STUDIES IN GEOCHEMISTRY

PART TWO

PETROLOGY AND GEOCHEMISTRY OF SYENITE INTRUSIONS IN THE EASTERN PROVINCE OF ZAMBIA

BY

FRANCIS TEMBO

Dissertation submitted as fulfilment for the requirement of the Degree of Master of Mineral Sciences (Geology) of the School of Mines, University of Zambia.

June, 1985

APPROVAL PAGE

This dissertation of Francis Tembo is approved as fulfilling the requirements of the Degree if Master of Mineral Science in Geology by the University of Zambia

Signature of Examiners

Chairman: Prof J. Cornah

1st Examiner: Lars Show Andersen

2nd Examiner: .....

External Examiner:

DECLARATION

This dissertation was written and submitted in accordance with the rules and regulations governing the award of Master of Mineral Sciences Degree of the University of Zambia. I further declare that the dissertation has neither in part nor in whole been presented as substance for award of any degree, either to this or to any other University. Where other peoples work has been drawn upon, acknowledgement has been made.

Signature of author: 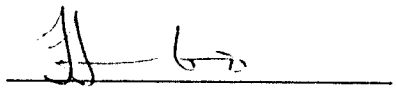

F. Tembo

Signature of Supervisor: 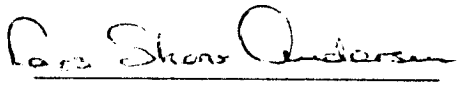

L.S. Andersen

Date: 13th June, 1985

CONTENTS

Chapter

Page

TABLES

FIGURES

PLATES

ABSTRACT

Syenitic rocks in Eastern Zambia are represented by both oversaturated quartz bearing types and undersaturated nepheline-sodalite varieties.

The Sinda syenite intrusions are oversaturated potassic syenites which form a petrogenetically related N-S trending string of intrusions at the eastern margin of the Sinda batholith.

The northernmost Lusandwa intrusion is a composite diapir covering some 70sq Km whilst the smaller Mayira, Seya, Pule and Tantha intrusions to the south are increasingly sill-like reflecting a strong structural control to their emplacement.

Petrographically, the syenites range from mafic pyroxene syenite through hornblende syenites to leucosyenites in the Lusandwa and Mayira intrusions, whilst the Pule, Seya and Tantha intrusions are homogeneous hornblende syenites.

The intrusions show systematic variations in their chemistry from the mafic syenites to the felsic syenites which are attributed to fractional crystallization. The Lusandwa and Mayira intrusions define an alkaline trend representing fractional crystallization of a mafic alkaline syenite magma whilst the Pule, Tantha and Seya intrusions deviate from this trend towards calc-alkaline compositions reflecting a change in the crystallizing assemblage induced by changes in the physical conditions during crystallization.

The apatite rich bodies within the Mayira intrusion, which are under investigation as phosphate ore have a mineralogy and mineral chemistry which indicates an origin as cumulates, with subsequent emplacement at a late stage of solidification.

The Lunkhwakwa intrusion in the Chipata area is an oversaturated potassic syenite which ranges in petrography from a mafic pyroxene syenite to a leucosyenite whilst the Bandawe intrusion in the south comprises a homogeneous sodi-potassic nepheline syenite.

The two intrusions also exhibit systematic chemical variations which are attributed to fractional crystallization. The chemistry of the Bandawe syenite is significantly different from that of the Lunkhwakwa syenite suggesting that the two intrusions originated from two different magmas. The Bandawe magma is considered to be a derivative of an alkaline magma of mantle origin whilst the Lunkhwakwa magma has a partly crustal origin.

The Mivula Hill intrusion is an undersaturated layered intrusion which petrographically is a nepheline sodalite syenite.

Chemically, the intrusion is miaskitic and peralkaline. The chemical variation within the exposed part of the intrusion is attributed to both fractional crystallization and crystal-liquid mixing processes with the latter predominating.

Rb-Sr isotope data have yielded an isochron with an age of 1340±16 Ma and an initial Sr isotopic ratio of 0.7028±0.0001. The Sr ratio suggests a mantle origin for the magma whilst the age is somewhat controversial and suggests the intrusion to have taken place in the early stages of the Kibaran orogeny.

ACKNOWLEDGEMENTS

Support from the University of Zambia Research and Grants committee and a Danida Fellowship to the author is gratefully acknowledged.

Professor H. Sørensen of the Institute of Petrology, Copenhagen University, Mr. L.S. Andersen and Professor D.C. Turner both of the University of Zambia, supervised the thesis.

The author is grateful to Drs. I. Sørensen, J.C. Bailey, O. Larsen and J. Rønsbo for carrying out the analytical work and assisting on the microprobe.

The following are thanked for their educative and fruitful discussions Professor E.H. Neumann, Dr. J.C. Bailey, Dr. L. M. Larsen Dr. A.K. Pedersen, D. Olsen and A. Garde.

Thanks are due to Ms. G. Sjørring, L. Andreasen and F. Phiri for typing the report and to Messrs. Sumbukeni and Phiri in the drawing office.

The author is indebted to Mr. B. Kabamba for his assistance in the field, Mr. W. Zimba for the preparation of thin sections and Mr. W. Nundwe in the photographic laboratory.

CHAPTER ONE

Introduction

1.1 Syenitic Rocks in the Eastern Province of Zambia.

Rocks of syenitic composition are known to occur at several localities within the basement complex of eastern Zambia (Fig. 1.1)[1].

Several of the syenite intrusions are either host to potentially economic mineralisation, or situated within mineralised country rock. At Nyimba, Petauke and Sinda, the syenites host disseminated sulphide deposits (2-5). At Sinda, concentrations of apatite are currently being evaluated as potential phosphate ore (6). In the Muchinje hills, radioactive boulders of monazite bearing syenite have been found (7), and in Mivula hill syenite asbetiform amphibole has been observed (8).

1.2 Scope and aims of present work.

Plutonic rocks of igneous origin constitute a significant part of the geology of the eastern part of Zambia. The intrusions are varied, both in their relative sizes and in their petrologic affinities. The largest pluton in the eastern part of Zambia is the Sinda batholith which covers an area of about 2,000 km^2 and is represented by rock types ranging from syenites to granites. Smaller syenitic, granitic and gabbroic intrusions are also present in the region. Information on these igneous rocks is so far limited to brief descriptions of their petrography and field relationships. Petrologic relationships between the various rock types are largely inferred from this information. An improved understanding of the

Fig. 1.1 Localities of syenitic rocks in E. Zambia within the framework of the geological map of Zambia (after Drysdall et al, 1972).

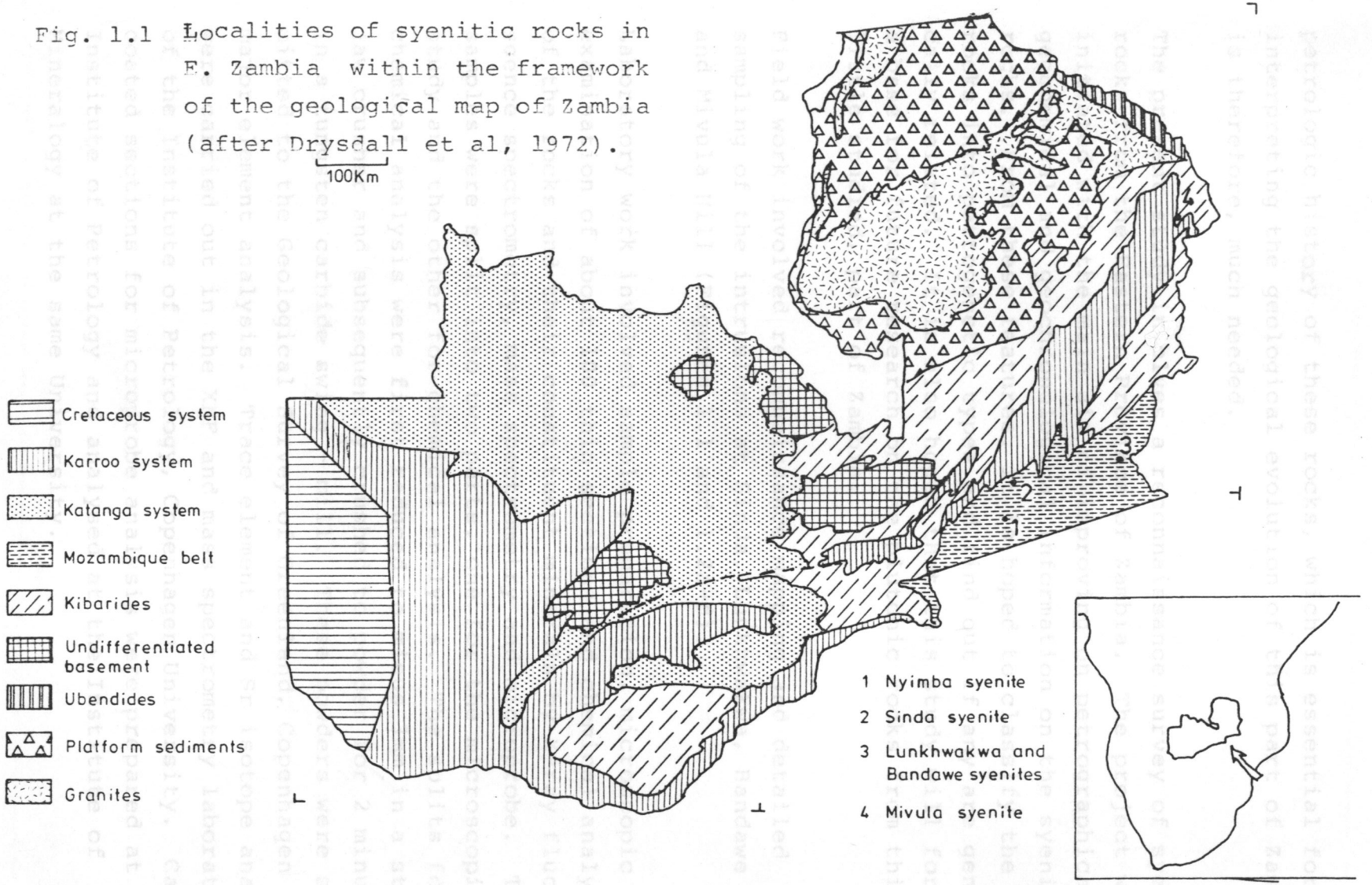

petrologic history of these rocks, which is essential for interpreting the geological evolution of this part of Zambia, is therefore, much needed.

The present study involves a reconnaissance survey of syenitic rocks from the Eastern Province of Zambia. The project was initiated with the main aim of improving on petrographical, geochemical and geochronological information on the syenitic rocks. From these features, it is hoped to classify the rocks into petrogenetic types and find out if any are genetically related. It is also hoped that this study will form a base for future research on the plutonic rocks from this, little studied, part of Zambia.

Field work involved reconnaissance mapping and detailed sampling of the intrusions at Sinda, Lunkhwakwa, Bandawe and Mivula Hill (Figures 1.1 and 1.2a-d).

Laboratory work involved sample preparation, microscopic examination of about 100 thin sections and chemical analysis of the rocks and their constituent minerals by X-ray fluorescence spectrometry, mass spectrometry and microprobe. The samples were split into two parts, one for the microscopic study and the other for chemical analysis. The splits for chemical analysis were first reduced to minus 3mm in a steel jaw crusher and subsequently crushed to powder for 2 minutes in a tungsten carbide swing - mill. These powders were submitted to the Geological Survey of Greenland, Copenhagen for major element analysis. Trace element and Sr isotope analysis were carried out in the XRF and mass spectrometry laboratories of the Institute of Petrology, Copenhagen University. Carbon coated sections for microprobe analysis were prepared at the Institute of Petrology and analysed at the Institute of Mineralogy at the same University.

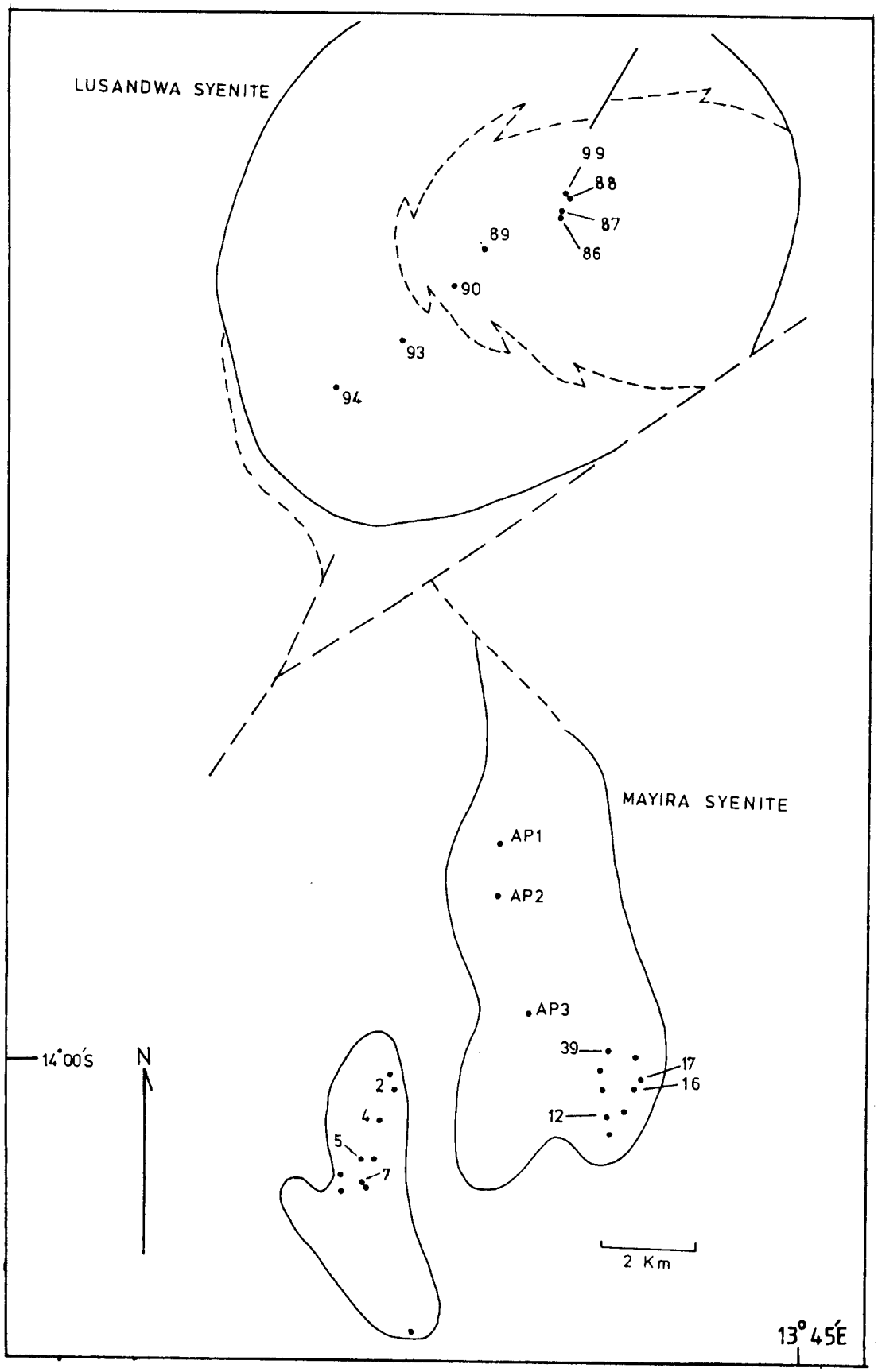

Fig. 1.2a Sample localities.

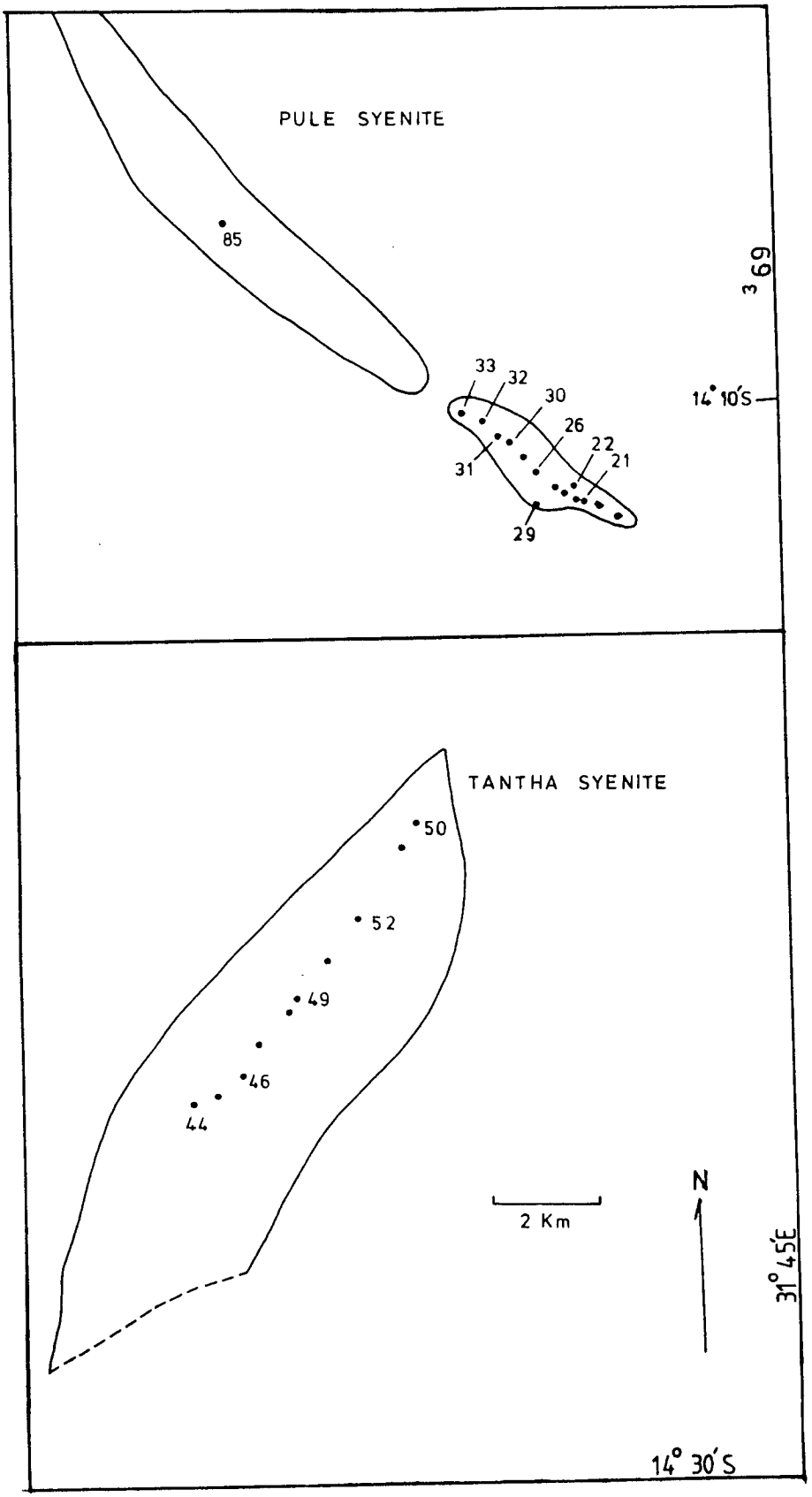

Fig. 1.2b Sample localities.

LUNKHWAKWA SYENITE

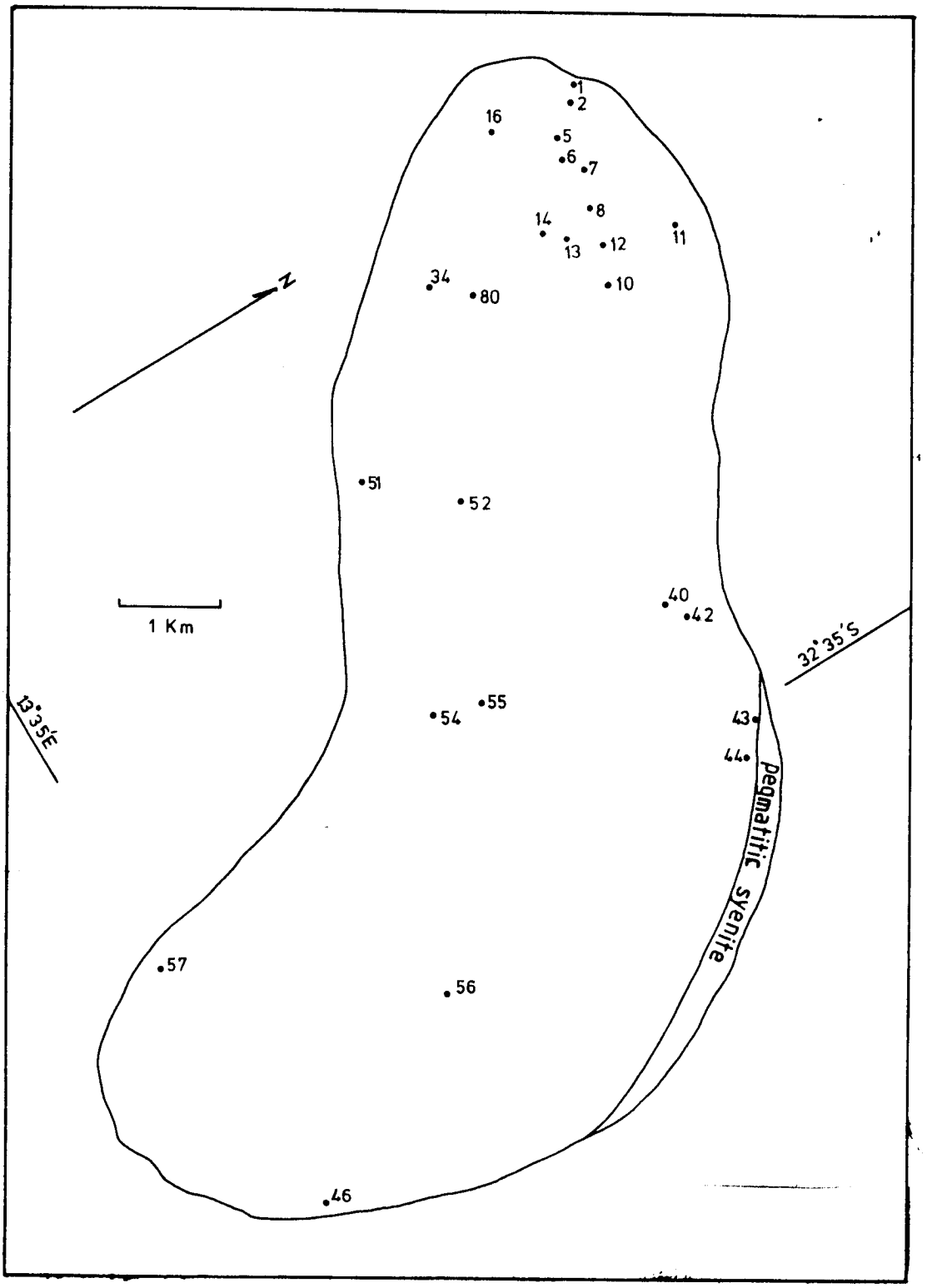

Fig. 1.2c Sample localites.

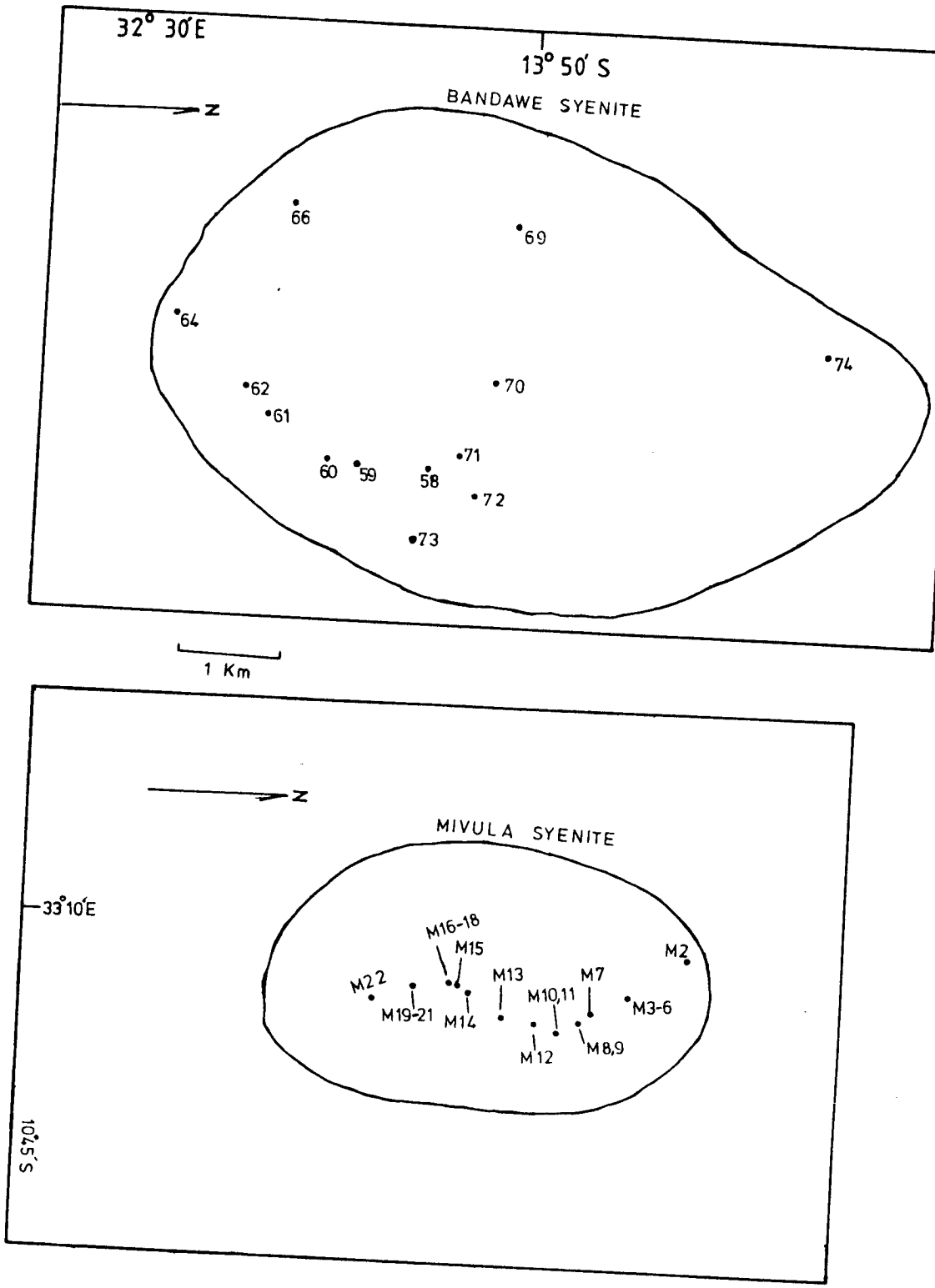

Fig. 1.2d Sample localities.

1.3 Previous Work

The first description of syenites in Zambia was given by Adams and Osborn (9). They described a nepheline syenite 60 Km west of Solwezi in the Northwestern Province and a nepheline - sodalite syenite in the north-east corner of Zambia between the Luangwa river and the border of Malawi. For the latter, they note its location in Karroo rocks but also mention its proximity to gneisses and schists of the basement complex. From their study, the authors concluded that the nepheline sodalite syenite was similar to the sodalite syenites of the Haliburton district, Ontario. From the location and geological description, there can be little doubt that the syenite in question is the Mivula Hill syenite.

Newton (10) later described the Mivula Hill syenite in more detail in relation to its potential for uranium mineralisation. The faulted contacts of the syenite against Karroo rocks on the eastern and southern boundaries and a possible contact with gneisses and schists in the north were noted. From this survey Newton concluded that the syenite is intrusive into the basement rocks.

Two main rock types were recognised at the Mivula Hill: the main syenite type is a coarse grained biotite sodalite syenite. The other is a fine grained porphyritic nepheline syenite which is sodalite free and has recrystallization and disequilibrium textures (10). Veins of aplitic syenite and amphibole bearing pegmatite are locally present. Newton also noted the possibility of a fault transecting the syenite towards its northern end.

Mapping in the Chipata area by Vavrda (11) delineated four syenite intrusions, the largest of which are the Lunkhwakwa and Pandawe syenites. All are intrusive into basement rocks. The south-eastern part of the Lunkhwakwa syenite is a fine to medium grained foliated aegirine syenite (11). Further northwest, Vavrda's mapping of the Lunkhwakwa syenite,was extended by Felton (7) who described it as a coarse grained massive rock which is in places composed entirely of aegirine.

The Pandawe syenite is a coarse grained porphyritic rock (11).

The Sinda syenites are considered to be part of the Sinda Plutonic complex, a composite batholith which covers an area of approximately 2,000 Km^2. The syenites are marginal to the central granite intrusion which they are considered to have preceded. (12).*

The Lusandwa syenite, which is the largest of the syenite intrusions, was first described by Bailey(13) who termed it a ring structure owing to its circular nature and the concentric layering within it. He also concluded that the rock composition ranges from a dioritic monzonite at the centre to a syenite at the margin. The margin is separated from the country rocks by a granitic border phase. The contact between the monzonite and the syenite is gradational.

Phillips (2-3) later mapped the Sinda area in detail and concluded that the syenite to the north is a stock whereas the other intrusions are sills. He recognised two rock types in the area: syenites which range in composition from hornblende syenite to quartz syenite and monzonites which make up the centre of the Lusandwa and Mayira hills intrusions. He recognized the

*NOTE: However, the present study shows that the syenites

gradational boundaries between the two rock types and concluded that the monzonite was an earlier phase.

Current work on the Sinda syenites by the Mineral exploration department of Zimco is concerned with prospecting for phosphate deposits which occur as apatite rich bodies within the syenites (6).

CHAPTER TWO

Regional Geology

2.1 Stratigraphy

The eastern part of Zambia is mainly underlain by a basement complex (Fig. 1.1) which can be subdivided into:

1) Proterozoic gneisses and granulites having a Rb-Sr whole rock isochron age of 2315±24 Ma (14) and
2) a Mid-Proterozoic metasedimentary cover which includes the Mvuvye, Sasare, Mwami and Mafingi Groups.

The Mvuvye Group rocks crop out in the Petauke and Mwanjawanthu areas. It comprises quartzo-feldspathic gneisses, marbles, quartzites and schists with minor metarhyolites and amphibolites. The eastern contact of the Mvuvye Group is the Sinda batholith, which is considered to have caused extensive migmatisation of the former (3). The Mvuvye Group sediments are considered to have been deposited in a shallow marine environment (4) and have not been correlated with any other lithological group in eastern Zambia.

The Sasare Group which crops out in the Sasare area is comprised of a basal unit of marbles, graphite schist and conglomerates followed by a metavolcanic unit composed of amphibolites, epidosites and minor acid metavolcanics and terminated by conglomerates and quartzites (15). The Sasare Group is correlated with the metasediments and metavolcanics of the Mpanshya Group (15) which are in turn correlated with the meta-sediments and meta-volcanics in the Mulungushi area (16). These sediments

and volcanics form part of the Pre-Irumide sedimentation and igneous activity.

The Mwami Group in the Chipata area is a sequence of psammitic and pelitic metasediments which begins with a basal conglomerate, grading into meta-arkosic sandstones and meta-tuffs. The upper unit is mainly composed of meta-argillites and meta-tuffs. The Mwami Group has been correlated with the Mchinji Group in Malawi (11) which is in turn correlated with the Mafingi Group of northeastern Zambia and northern Malawi (17).

The Mafingi Group which has its type locality in northern Malawi is composed of psammitic and pelitic metasediments of variable composition. The sequence reaches a maximum thickness of about 1350m in the Mafingi basin where it begins with a 29m thick basal conglomerate which passes into 1290m thick quartzites and terminates with 50m thick meta-pelites. The major part of the sequence is believed to have been deposited in a shallow marine environment (18). The Mafingi Group has been correlated with the Manshya River Group in northern Zambia (19).

Thus it appears that the Sasare, Mwami and Mafingi Groups were all deposited within the same period of time in a similar sedimentary environment.

2.2 Deformation

The basement complex in the eastern part of Zambia has been subjected to at least three major phases of deformation (3, 11, 20). The earliest phase is represented by north-south trending structures and is limited to the crystalline basement and the Mvuvye Group cover rocks.
The structural trends are attributed to the

Ubendian phase of the Eburnian Orogeny (21). This correlation leads to the conclusion that the Mvuvye Group rocks are pre-Ubendian sediments. The north-south structural trends are strange as further north, Ubendian structures have east-southeasterly to east-westerly trends (22). The observed trends probably reflect a re-orientation of the Ubendian structures during later orogenies.

The second and third phases of deformation affected all rocks of the basement complex, but some more severely than others. Thus phase II is more prominent in the Mafingi, Mwami and Sasare Groups and is characterized by northeast-southwest trending structures. These structures are attributed to the Kibaran Orogeny (1340±25 Ma) (23) which resulted in the formation of the Irumide fold belt. Phase three which is correlated with the Mozambiquian phase of the Katangan Orogeny (650 -485Ma)(23) produced north-northeast to south-southwest trending structures and is more easily recognised in the Mwami and Sasare Groups. This is presumabely because the Mafingi Group is outside the major influence of the Mozambiquian orogeny. Each deformation was accompanied by regional metamorphism ranging from greenschist facies to granulite facies and by widespread magmatic activity resulting in the formation of high grade metamorphic rocks, migmatisation and the emplacement and extrusion of a variety of plutonic and volcanic rocks respectively. Among the plutonic rocks intruded during these periods are the Sinda plutonic complex and the syenites of the Chipata and Mivula hill areas.

3 Geochronology

Little geochronological data exists on the syenites of the Eastern Province. However, relative ages of the syenites can be inferred from local field evidence.

2.3.1 Sinda area

The syenites in the Sinda area are marginal to the main granite intrusion of the batholith which is intrusive into the Mvuvye Group rocks (2).

A metamorphic biotite from the Lusandwa syenite has yielded a Rb-Sr age of 480 Ma whilst the main granite yield/s a Rb-Sr whole rock age of 400 Ma (3). These ages are doubtful as it is not reported whether it is an isochron age or not. Furthermore, the number of samples analysed is not reported. However, these ages are within the age limits of the Mozambiquian orogenic episode, 650-485 Ma (23) and probably reflect its effects. It is therefore concluded that the Sinda syenites and the Sinda granite are younger than the Mvuvye Group, deformed at 1930±30 Ma (21) and older than or coeval with the Mozambiquian episode.

2.3.2 Chipata area

The syenites in the Chipata area are intrusive in the basement complex of granulites and gneisses which have a Rb-Sr whole rock age of 2315±24 Ma (14). The relationship of the syenites to the Mwami Group is obscure as there is no observable contact between them. As such, the age of the syenites cannot be bracketed, but they have been correlated with the Sinda syenites on petrological grounds (11).

2.3.3. Mivula Hill syenite

The Mivula Hill syenite is intrusive into the Mafingi Group rocks which were deformed during the Kibaran orogeny, at 1340±25 Ma (23), thus suggesting that it is younger than this orogenic event. The syenite has yielded a K-Ar mineral age of 550 Ma (24).

As part of this study, a Rb-Sr whole rock isochron age of 1341±16 Ma has been obtained for the intrusion, thus placing it in the early Kibaran. The 550 Ma age and the implications of the present age will be discussed further in Chapter 7.

CHAPTER 3

Field relations and structure of the syenitic rocks.

The syenitic rocks of the Eastern Province intrude rocks of the basement complex with which they have various morphological and structural relationships. Internally, the syenite bodies exhibit both igneous and metamorphic structures.

Previous workers have described the syenites as unmetamorphosed igneous rocks (2,3,4,7,11). However, the present study has revealed that some of the rocks have been metamorphosed.

3.1 Sinda area

The syenite intrusions (fig.3.1) outcrop as ridges and hills in a terrain which ranges in topography from flat or gently undulating in the south to rugged and hilly in the north. The main intrusions occur in the Tantha hills, Pule hill, Mayira and Loli hills (Lusandwa stock). Contacts with the surrounding country rocks are in most cases not exposed owing to a thick soil cover.

The Lusandwa syenite is a rounded body occupying about $70Km^2$. It is in gradational contact with the Lusandwa granite in the south and has both concordant and discordant relationships with the Kasangazi and Chindeni gneisses in its northern, eastern and western contacts (3). The intrusion is characterized by an internal coarse flow foliation which is defined by a parallel alignment of tabular feldspar crystals up to 2cm x 3cm in size.

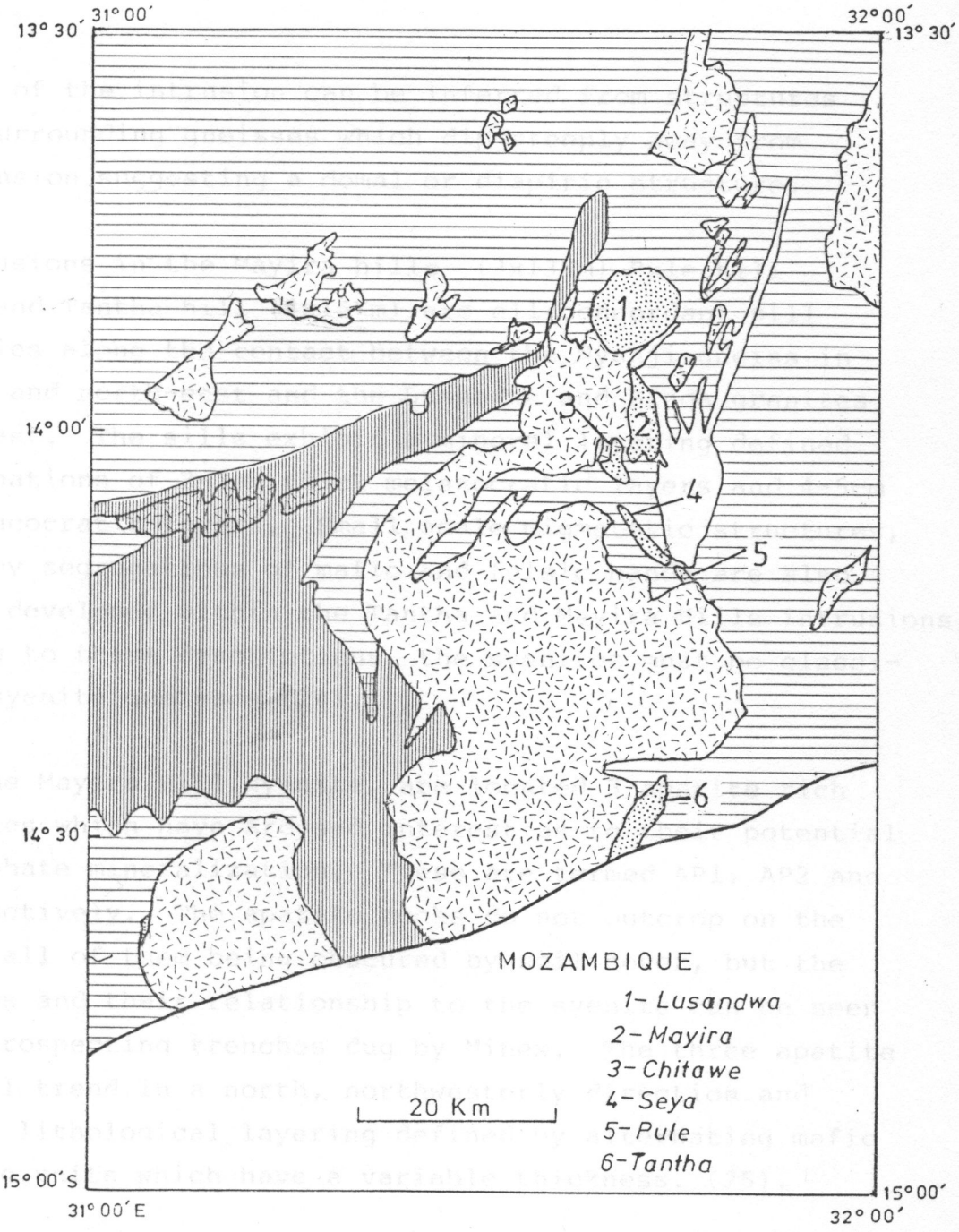

Fig. 3.1 Regional geology of the Sinda and Lusandwa River areas (after Phillips, 1964).

The form of the intrusion can be inferred from structures in the surrounding gneisses which dip steeply away from the intrusion suggesting a domal or diapiric structure.

The intrusions in the Mayira hills (3x13Km) Pule hill (1x4Km) and Tantha hill (4x15Km) are all concordant sill like bodies along the contact between the Nyanji gneiss in the east and north-east and the Lusandwa and Sinda granites in the west. The sills exhibit a mineral layering defined by alternations of 2-3cm thick melanocratic layers and 4-5cm thick leucocratic layers. Small scale migmatitic structures, defined by segregations of mafic and felsic bands are also locally developed within the Tantha and Mayira Hills intrusions. According to these descriptions, the syenites must be classified as syenite gneisses (24).

Within the Mayira Hill syenite, are located 3 apatite rich rock bodies which have aroused interest as to their potential for phosphate mineralization. These are termed AP1, AP2 and AP3 respectively. The apatite rocks do not outcrop on the surface, all of them being obscured by soil cover, but the rock types and their relationship to the syenite can be seen in some prospecting trenches dug by Minex. The three apatite bodies all trend in a north, northwesterly direction and exhibit a lithological layering defined by alternating mafic and felsic units which have a variable thickness. (25).

Apatite body AP1 is the largest of the bodies and it occurs as lenticles and veins which have sharp contacts with the enclosing syenite. These veins and lenticles are presumed to meet at depth to form one large body (6). Brecciation of the rock is visible in handspecimen.

Apatite rock body AP2 is a vein like mass which covers an area of 6m x 130m. It also has sharp contacts with the surrounding syenite and is also brecciated.

Apatite rock AP3 is also a vein like body covering an area of 5m x 35m which is in sharp contact with the enclosing syenite. In contrast to the other two rock types, rock AP3 does not show any signs of brecciation.

Smaller apatite rich bodies have also been observed at the contact between the syenites and the Nyanji gneisses (Mujokotwaki, Pers. Comm. 1984).

Another type of inclusion in the syenite intrusions are rounded mafic inclusions which may reach up to 5cm across. These inclusions have sharp contacts with the enclosing syenites and are made up of an aggregate of mafic minerals which were visually identified as pyroxene. Pale green apatite grains are also present in the inclusion. In the foliated syenites, the inclusions lose their round shapes and are elongate parallel to the foliation, showing that they have been deformed together with their host rock.

3.2 Chipata area

The Lunkhwakwa syenite (fig. 3.2) covers an area of about 50Km^2 and occupies a flat depression surrounded by ridges of quartzite, belonging to the basement complex (11).

The Bandawe syenite in the south, occupies an area of about 18Km^2 in a flat undulating terrain. Outcrop of both intrusion/s is isolated and often in the form of small hillocks. Contacts with the surrounding country rocks are almost always obscured by soil cover.

The Lunkhwakwa syenite has sharp concordant contacts with granulites and quartzites in the north and south. In the northwest, it has/a discordant contact with quartzo

Fig. 3.2 Regional geology of the Chipata and surrounding areas (after Vavrda, 1972).

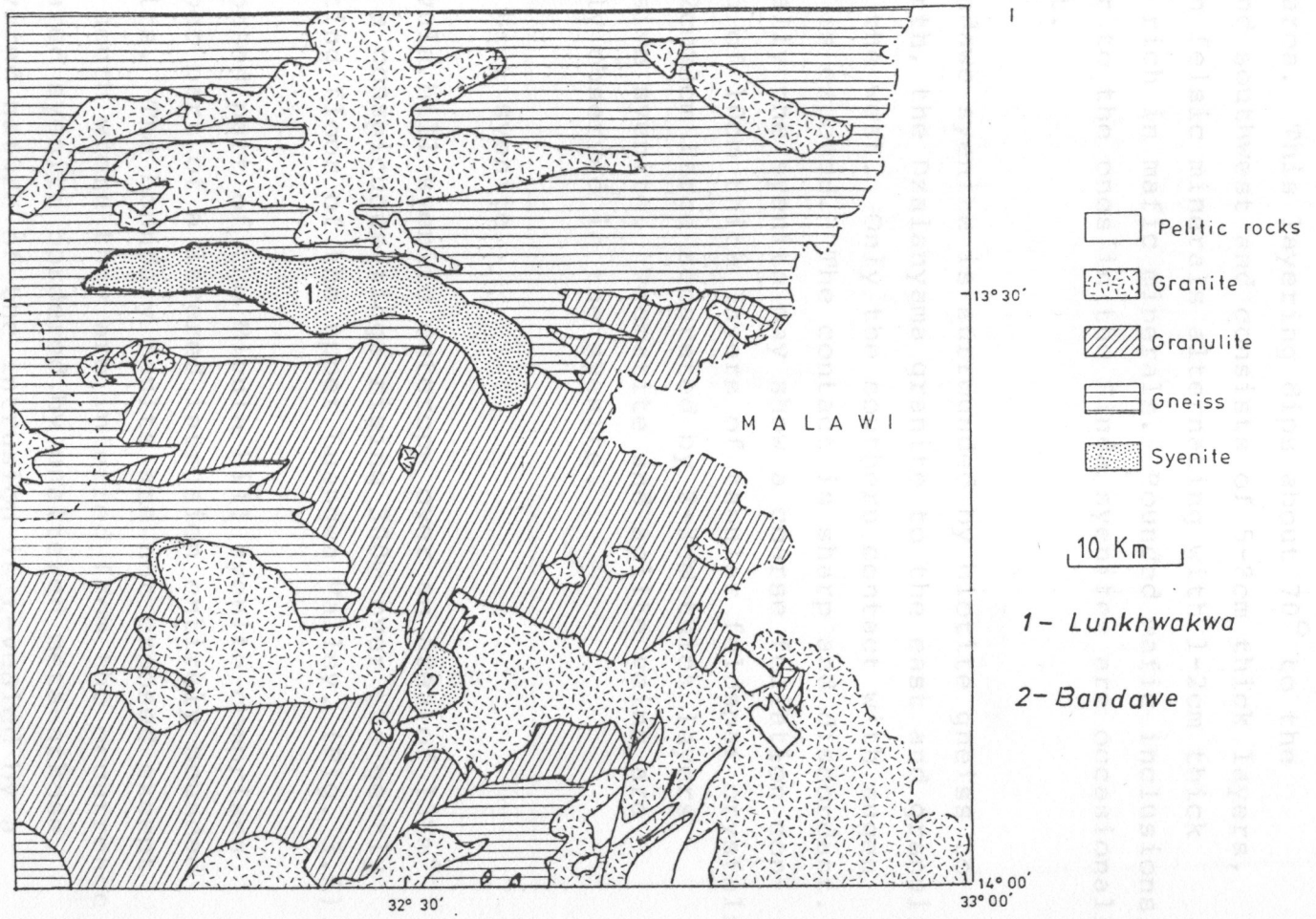

feldspathic gneiss. In all cases, the contacts are defined by pegmatite veins. The intrusion exhibits a mineral layering similar to that observed in the Sinda area. This layering dips about 70° to the west and southwest and consists of 5-8cm thick layers, rich in felsic minerals alternating with 1-2cm thick layers rich in mafic minerals. Rounded mafic inclusions, similar to the ones in the Sinda syenites are occasionally present.

The Bandawe syenite is surrounded by biotite gneiss to the north, the Dzalanyama granite to the east and granulites to the west. Only the southern contact with augen gneiss is exposed. The contact is sharp and discordant. Internally the syenite may show a coarse foliation consisting of 10cm thick layers of tabular feldspar crystals up to 2cmx3cm large separated by 2-3cm thick layers of massive syenite. Pegmatite and aplite veins are commonly observed in the syenite.

3.3 Mivula hill syenite

The Mivula hill syenite outcrops over an area of 13Km^2 forming a conspicuous ridge rising 300m over the gently undulating floor of the upper Luangwa Valley. (Fig. 3.3).

The exposed part of the Mivula hill syenite comprises the upper part of a layered intrusion entirely bounded by faults. The boundary faults are not exposed except to the south where they are inferred from the occurrence of sheared syenite bordered by unaltered meta-arkose. The layered nature of the intrusion is revealed by a variably developed mineral lamination which has a consistent north-east strike and southerly dip ranging from 70° at the northern most outcrop to 30° in the central part. The decrease of dips is accompanied by a weakening of the lamination, an increase of grain size and changes in the cumulus assemblages consistent

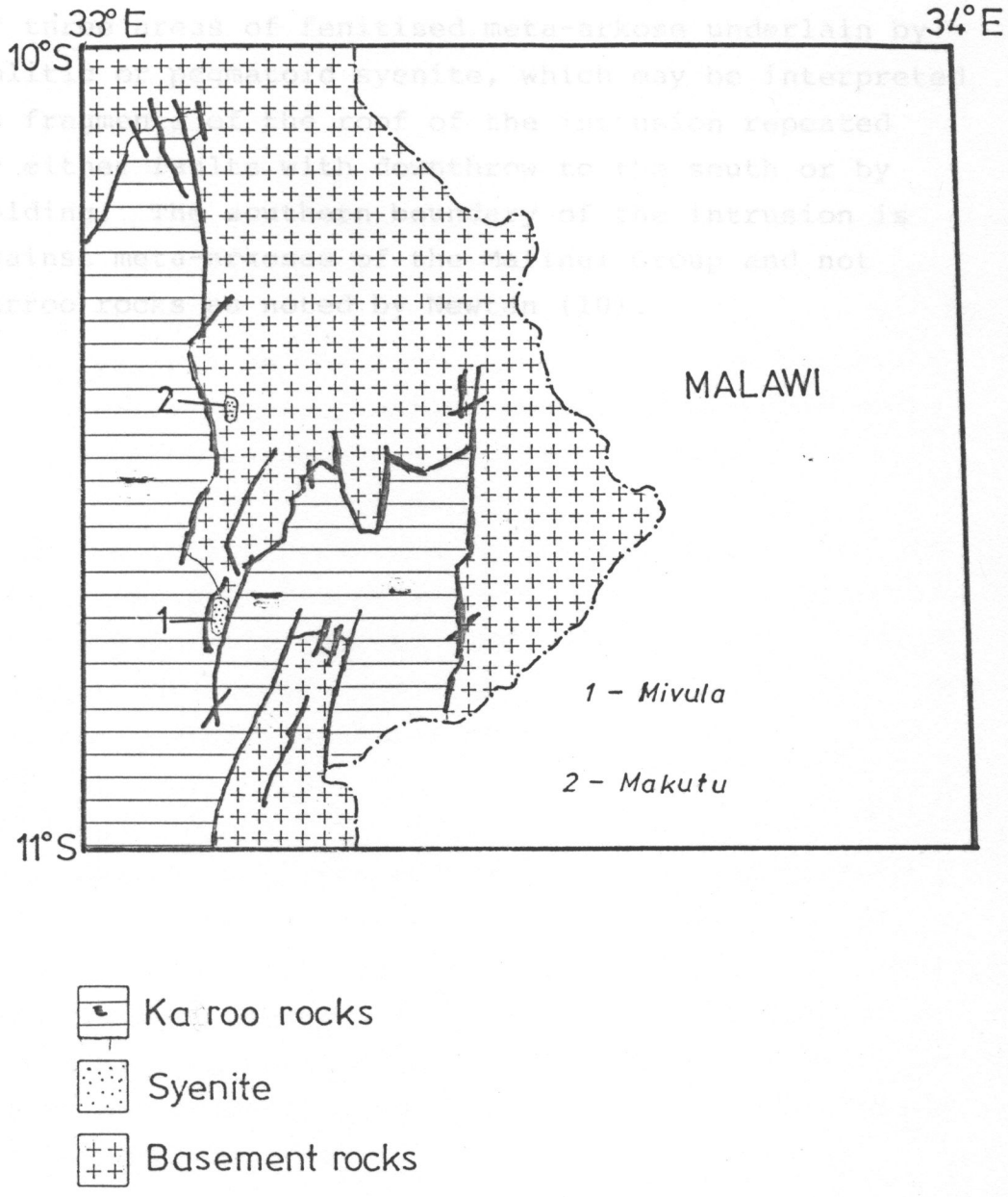

Fig. 3.3 Regional geological setting of the Mivula Hill syenite (after Drysdall et al, 1972).

with higher levels of an intrusion. The changes are corroborated by the occurrence along the ridge crest of three areas of fenitised meta-arkose underlain by aplitic or pegmatoid syenite, which may be interpreted as fragments of the roof of the intrusion repeated by either faults with downthrow to the south or by folding. The southern boundary of the intrusion is against meta-arkoses of the Mafingi Group and not Karroo rocks as noted by Newton (10).

CHAPTER FOUR

Petrography

4.1 Introduction

The syenites can primarily be classified into saturated, quartz bearing types and undersaturated feldspathoid bearing ones. The saturated types are represented by the syenites in the Sinda area and by the Lunkhwakwa syenite at Chipata, whilst the undersaturated rocks include the Bandawe and Mivula Hill syenites.

A characteristic feature of the syenites in the Sinda and Chipata areas is the presence of metamorphic textures. The Mivula Hill syenite is also foliated but it will be shown that these are primary igneous foliations. Some of the textural features of the syenites are shown in plates A-C.

The metamorphic syenites of the Sinda and Chipata areas must be classified as syenite gneisses (24). According to the definition of Floor (24), an alkaline gneiss is a leucocratic metamorphic, metasomatic or igneous rock containing feldspar as an essential component and characterized by one or more of the following structural features:

1) a banded appearance, caused by alternating layers with different mineralogical composition
2) a laminated appearance, caused by alternations of thin laminae of dark and ligh minerals within one rock type.
3) a foliated appearance defined by a (sub) parallel arrangement of one or more mineral species.

The above definition is purely petrographical and does not take into account the mode of origin of these rocks. Field evidence from the Sinda, Chipata and Mivula Hill areas clearly indicates that these are intrusive rocks, hence while keeping their metamorphic aspect in mind, they are described as igneous rocks and therefore the term syenite is used throughout this text.

4.2 Sinda Syenites

The syenites can be grouped into two types based on their mineralogical composition. The Lusandwa syenite contains two pyroxenes and biotite whereas those from the other intrusions contain amphibole and biotite with subordinate amounts of pyroxene. The feldspars change from microperthite and calcic plagioclase in the pyronexe syenites to mesopherthite and a sodic plagioclase in the amphibole syenites. Constant accessory minerals are Fe-Ti-oxides, apatite, sphene and calcite, whilst zircon and epidote may be present.

The pyroxene syenite has an approximate modal composition of 80-90% alkali feldspar, 1-3% plagioclase feldspar, 5-15% pyroxenes, 3-5% biotite, .5% quartz and 1-2% accessories whereas the modal composition of the amphibole syenite is 85-90% alkali feldspar, 0-1% pyroxene, 3-10% amphibole 1-2% biotite, 4-5% quartz and 1-4% accessories.

The rocks are typically coarse to medium grained and have granular textures (Plate A, Figs a and b). Foliated textures are also present, with the foliation being defined by an orientation of all the constituent minerals. (Plate A Fig. c). Locally porphyritic textures are developed. In hand specimen, the mafic minerals are patchily distributed.

Plate A Textures of the Sinda syenites

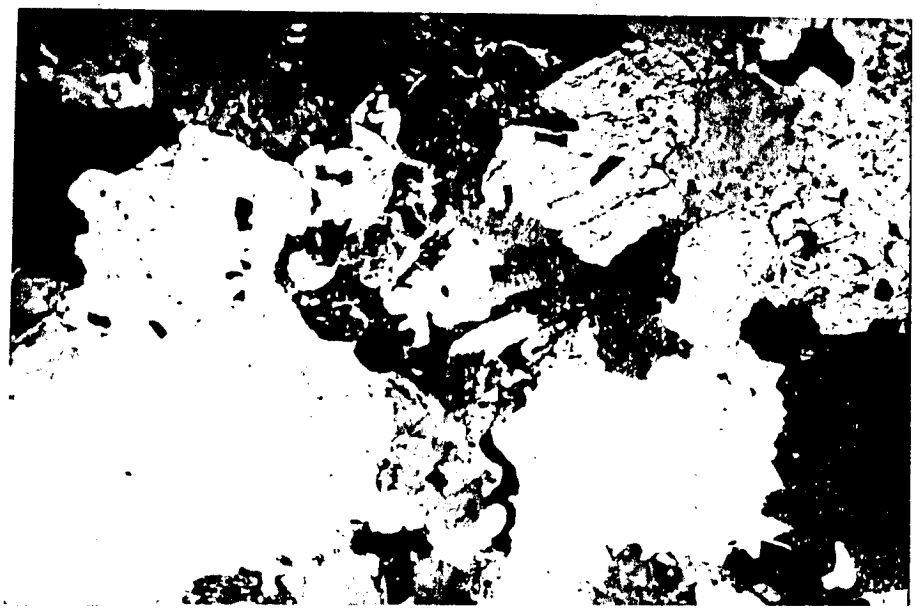

Fig. a. Granular texture in pyroxene syenite. Note replacement of pyroxene (light grey) by biotite (dark coloured with birds eyes structure) crossed nicols 20 x magnification. (Lusandwa syenite).

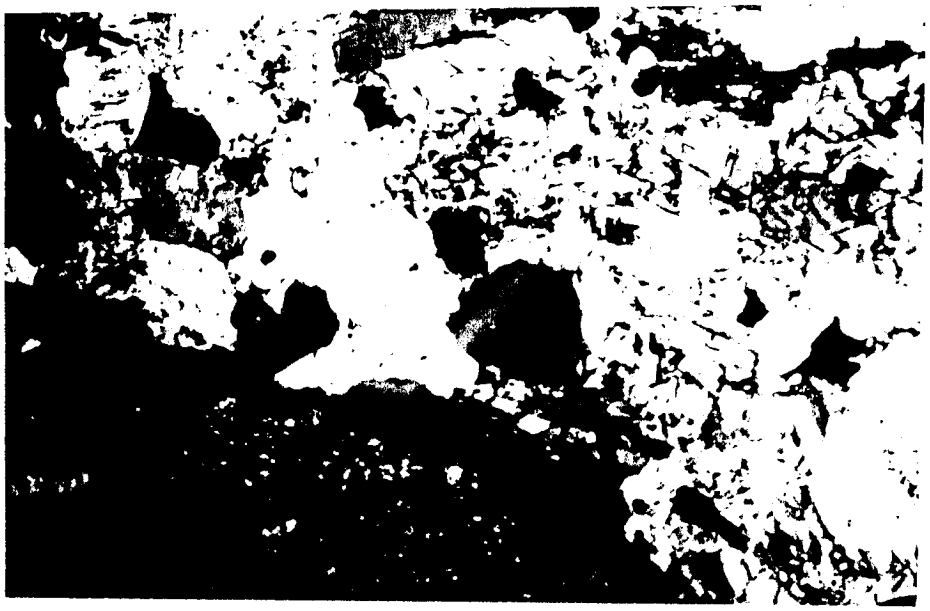

Fig. b. Granular texture in pyroxene syenite (Mayira) note replacement of pyroxene by hornblende crossed nic ols, 20 x magnification.

Feldspar: the microperthite of the pyroxene syenites commonly occurs as 2mm x 4mm anhedral, irregularly shaped grains containing patches of exsolved albite. Less common phenoclasts are present as .5cm x 2cm tabular clouded grains, which are granulated at the margins. Oscillatory zoning and inclusions of clinopyroxene, iron oxide and plagioclase are common in the microperthite. The plagioclase inclusions are characteristically arranged parallel to the zoning in the larger grains. This is interpreted as a synneusis texture in which co-existing plagioclase grains are physically stuck onto the crystal faces of a growing K-feldspar grain.

The amphibole syenites contain a mesoperthite which in the most deformed rocks has completely inverted to microline (Plate A, Fig. d). The grains have an average size of 3mm x 4mm and are anhedral with irregular grain boundaries. Locally, the grains show a preferred orientation. Zoning of the perthite grains is defined by alternation of microcline and microperthite in a single grain. Recrystallization of the perthites is shown by the development of smaller, .1mm x .2mm, microcline and albite grains at the margins of the large grains. These show undulatory extinction and are arranged in a polygonal texture.

Plagioclase feldspar ranges in composition from An25-35 in the pyroxene syenites to An_{0-10} in the amphibole syenites. The plagioclase of the pyroxene syenite occurs as euhedral, 2mm x 4mm large grains, which together with biotite may outline a foliation, (Plate A, Fig. c). These oriented grains are occasionally bent and have a wavy extinction. In the amphibole syenites, the albite occurs interstitially and is commonly recrystallized to define a granoblastic texture together with quartz (Plate A, Figs. e and f).

Fig. c. Foliated texture in pyroxene syenite (Lusandwa), note preferred orientation of all mineral grains, crossed nicols, 20 x magnification.

Fig. d. Granular texture in hornblende syenite (Pule), note mesoperthitic alkali feldspar and interstitia albite, crossed nicols, 20 x magnification.

Pyroxene: the common pyroxene is non pleochroic, colourless and was chemically determined to be a salite. A pale green, weakly pleochroic type, which is probably hedenbergitic is occasionally seen in the pyroxene syenite. The individual pyroxene grains have an average size of 1mm x 2mm. In the amphibole syenite, the pyroxene grains may be smaller due to replacement by amphibole. The common mode of occurrence of the pyroxene is as anhedral interstitial grains which are usually clustered and occasionally show a preferred orientation. Simple twinning and inclusions of iron oxide are common in the pyroxene. These inclusions may give the pyroxenes a poikilitic appearance. The pyroxene of the amphibole syenite is always broken up and replaced by amphibole.

Orthopyroxene is present in the pyroxene syenite where it occurs as rounded interstitial grains less than 1mm across. It has corroded margins against the clinopyroxene. In one case, the orthopyroxene is enclosed by clinopyroxene.

Amphibole: the amphibole of the pyroxene syenite is an actinolite which replaces clinopyroxene. In the amphibole syenite, the common amphibole is an edenite which is present as 1mm x 1.5mm anhedral grains interstitial to the feldspar. It also pseudomorphs clinopyroxene. The amphibole is replaced by biotite and locally exhibits polygonal textures. Inclusions in the amphibole are iron oxide, apatite and less commonly quartz.

An inclusion free secondary actinolite is seen to replace both the early amphibole and the pyroxene.

Fig. (e) Massive texture in hornblende syenite (Tantha), note discrete microcline and albite grains, crossed nicols, 20 x magnification.

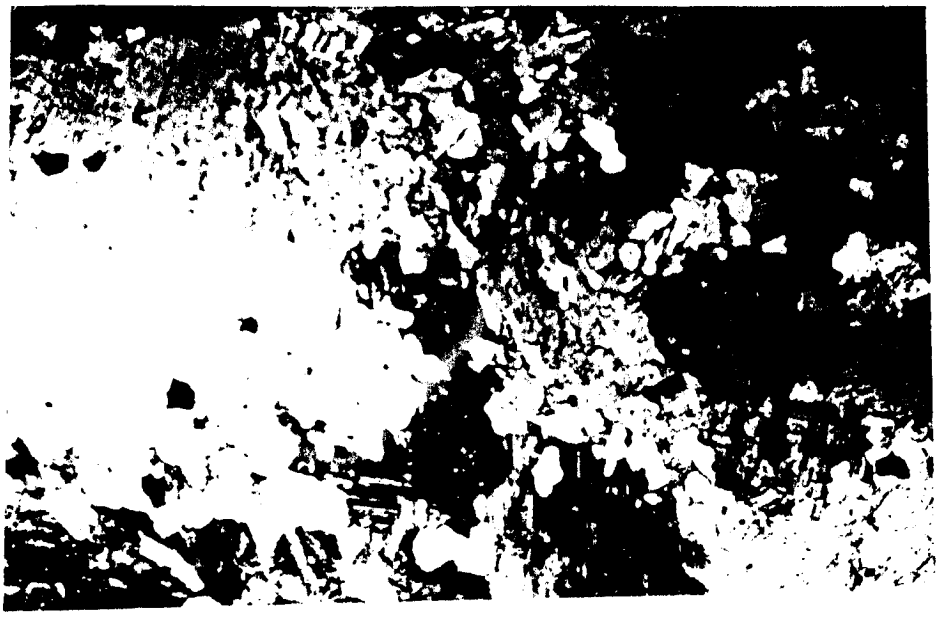

Fig. (f) Granulated alkali feldspar grains in leucocratic syenite, note interstitial albite, crossed nicols 20x magnification.

Biotite - two generations of biotite are observed in the pyroxene syenites. Biotite considered to be primary is present as .5mm x 1mm subhedral plates partly or completely replacing pyroxene. These biotites are pleochroic with X = greenish brown Y = Z = brown and often contain euhedral inclusions of apatite and iron oxide. The second generation biotite occurs as large, anhedral grains which have deep brown colours. These grains replace primary biotite, pyroxene, and enclose feldspar and iron oxide. In the amphibole syenites, the biotite occurs as small flakes often replacing amphibole and containing zircon inclusions. These biotites show a preferred orientation.

Quartz - in the pyroxene syenites, quartz is in accessory amounts and has three modes of occurrence (a) as interstitial anhedral grains, together with plagioclase (b) as recrystallized rims around biotite and plagioclase and (c) as myrmekite in the plagioclase. Quartz is more abundant in the hornblende syenites where it occurs as interstitial polygonal grains, defining a granoblastic texture with albite, and as anhedral grains 1mm x 2mm large showing undulatory extinction.

Iron oxide, Sphene and Apatite.
These accessory minerals are always present in the syenites where they are associated with the mafic minerals.

Iron oxide in the pyroxene syenite occurs, firstly as anhedral, interstitial grains, occasionally enclosed by late biotite and secondly as euhedral rectangular inclusions in pyroxene, primary biotite and microperthite. In the amphibole syenites the

iron oxide is present as anhedral interstitial grains often mantled by sphene, and as an inclusion in the amphibole and biotite. Sphene occurs in amphibole syenites as anhedral to subhedral grains together with the mafics, often replacing iron oxide. The two minerals have an inverse relationship to each other: that is, samples abundant in sphene are relatively depleted in iron oxide whilst those abundant in iron oxide have little sphene. Sphene is absent from the pyroxene syenites.

Apatite in both syenite types has two modes of occurrence: as euhedral inclusions in feldspar and amphibole and as subhedral interstitial grains.

Calcite, epidote, zircon and colourless mica: Calcite is present as interstitial grains often recrystallized and sometimes filling cracks in the felspar grains. The calcite is in places associated with sphene and epidote. Zircon occurs as inclusions in the metamorphic biotite of the pyroxene syenite. Epidote is present as anhedral grains replacing the plagioclase phase of the perthite. The colourless mica is present as small flakes filling fractures in the perthites.

4.2.2 Apatite rich rocks.

The apatite rich rocks are dark to light coloured and medium grained. They are composed of clinopyroxene, apatite, alkali feldspar, quartz and amphibole with little biotite. Brecciation of the rock is apparent in the samples from the two bodies AP1 and AP2.

The rock from apatite body AP1 has an approximate composition of 60-65% alkali feldspar, 30-35% apatite and 5% quartz. That from AP2 has a composition of 70-80% apatite, 20-25% quartz and 3-5% clinopyroxene whilst that from AP3 is composed of about 49% apatite, 49% clinopyroxene, 1% amphibole and 1% iron oxide.

Feldspar - A clear, Carlsbad twinned alkali feldspar, probably orthoclase, is present only in rock AP1 where it occurs as anhedral grains, 0.5mm x 1mm large set in a fine grained slightly altered matrix of quartz, calcite and fibrous amphibole. Some feldspar grains are slightly strained and may contain amphibole inclusions.

Pyroxene - the clinopyroxene is present in rocks AP2 and AP3 and absent in rock AP1. In both rocks the pyroxene is a pale green and weakly pleochroic salite which has hedenbergitic composition. In rock AP2, the pyroxene is subordinate to amphibole and it occurs as .4mm x 2mm broken up grains, but still retaining its original subhedral to euhedral shapes. It is frequently replaced by amphibole and its cracks filled by secondary quartz. This pyroxene, together with amphibole and apatite are set in a fibrous matrix of quartz which shows undulatory extinction due to recrystallization.

In rock AP3, the pyroxene is also a pleochroic salite and is the main mafic mineral present. It occurs as .5mm x 2mm long subhedral to euhedral grains occasionally showing a preferred orientation. It contains inclusions of hematite and is replaced by a green amphibole.

Amphibole - a magnesian hornblende is present in rock AP2 as anhedral grains, 1mm x 2mm in size. These are usually broken up and altered to a fine micaceous mineral. The cracks in the hornblende , like in pyroxene are filled with secondary quartz. The amphibole may also enclose apatite.

Apatite - the apatite is present in all three rocks as subhedral to euhedral prismatic grains which are occasionally broken up and have a wavy extinction due

to granulation. Apatite in rock AP3 may reach up to 1mm x 3mm in size and has straight or slightly curving grain boundaries. In the brecciated rocks, the apatite has an average size of .5mm x 1mm.

Quartz and calcite - these are secondary minerals which are only present in the brecciated rocks where they form a major part of the matrix. Quartz is present as fibrous grains which may be recrystallized. Calcite occasionally occurs as large patches which fill cavities in the rocks, but its common mode of occurrence is as fine grained aggregates.

4.3 Syenites in the Chipata area.

The Lunkhwakwa syenite is a cream, medium to fine grained, foliated pyroxene syenite whose principal minerals are alkali feldspar (80-90%), sodic pyroxene (5-15%), sphene (2-5%) and quartz (1%) with rare secondary amphibole and biotite. Accessory minerals are iron oxide, apatite and calcite.

The Bandawe syenite is a bluish-grey coarse to medium grained rock which shows both massive and foliated textures. Mineralogically, the syenite is composed of alkali feldspar (70-80%), nepheline (10-20%)diopside (3-5%), hornblende (5-10%), biotite (2-5%), sodalite (1-2%) and scapolite (1%). Accessory minerals include iron oxide, apatite and rare sphene.

4.3.1 Lunkhwakwa syenite.

Feldspar - the common feldspar is a vein type mesoperthite. Inversion of the mesoperthite to a tartan twinned microline is a common feature especially in the leucocratic rock type. This microcline is of the same grain size as the perthite and contains veinlets

Plate B. Textures of the Chipata syenites

Fig. (a) Foliated texture in the Lunkhwakwa syenite, crossed nicols, 20x magnification.

Fig. (b) Mesoperthitic structures in the Lunkhwakwa syenite, note development of albite as rims on the perthite, crossed nicols, 20x magnification.

Fig. (c) Massive texture in the Lunkhwakwa syenite, note occurrence of mafic minerals in clusters, crossed nicols, 20x magnification.

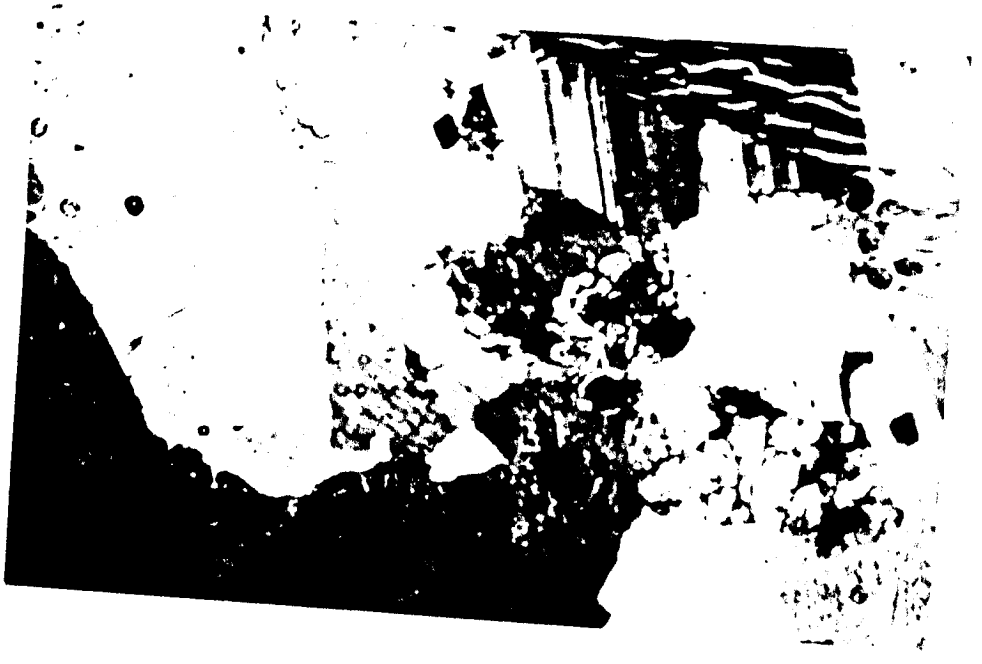

Fig. (d) Carlsbad twinning in mesoperthites in top left corner, amphibole overgrows pyroxene, crossed nicols, 20x magnification.

of an untwinned phase, probably albite. The perthite occurs as 2mm x 3mm grains having interlocking boundaries and shows a preferred orientation. Local polygonal textures are developed among the perthites. The plagioclase component of perthites occurs as irregular veins in some cases concentrated at the margins of the K-feldspar host suggesting an original zoning or advanced exsolution. Carlsbad twinning and a graphic intergrowth with quartz is observed in some of the perthites. In the leucocratic rock type, the perthites may assume an elongate shape and show wavy extinction due to recrystallization (Plate B, Figs a, b, d, e and g).

Plagioclase feldspar is represented by albite which has average sizes of .2mm x .3mm and .5mm x 1mm in the fine grained rocks and medium grain rocks respectively. It is an interstitial mineral which occurs interlocked together with microcline and quartz.

Pyroxene - the pyroxene is an aegirine-augite which ranges from a weakly pleochroic, pale green type in the leucocratic rocks to a strongly pleochroic, grass green variety in the melanocratic rocks. A single grain of a diopsidic pyroxene was seen in one sample. The pale green aegirine is rectangular and averages .5mm x 1mm and occurs as scattered grains. The grass green type is usually euhedral, averaging 1mm x 2mm in size and occurs as oriented evenly distributed clusters which may contain inclusions of iron oxide and sphene. (Plate B, Fig. c). Secondary amphibole and biotite are rare and replace pyroxene. The amphibole is an actinolite which occurs as pseudomorphs after pyroxene. Biotite is present as small laths intergrown with the amphibole.

Fig. (e) Foliated texture in the leucocratic syenite, note development of microcline from mesoperthite, crossed nicol's, 20x magnification. (Lunkhwakwa).

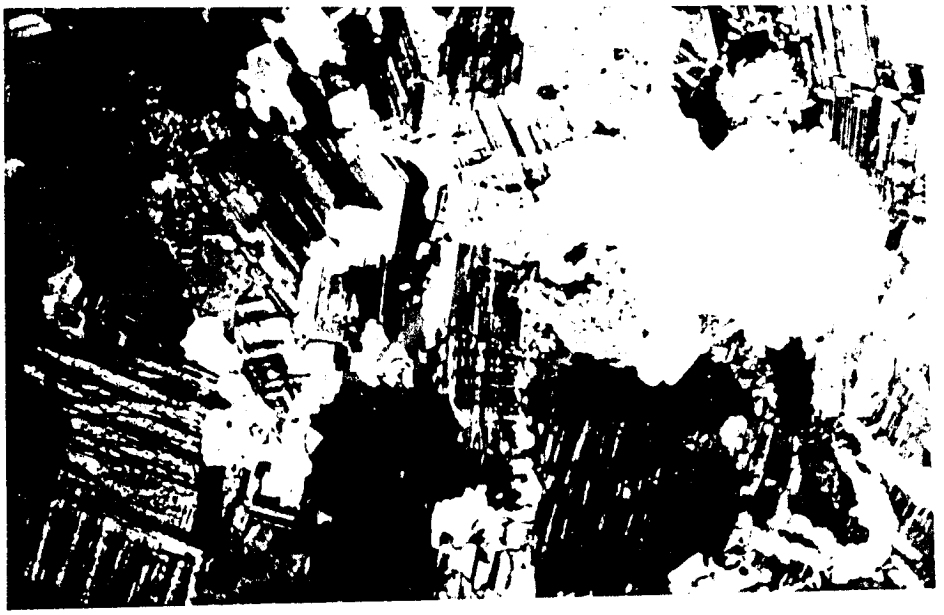

Fig. (d) Granulated alkali feldspar in the Lunkhwakwa syenite, crossed nicols, 20x magnification.

Sphene - the sphene is present as euhedral, grains .5mm x 1mm in size and is usually together with the pyroxene. It may also occur as lozenge shaped and anhedral grains some of which mantle iron oxide. Less common inclusions of sphene in feldspar are also present. The sphene, like the pyroxene and feldspar, shows a preferred orientation.

Quartz - In the leucocratic rock, the quartz is an interstitial mineral which occurs as elongate, .3mm x 1mm large grains and shows an undulatory extinction. The quartz may envelop some perthite grains. In the melanocratic rocks, quartz is present as smaller grains, interstitial to the other minerals and defines a granoblastic texture.

Iron oxide, apatite and zircon.

The iron oxide is present as anhedral interstitial grains and as an inclusion in pyroxene. Apatite is also an interstitial mineral but may also occur as an inclusion in the perthite. Zircon is rare and is present as an inclusion in pyroxene.

4.3.2 Bandawe syenite.

Feldspar - microperthitic alkali feldspar which occurs as 2mm x 2mm anhedral grains is the principal feldspar in the rock. In the coarse grained type, the microperthite may also occur as compositionally zoned euhedral grains up to 1cm x 1.5cm in size. Individual microperthite grains commonly have sutured grain margins which may also be granulated, the boundary between the grains exhibiting a granoblastic texture. Carlsbad twinning and a zoning defined by albitic cores and perthitic margins may also be present. Albite is usually present as small interstitial grains which define a granoblastic

Fig. (f) Oriented biotites interstitial to large (white) unexsolved alkali feldspar grains, crossed nicols, 20x magnification.

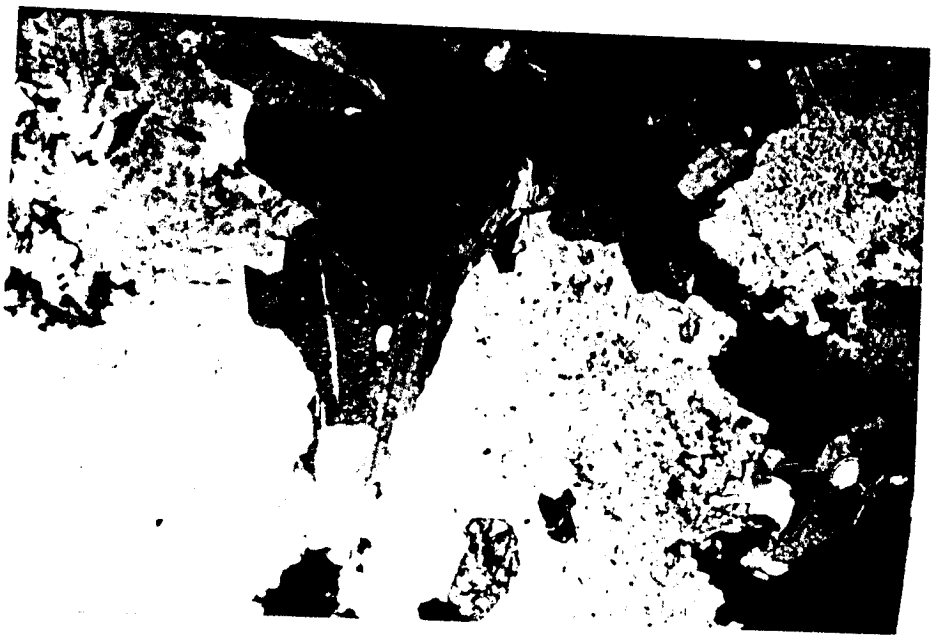

texture and is in most cases recrystallized. The albite may also be present as 1mm x 2mm grains, having straight grain boundaries.

Nepheline - In the massive rock, the nepheline occurs as 1mm x 2mm anhedral grains having sutured boundaries with the perthite and is always cloudy due to alteration.

In the foliated and more recrystallized rocks, the nepheline is present as interstitial .2mm x .3mm large grains which are always rimmed by scapolite.

Pyroxene - the pyroxene is a salite which occurs as evenly distributed .5mm x 1mm anhedral grains interstitial to the feldspar. Larger grains may also be present. These large grains have curving boundaries and may show simple twinning. The pyroxene is commonly overgrown by amphibole and biotite.

Amphibole - a hornblende which ranges from greenish - brown to deep brown is the main mafic mineral in the rock. It occurs as clear anhedral grains 1mm x 2mm in size and is interstitial to the feldspar grains. An actinolitic amphibole was observed in one sample. The hornblende is replaced by biotite.

Biotite - the biotite is deep brown and is present as 1mm x 1.5mm grains which may show a preferred orientation. The biotite may enclose iron oxide.

Sodalite and scapolite.
Sodalite occurs as anhedral, interstitial, elongate grains which may be altered containing tiny dust like inclusions. The sodalite is always rimmed by scapolite. The coronas of scapolite around nepheline and sodalite are a result of recrystallization (Plate B, Fig.1).

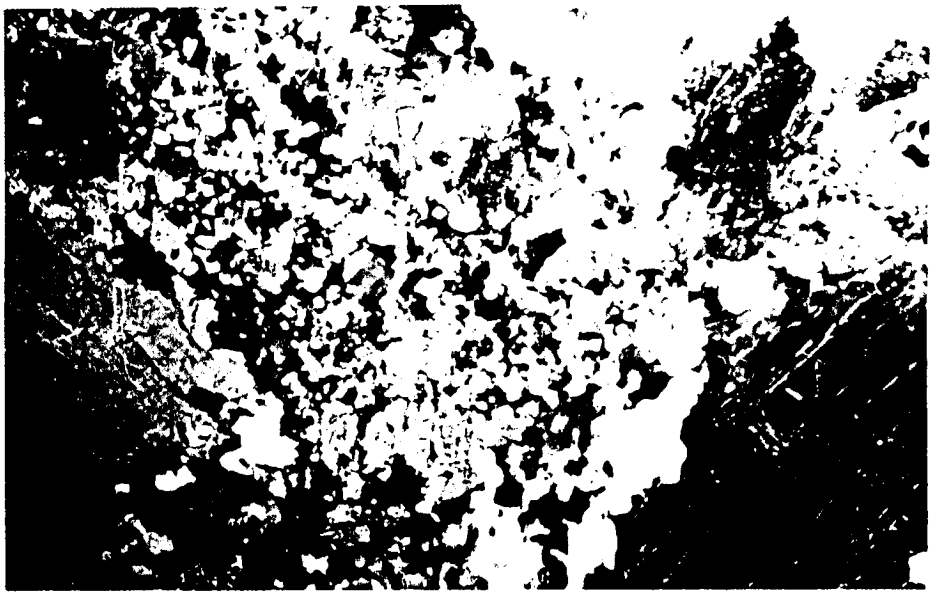

Fig. (h) Recrystallization texture in the Bandawe syenite, crossed nicols, 20x magnification.

Fig. (i) Recrystallization texture in the Bandawe syenite, note scapolite (pale grey) occuring as rims on sodalite (black), crossed nicols, 20x magnification.

Iron oxide, apatite and sphene - the three accessory minerals all occur as interstitial grains. The apatite may also occur as an inclusion in the feldspar.

4.4 Mivula Hill Syenite.

The rock ranges from a coarse to a fine grained, laminated bluish-grey amphibole-biotite syenite, which on the weathered surface is whitish and pitted owing to the preferrential weathering of nepheline and sodalite. The coarse grained variety typically consists of alkali feldspar crystals up to 1cm x 4cm large and 3mm x 5mm interstitial nephelines. Large nepheline grains are also present. The feldspars and nephelines of the finer grained variety has an average size of .2mm x 5mm. Feldspar phenocrysts up to 2mm x 5mm are also present. The syenite is locally cut by up to 1m thick discordant dark grey porphyritic dykes. The dykes have massive centres and weakly foliated margins which are sheared.

In thin section the rock has a predominantly panidiomorphic granular texture chiefly consisting of euhedral to subhedral alkali feldspar (60-79%) and nepheline (10-15%) with interstitial, nepheline, sodalite (3-5%), biotite (5-10%), amphibole (1-3%) and rare pyroxene (Plate c, Fig. a and b).

Alkali feldspar - The alkali feldspar usually shows Carlsbad twinning and poorly developed perthitic structures. Microline microperthites are occasionally observed in some rocks. The grains have interlocking boundaries and occasionally show compositional zoning.

Some grains show corroded boundaries against nepheline and sodalite. Albite is present in the fine grained rock types where it occurs as an interstitial mineral.

Plate C. Textures in the Mivula Hill syenite

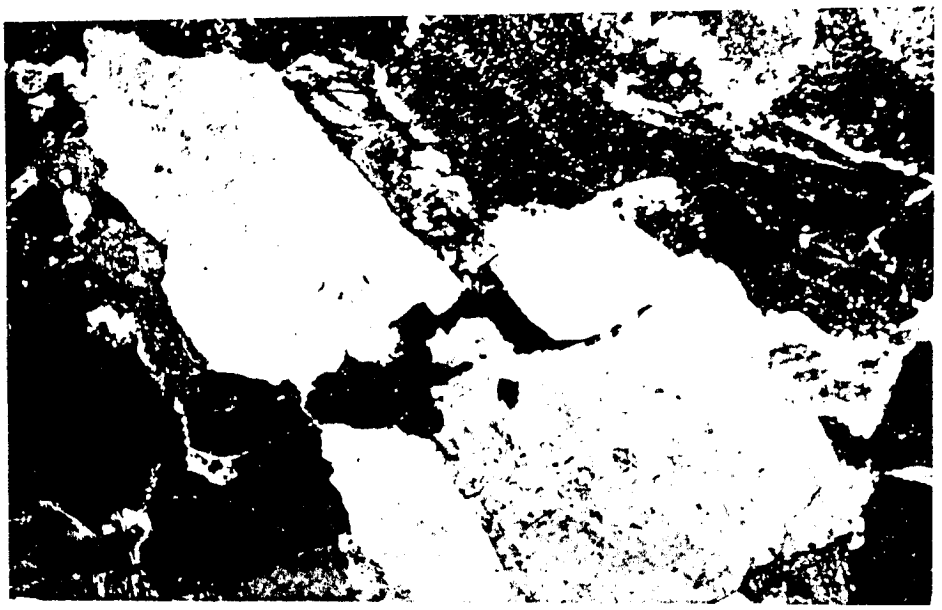

Fig. (a) Granitic textures in the syenite, note interstitial sodalite (black) and amphibole pale grey. Nepheline (upper right corner) is replaced by cancrinite (white), crossed nicols, 70x magnification.

Fig. (b) Granitic texture in the syenite, crossed nicols, 20x magnification.

The albite observed in the coarse grained varieties is commonly developed at alkali feldspar grain margins but interstitial grains are also present. The feldspars of the dyke rocks are phenocrystic, perthitic microclines and matrix microclines and albite which show corroded boundaries and granulation often occurring as cloudy grains due to alteration. The phenocrysts may contain inclusions of biotite and amphibole. The feldspar and nephelines in these rocks are usually separated by secondary brown micaceous material.

Nepheline - in the coarse grained varieties nepheline occurs both as a framework and an interstitial mineral. The framework nepheline is subhedral to euhedral, having interlocking boundaries with feldspar whereas the interstitial grains are anhedral and have corroded margins. In the fine grained varieties and in the dyke rocks, the nepheline has the same grain size as the feldspars and occurs as interlocking grains. In almost all cases the nephelines are altered to cancrinite especially at their margins, and often contain inclusions of amphibole laths.

Sodalite - the sodalite is interstitial and occurs as 0.5mm x 1mm anhedral grains containing highly birefringent inclusions of possibly cancrinite. In the coarse grained rocks, the sodalite grains may occasionally occur as larger grains. In general, the sodalite constitutes a greater proportion of the fine grained rocks than of the coarse ones. The sodalite like the nepheline, always has corroded margins and is often altered to cancrinite. The sodalite may enclose nepheline and amphibole.

Biotite, amphibole and pyroxene:
Biotite and amphibole represent the main mafic component of the rock. Biotite is usually present as small anhedral flakes, interstitial to the felsic minerals

and often evenly distributed in the rock. The biotite is more abundant in the fine grained varieties where it may make up to 90% of the mafic minerals. The biotite also occurs as overgrowths on amphibole, but this is rare. The coarser grained rocks may contain larger 4mm x 2mm anhedral biotites clustered together with amphibole. In the sheared dyke rocks it occurs as stretched out flakes along the shear zones. The amphibole, like the biotite, is more abundant in the finer grained rocks and in the dyke rocks than in the coarse varieties. The amphibole is a ferro-edenite which occurs as anhedral interstitial 2mm x 3-4mm large grains interstitial to the felsic minerals. Samples close to the roof of the intrusion have a pale green asbestiform amphibole (determined by Phillips and Drysdall (99)) as arfverdsonite which often shows a preferred orientation. In general, there are no significant textural differences between the amphibole rich syenites and the biotite rich ones.

Pyroxene was observed in two samples of the biotite syenite. It occurs as rare anhedral, interstitial grains .2mm x 1mm large and often replaced by calcite. It may also occur as an inclusion in alkali feldspar. The pyroxene like the amphibole has a sodic composition.

Accessory minerals, - Calcite is often recrystallized and occupies fractures and the intergranular space between feldspars and nepheline. Apatite is present as euhedral grains included in feldspars and as anhedral interstitial grains. Cancrinite occurs as a replacement of nepheline and sodalite while iron oxide and sphene are present as anhedral interstitial grains together with the mafics.

Fenite

The roof of the Mivula intrusion consists of a fenite which in handspecimen is a pink, coarse to medium grained granular rock consisting of 1 x 3cm pink alkali feldspar grains set in a fine grained matrix of alkali feldspar, amphibole and biotite.

In thin section the rock is seen to have a mortar texture in which large alkali feldspar and quartz grains are set in an intergranular matrix of alkali feldspar, aegirine augite, sodic amphibole and biotite with accessory amounts of sphene, apatite and iron oxide.

The large alkali feldspar grains are angular and show complete alteration to a clay mineral, probably sericite. This alkali feldspar is interpreted to be the original feldspar of the meta-sedimentary rock which was later altered to a clay mineral probably by the metasomatic fluids causing fenitisation. The matrix feldspar, which occurs as smaller tabular grains shows no signs of alteration and has developed perthitic structures similar to those observed in the main syenite. This second generation feldspar is interpreted to have been crystallized from the metasomatic fluids causing fenitisation.

The quartz which occurs as angular grains showing undulatory extinctiction due to recrystallization is also interpreted to be an original mineral of the meta-sediment.

The mafic minerals aegirine augite, sodic amphibole and biotite are all interstitial minerals which form irregular aggregate/s between the feldspar grains. The

minerals are all second generation, showing no signs of alteration or recrystallization and are therefore interpreted to have crystallized from the metasomatic fluids.

4.5 Discussion on the petrography of the syenites.

A significant result which emerges from this study is the presence of distinct mineralogical and textural differences among the syenites. Textures and mineral assemblages in the Sinda, Lunkhwakwa and Bandawe syenites indicate that the intrusions have been metamorphosed. In contrast, the Mivula Hill syenite is relatively unmetamorphosed.

4.5.1 Sinda syenites

From the petrographic description it is clear that there is a crystallization sequence which ranges from anhydrous mafic syenites characterized by pyroxenes and sodic plagioclase through hydrous felsic syenites whose main minerals are amphibole, biotite and alkali feldspar to leucocratic syenites devoid of mafics. This mineralogical variation and the presence of sphene in the more hydrous rocks indicates a relative increase in alkalis, volatiles and oxygen pressures with crystallization. (26). The petrographic data also shows that there is a progressive increase in the metamorphic character of the rocks from the northern Lusandwa intrusion to the southern intrusions. This observation is in agreement with field evidence which shows a progressive development of lenticular intrusions southwards, suggesting that there is relationship between igneous intrusion and metamorphism.

The apatite rocks are interpreted as cumulates which originated as a result of the accumulation of early

crystallized minerals, namely apatite, pyroxenes hornblende and alkali feldspar, hence their layered nature (Sililo pers. comm. 1984). The mafic nature of some of the cumulates, shown by their mineralogy, is consistent with the differentiation sequence of the mineral assemblages observed in the syenites but the presence of felsic cumulates suggests the operation of more than one mechanism of accumulation or the mixing of the mafic cumulates with syenitic material. The brecciation of some of the cumulates suggests that they cystallized at a different level and were emplaced into their present position at a later stage.

The occurrence of orthopyroxene in the mafic syenites is an indication that they have a charnockitic affinity and suggest that they were emplaced in a high-grade metamorphic environment.

Feldspar exsolution textures represented by microperthitic structures in the pyroxene syenite and mesoperthitic and patch perthitic structures in the amphibole syenite confirms the falling anorthite contents of the feldspars from the former to the latter and indicate a subsolidus interaction of the feldspars from the amphibole syenite with fluid phase (39).

The alkali feldspar in the syenites shows most of the features listed by Frasl (27), in Droop (28), as evidence of a high temperature igneous origin, namely a) large size, b) coarse perthitic exsolution structures c) oscillatory zoning outlined by exsolved plagioclase, d) crystallographically oriented euhedral plagioclase inclusions, e) simple twinning (Carlsbad law).

In addition, the perthite grains display similar features to those observed in high temperature igneous

alkali feldspars of metamorphosed syenites (28-30). These are: a) partial or complete inversion to microcline b) granulation at the margins and the development of recrystallized microcline and albite grains at their rims c) the presence of epidote inclusions in the plagioclase phase of the perthite. The epidote is believed to form during metamorphism to accomodate the Ca released as the plagioclase reverted to albite (28).

Thus it seems reasonable to conclude that the perthites were originally homogeneous hypersolvus alkali feldspars.

Albite in the syenites has two modes of origin. The first, which has already been discussed is an exsolution of the original monoclinic K-feldspar. This albite is always at the margin of nearly completely exsolved microcline perthites and is in optical continuity with them. The second albite occurs as discrete interstitial grains often together with quartz.

Alteration of the primary minerals is common in the syenites: calcite, epidote and colourless mica formed at the expense of plagioclase, uralitised grains of pyroxene indicate that the amphibole at least in part formed by replacement of clinopyroxene relicts of which are preserved. Actinolitic amphibole formed at the expense of both clinopyroxene and early amphibole. Biotite crystallized in two generations. Primary biotite in part formed at the expense of clinopyroxene and amphibole in the pyroxene syenites and amphibole syenites respectively. The second generation biotite formed at the expense of all the primary mafics. Iron oxide associated with this biotite may be a secondary product. The inverse relationship existing between sphene and iron oxide and their textural relationship indicate that some sphene has formed at the expense of iron oxide.

In summary, the petrographic features displayed by the syenites show a complex interaction between igneous and metamorphic processes. The syenites are magmatic rocks which were emplaced in an area of regional metamorphism, hence the occurrence of most of the intrusions as sills. Textures in the Lusandwa and Mayira intrusions suggest that their magmas were in a partly crystalline state on emplacement whilst the relatively homogeneous textures in the Pule, Seya and Tantha intrusions indicate that their magmas were largely in a liquid state.

The syenites were crystallized from a magma in which the early crystallizing phases were sodic plagioclase and pyroxene. Alkali feldspar was earlier than biotite and hornblende. Albite, microcline and quartz crystallized late.

4.5.2 Chipata syenites

A. Lunkhwakwa syenite.

A feature of petrographic interest in the Lunkhwakwa syenite is its foliated appearance. The rock is relatively homogeneous consisting of alkali feldspar, sodic pyroxene, sphene and quartz with accessory iron oxides and apatite.

The perthite is in some respects similar to that of the Sinda rocks exhibiting the same high temperature characteristics which are indicative of a hypersolvus crystallization. However the perthite shows some significant differences, namely a) it is not granulated, suggesting either limited post-igneous deformation or annealing, b) it has a uniform grain size suggesting a deep level of crystallization or high level emplacement of magma at near liquidus temperatures, c) complete inversion to microcline.

Albite and microcline are a result of both exsolution and late crystallization. The grains related to exsolution are always in optical continuity with the larger perthitic grains from which they exsolved. In contrast the late crystallized albite and microcline occur as discrete interstitial grains.

The presence of mesoperthitic microcline, discrete microcline and albite grains in the finer grained varieties is best explained either by the introduction of a fluid phase after the main crystallization or a reheating process leading to the conversion of K-feldspar to microcline and albite (31,32). The reheating event would probably have been caused by one of the many metamorphic events recorded from the area (11).

The foliation shown by all the constituent minerals of the rock is interpreted as a primary igneous feature having been attained either as a result of flow alignment of the magma during emplacement or during the late stages of consolidation of the magma. Post crystallization deformation shown by recrystallized quartz, albite and perthite was localized.

It is concluded that the Lunkhwakwa syenite was formed from a magmatic source crystallizing sodic pyroxene, alkali feldspar, sphene and quartz. The intrusion was affected by a severe "thermal event" after solidification but suffered little deformation.

The petrographic features described above are similar to those observed in the aegirine gneisses of central Malawi for which a sedimentary origin has been postulated (33).

B. Bandawe nepheline syenite.

Mineralogical and textural features of the nepheline

syenite show that the rock crystallized from an undersaturated magma. The principal phases crystallising were alkali feldspar, nepheline, clinopyroxene and sodalite. The rock was subjected to a metamorphic event during which amphibole, biotite and scapolite were formed.

The alkali feldspar is a microperthite, in contrast to that in both the Sinda and Lunkhwakwa syenite, and exhibits features consistent with a high temperature origin and a later metamorphic re-equilibration, shown by granulation and recrystallization of the grains.

The presence of phenocrystic microperthite grains again suggest a high level of intrusion. Nepheline and sodalite exhibit a characteristic metamorphic texture in which they are both rimmed by coronas of scapolite. The scapolite probably formed as a result of metamorphic reactions between nepheline, sodalite and feldspar.

The formation of amphibole and biotite at the expense of pyroxene are evident in the syenite. Amphibole and biotite are both typically greenish brown, to deep brown in contrast to the normal green varieties found in the other syenites. Brown amphiboles and biotites are only reported from metamorphic rocks (34), hence it is likely that the Bandawe syenite suffered metamorphism of higher grade than the Sinda syenites.

4.5.3 Mivula Hill syenite

The syenite displays a typical hypersolvus mineral assemblage in which the original single feldspar has exsolved into a perthite. The alkali feldspar is an early mineral followed by nepheline, amphibole and biotite, whereas sodalite and cancrinite crystallized late. This indicates that the magma was slightly undersaturated and had a low volatile content (35).

Albite is also a late mineral which was either exsolved from the microperthite or crystallized late. The mineral lamination observed in the syenite is in some respect similar to the layering in the kakortokites of the Ilimaussaq intrusion which has been attributed to the gravitative settling of the mineral grains during crystallization (36). The inverse relationship in the relative abundance of nepheline and sodalite in the two textural types is similar to that observed in the miaskitic nepheline syenite of the Red Hill syenitic complex (35). This reflects an increase in the water and chlorine contents with crystallization resulting in the formation of sodalite rather than nepheline (36-38).

4.5.4 Comparison of the petrographic features of the syenites.

The Sinda syenites are composed of mesoperthite, plagioclase, diopside, orthopyroxene, green hornblende, biotite and quartz with accessory iron oxide, sphene, apatite and zircon. The rocks also contain a metamorphic assemblage of green hornblende, biotite, epidote, calcite and probably albite and sphene. Both metamorphic and igneous textures are present in the rocks.

The Lunkhwakwa syenite has igneous and metamorphic textures and is mineralogically composed of mesoperthite, aegirine, sphene and quartz with late albite and microcline. Accessory minerals are iron oxide, calcite and zircon. The rare amphibole and biotite present is attributed to late magmatic effects rather than metamorphism.

The Bandawe syenite like the Sinda syenites also contains igneous and metamorphic textures, but is mineralogically different from the Sinda syenites in

being made up of microperthite, nepheline, sodalite and clinopyroxene. Metamorphic minerals are greenish brown calcic amphibole, brown biotite and scapolite. Accessories include apatite, iron oxide and zircon.

The Mivula hill syenite is petrographically similar to the Bandawe syenite in being composed of microperthite, nepheline and sodalite but differs in having primary biotite and amphibole as the mafic minerals. Accessory minerals are apatite, iron oxide, cancrinite, calcite and zircon. Metamorphic textures are absent. The similarities and differences in the petrography of the syenites are summarized to table 4.1.

Table 4.1 Comparison of the petrographic characteristics of the syenites

Sinda area	Chipata area	Mivula hill
Rock types: Biotite-pyroxene syenite and Biotite-amphibole syenite, charnockitic association. Textures: a) Igneous-granular with rare foliated. b) Metamorphic-granoblastic and foliated. Mineralogy: Primary. Feldspars: plagioclase and microperthite in pyroxene syenite and mesoperthite in amphibole syenite. Microcline only as a component of perthite. Pyroxene: orthorhombic pyroxene-(hypersthene), and a diopsidic clinopyroxene Amphibole: green amphibole of hornblende composition Biotites: green-palebrown Quartz. Accessory: Iron oxide, sphene, apatite zircon Metamorphic: hornblende, brown biotite, epidote ± sphene, calcite and colourless mica.	<u>Lunkhwakwa syenite.</u> Rock type: pyroxene syenite Textures: Igneous-foliated. local granoblastic. Mineralogy: Primary: Feldspars - mesoperthite, albite, microcline. Pyroxene: aegirine, sphene, quartz Accessory: Iron oxide, apatite Secondary: actinolite, biotite. <u>Bandawe syenite</u> Rock type: nepheline sodalite syenite. Textures: Igneous - rare granitic, metamorphic-massive, granoblastic and rare foliated. Mineralogy- Primary: Feldspars- microperthite and albite. nepheline, diopsidic pyroxene and sodalite, accessory; iron oxide, apatite and sphene. Metamorphic: brown amphiboles of pargasitic composition. deep brown biotite, scapolite	Rock type: nepheline sodalite syenite Textures: granitic Mineralogy: Feldspar - microperthite and albite. nepheline, sodalite biotite - greenish brown amphibole - sodi-calcic amphibole of edenitic composition. Pyroxene - rare aegirine. Accessory: iron oxide, calcite, sphene, cancrinite, apatite and zircon.

CHAPTER FIVE

Mineral Chemistry

1 Introduction

The discussion of the mineral chemistry of the syenites is based upon microprobe analysis of pyroxenes, amphiboles, biotites, sphene, iron oxides, feldspars and nephelines in eight rock samples. Table 5.1 lists the rock types and mineralogy of the analysed samples.

Table 5.1

Locality and Sample number	Rock type	Mineralogy
Sinda area		
FTS 87	pyroxene syenite	Opx,Cpx,Fsp,Bt,FeOx.
AP1	apatite rich cumulate	Fsp,Ap,Amph.FeOx.
AP3	apatite rich cumulate	Cpx,Ap,Amph.
FTS 13	amphibole syenite	Cpx, Amph,Fsp,Bt,Feox, Sph.
Chipata area		
FTC 9	pyroxene syenite	Fsp,Cpx,Sph,Feox.
FTC 65	nepheline syenite	Fsp,Cpx,Amph,Bt. FeOx,Neph,Sod,Scap.
Mivula Hill		
M3	nepheline syenite	Fsp,Bt,Amph.Neph, Feox,Sod.
M11	sodalite syenite	Fsp,Neph,Sod.Bt,Amph FeOx.

.2 Analytical procedure

The mineral analyses were carried out on a Jeol electron microprobe instrument. General operating conditions were 15KV accelerating potential and lnA sample current. Natural and synthetic standards of known composition were used. Matrix effects on the analysed minerals were corrected for by Z.A.F correction procedures.

In each thin section, an average of three grains of each mineral were analysed, the grains being probed at their centre and margin to check for chemical homogeneity. The exsolved phases in alkali feldspars and iron oxides were analysed separately.

.3 Chemistry.

Pyroxenes.

Chemical analyses of the pyroxenes from the syenites are presented in table 5.2 and are plotted in figures 5.1 - 5.5. The Fe^{3+} content is calculated on the basis of six oxygens and four cations, assuming complete site occupancy of both octahedral and tetrahedral sites in the pyroxene formula (44).

Figures 5.1 - 5.3 show the general chemical trends of the pyroxenes whereas figure 5.4 is a comparison of the pyroxene with common trends of pyroxenes of alkaline rocks (45). Figure 5.4 also shows that there is a general increase in the alkalinity of the pyroxenes from the Sinda syenites to the Chipata syenites suggesting that they may represent different stages of evolution of an alkaline magma.

Element variations in the more varied Sinda syenites are plotted in figure 5.5. Al,Ti,Mn,Fe and Na show a progressive increase from the cumulate rocks through the

Table 5.2 Chemical results of pyroxenes

sample No.	AP3			FTS 87			FTS 13		
	1	2	3	1(OPX)	2	3	1	2	3
SiO_2	52.756	51.617	52.871	52.677	52.832	51.882	52.184	49.635	52.240
Al_2O_3	1.152	1.832	1.152	.729	.964	1.820	1.145	3.020	0.874
TiO_2	0.086	-	-	0.303	0.142	0.440	-	0.464	0.358
FeO_1^*	7.060	7.753	7.079	21.247	8.258	8.120	9.917	11.619	10.314
MnO	.114	.220	.204	.988	.179	.115	.497	0.591	0.530
MgO	14.200	13.346	14.227	22.230	14.338	14.075	12.340	12.600	11.819
CaO	23.475	21.585	23.295	.732	21.906	21.860	22.120	18.909	22.377
Na_2O	.570	.482	1.012	-	-	.263	1.160	1.867	0.864
K_2O	-	-	-	-	-	-	-	0.299	-
Total	99.937	97.04	100.303	99.036	99.386	99.573	99.363	99.069	99.494
$Mg/Mg+Fe$	78.2	75.2	78.2	65.5	75.5	75.5	67.0	65.9	67.1
Structural formulae based on 6 oxygens atoms									
Si	1.960	1.977	1.950	1.978	1.978	1.950	1.958	1.866	1.973
Al	.051	.046	.050	.032	.043	.081	0.050	.133	.039
Ti	.002	-	-	.009	.004	.013	-	.013	.010
Fe^{3+}	.066	.074	.126	.012	.056	.026	.118	.243	.057
Fe^{2+}	.154	.175	.092	.655	.203	.229	.193	.123	.269
Mn	.004	.007	.006	.031	.005	.003	.016	.019	.017
Mg	.787	.760	.782	1.245	.800	.789	.691	.706	.666
Ca	.935	.887	.920	.029	.879	.884	.890	.762	.906
Na	.041	.074	.072	-	-	.019	.084	.136	.064
K	-	-	-	-	-	-	-	-	.032
Atomic %									
Ca	48.0	47.0	48.0	1.3	45.0	46.0	47.0	40.0	48.0
Mg	41.0	40.0	41.0	64.1	42.0	41.0	36.5	38.0	35.0
Fe	11.0	13.0	11.0	34.4	13.0	13.0	16.5	20.0	17.0

FeO_1^* - Total iron as Fe^{2+}

Table 5.2 contd.

sample No.	FTC 9			FTC 65	
	1	2	3	1	2
SiO_2	50.586	50.882	50.687	49.627	49.716
Al_2O_3	.923	.882	1.067	4.037	4.531
TiO_2	.184	-	-	1.516	1.352
FeO_1^*	20.024	18.825	20.186	9.574	8.664
MnO	.710	.633	.377	.569	.363
MgO	5.442	6.041	5.380	10.587	11.210
CaO	17.284	17.927	17.367	20.934	21.295
Na_2O	3.751	3.820	4.026	1.966	2.269
K_2O	-	-	-	-	-
Total	99.027	98.996	99.384	98.838	99.433
$Mg_{/Mg+Fe}$	32.6	36.4	32.2	66.7	69.9
structural formulae based on 6 oxygens atoms					
Si	1.962	1.960	1.957	1.893	1.879
Al	.042	.040	.050	.182	.202
Ti	.002	-	-	.043	.038
Fe^{3+}	.298	.325	.334	.003	.006
Fe^{2+}	.352	.282	.318	.302	.266
Mn	.023	.020	.012	.018	.012
Mg	.315	.347	.310	.602	.631
Ca	.719	.740	.719	.856	.862
Na	.282	.287	.302	.145	.166
K	-	-	-	-	-
Atomic %					
Ca	42.0	44.0	43.0	49.0	49.0
Mg	19.0	20.0	18.0	34.0	35.0
Fe	39.0	36.0	39.0	17.0	16.0

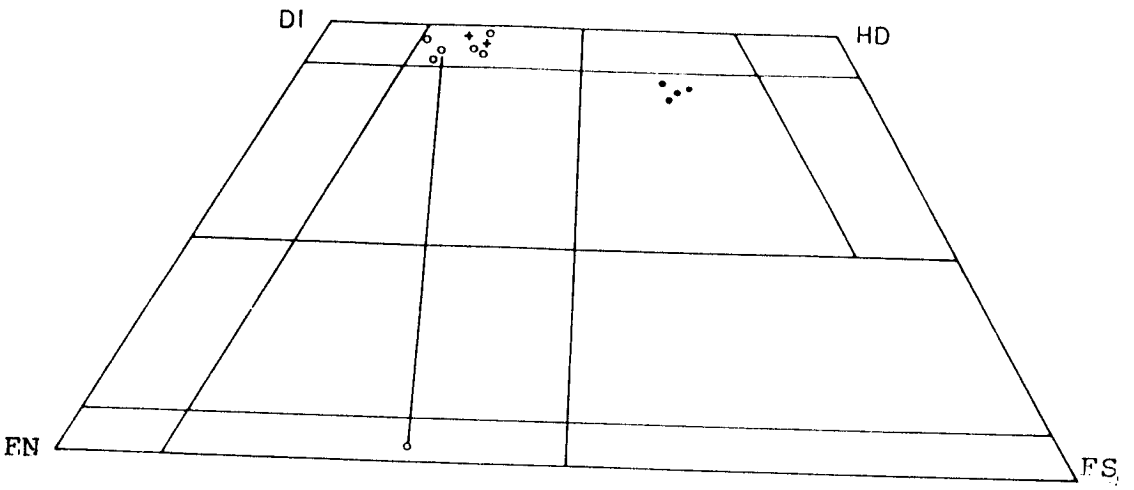

- ∘ Sinda syenites
- • Lunkhwakwa syenite
- + Bandawe syenite

Fig. 5.1 Di - Hd - En - Fs plot of the pyroxenes.

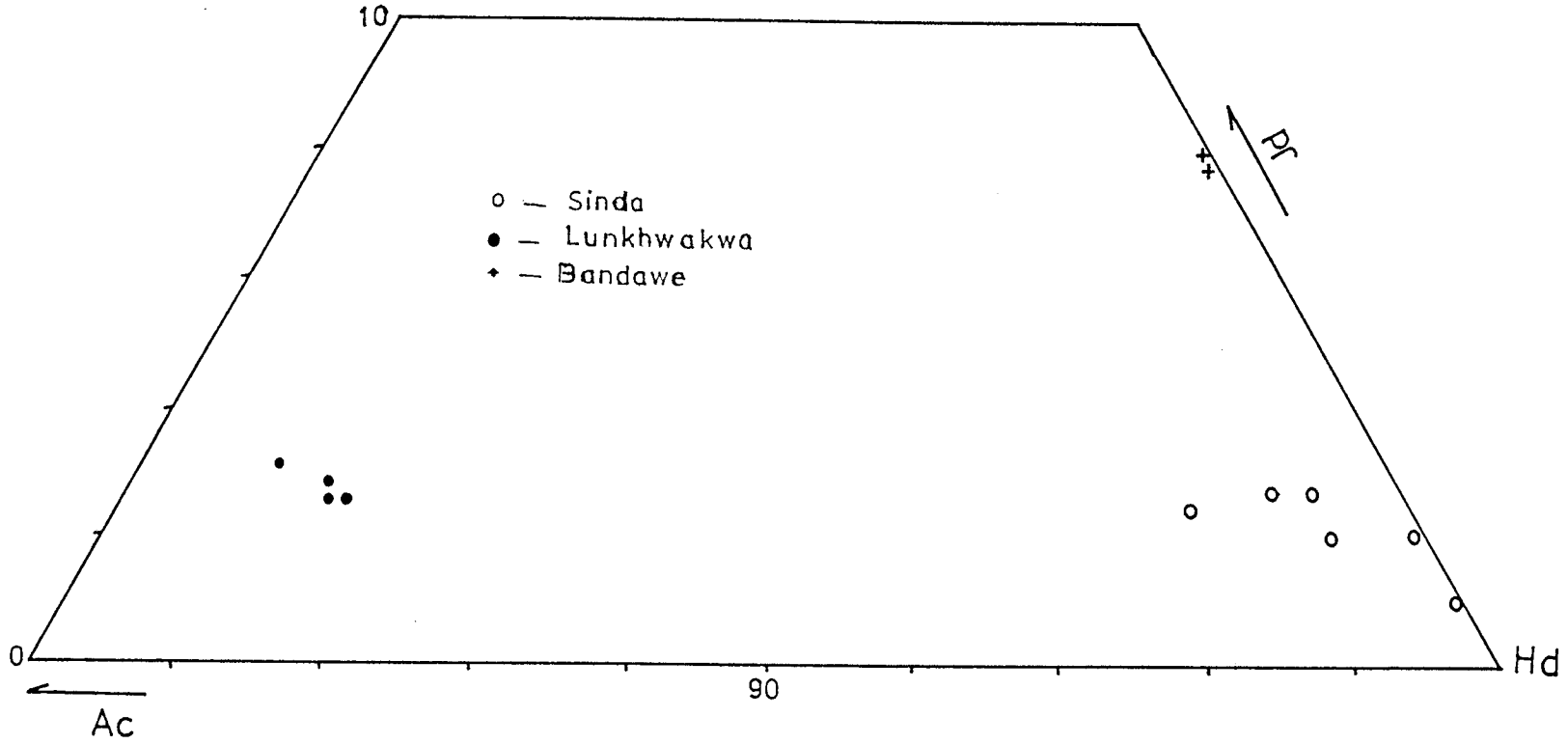

Fig. 5.2 Ac - Jd - Hd plot of the pyroxenes

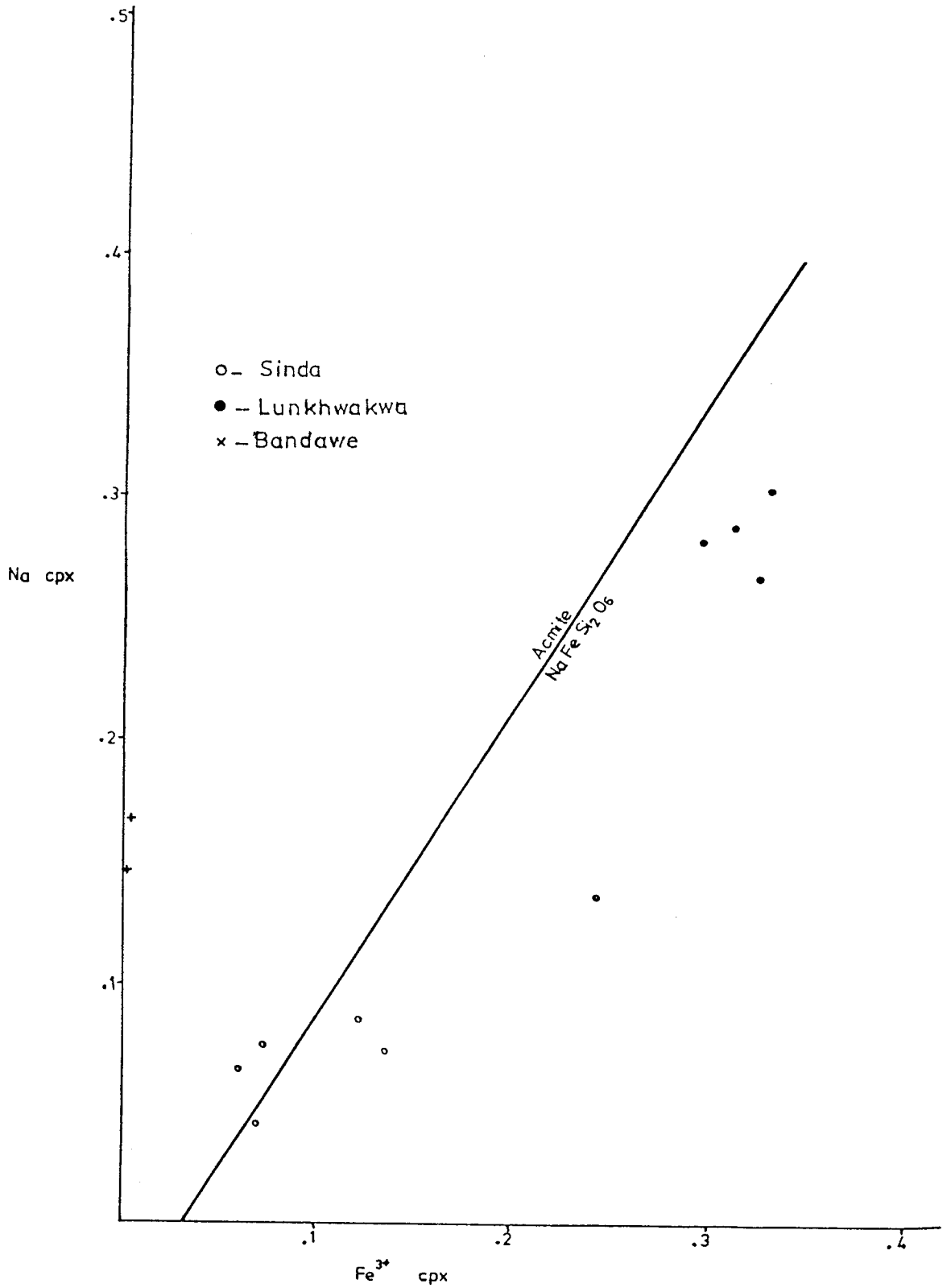
.5
.4
.3
.2
.1
Na cpx
o– Sinda
● – Lunkhwakwa
× – Bandawe
Acmite
NaFeSi2O6
.1
.2
.3
.4
Fe3+ cpx

3+

pyroxene syenite to the amphibole syenite whereas Mg and Ca show the opposite.

Clinopyroxenes from the Sinda syenites (Fig. 5.1) are sodian salites whereas that from the Bandawe syenite may be regarded as a titaniferous sodian salite (46). The clinopyroxene of the Lunkhwakwa syenite is an aegirine-augite in which there is an increasing replacement of Ca (Mg,Fe^{2+}) by $NaFe^{3+}$ (fig. 5.2 and 5.3). The chemical formula of the Lunkhwakwa syenite pyroxene shows a tendency toward acmite enrichment, an indication of high Fe^{3+}/Fe^{2+} ratios.

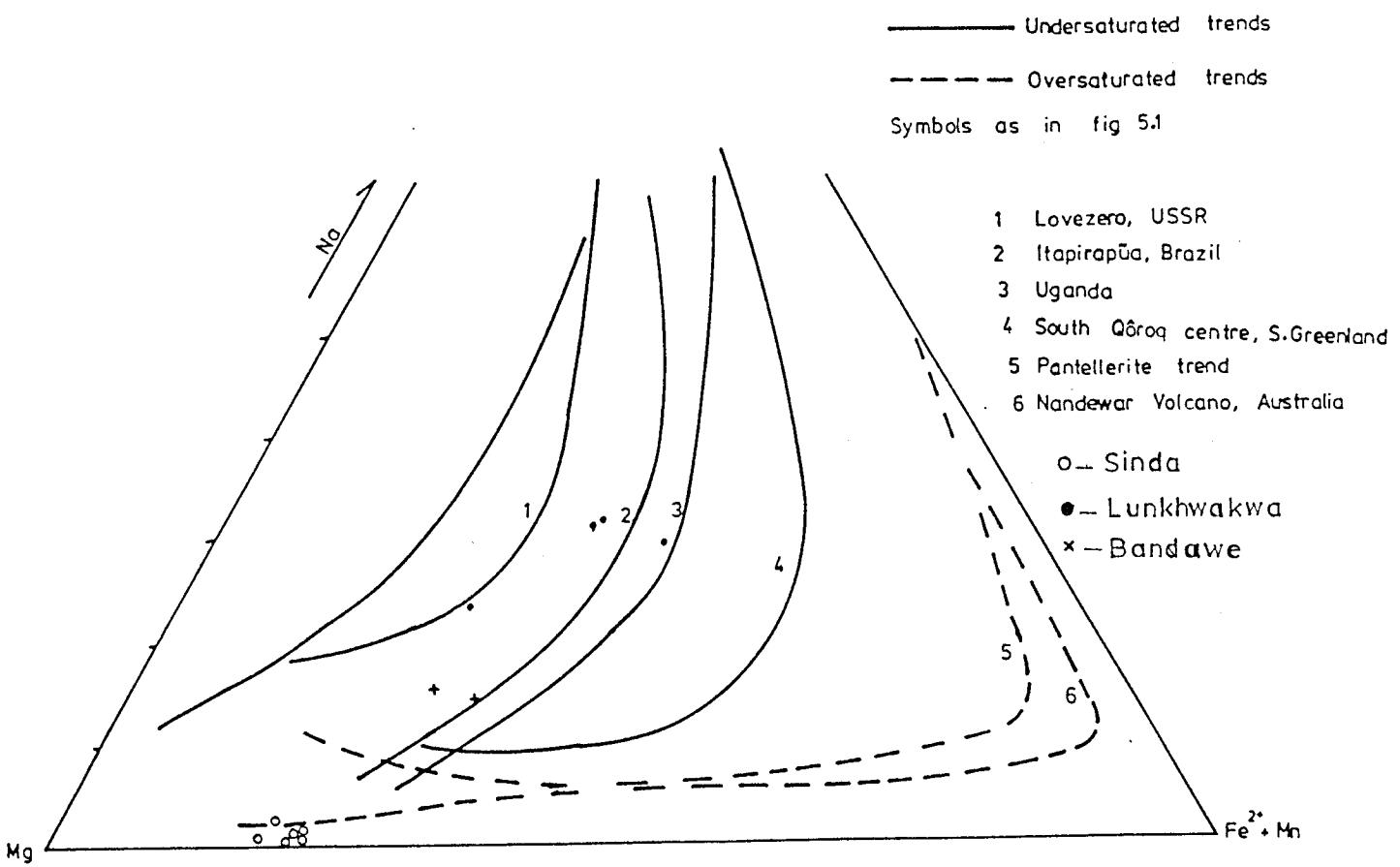

Fig. 5.4 Pyroxene from the syenites of the Eastern Province compared with published alkaline pyroxene trends

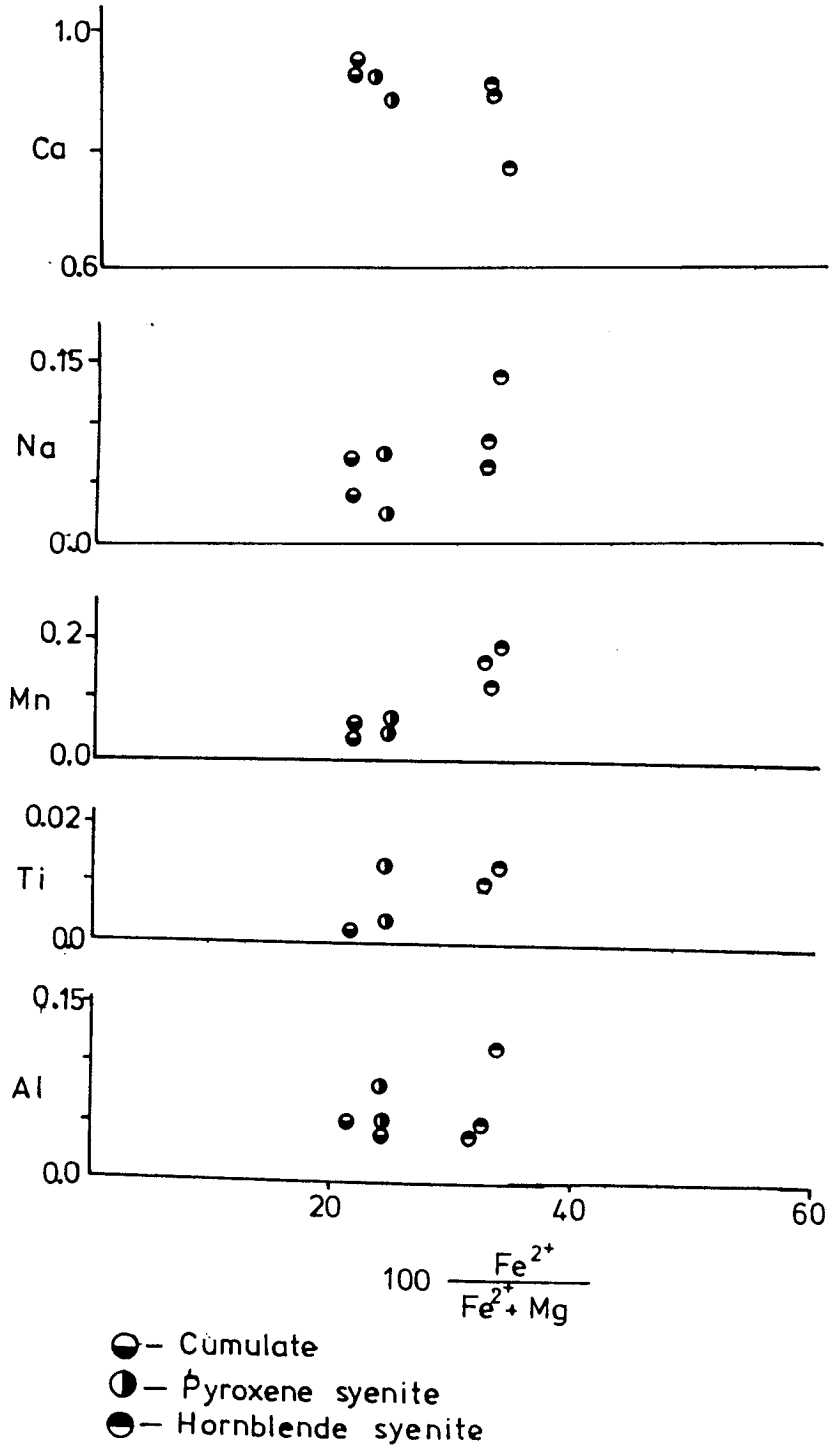

Fig. 5.5 Chemical variation in pyroxenes from the Sinda syenites.

Amphiboles.

Results and structural formulae (based on 23 oxygen atoms) of amphiboles are presented in table 5.3 and plotted as figures 5.6 and 5.7, the latter of which shows chemical variation in amphiboles from the Sinda syenites.

According to the classification of Leake (47), the amphiboles of the Sinda syenites are magnesio-hornblendes (AP3) and edenites (FTS13), (Fig. 5.6). The amphibole from the Bandawe syenite is a pargasite whereas that from the Mivula hill syenite is ferro-edenite. The second generation amphibole from the Lunkhwakwa syenite is a tremolite.

Biotites.

Chemical results and structural formulae (based on 22 oxygen atoms) of biotites from the syenites are presented in table 5.4 and plotted as figure 5.8.

Iron-Titanium oxides.

The oxide minerals from the Sinda and Bandawe syenites are inhomogeneous and contain lamellae of titanium rich phases. Oxides from the Lunkhwakwa and Mivula hill syenites, in contrast, are homogeneous. Chemical results of the oxide minerals are presented in table 5.5. The inhomogeneous phases in the oxide from the Sinda area may be divided into a host magnetite' phase, and an ilmenite phase. The magnetite phase has high Ti contents which are highest in the pyroxene syenite and lowest in the amphibole syenite. In the Bandawe syenite, the oxide phases can be divided into a spinel phase and an ilmenite phase. The spinel is a solid solution of $MgAl_2O_4$ and Fe_3O_4 and contains unusually high Si,Mn,Ca and Na. The ilmenite phase is also unusually high in Mn. A characteristic feature of the iron oxides in the Lunkhwakwa syenite is the absence of Ti. The oxide mineral in the Mivula syenite is an ilmenite.

Table 5.3 Chemical results of amphiboles

sample No.	AP 3			FTS 13			FTC 9
	1	2	3	1	2	3	1(Sec.)
SiO_2	45.799	48.804	49.180	45.751	46.241	45.286	52.125
Al_2O_3	7.970	5.912	5.975	7.335	7.185	7.370	.980
TiO_2	1.062	.902	1.000	1.284	1.351	.990	-
FeO^*_1	12.285	10.510	10.473	14.016	14.995	15.015	17.128
MnO	-	-	-	.237	.383	.324	.857
MgO	14.612	15.890	15.941	13.515	13.161	13.450	12.431
CaO	11.384	11.900	12.682	11.318	11.068	11.351	9.706
Na_2O	2.230	2.003	1.762	2.531	2.290	2.576	1.973
K_2O	.897	.514	.509	1.272	1.281	1.218	.403
Total	96.748	96.778	97.638	97.081	98.222	97.914	95.828
$Mg/Mg+Fe$	67.9	72.9	73.0	63.2	61.0	61.5	56.4
structural formulae based on 23 oxygen atoms							
Si	6.161	7.134	7.142	6.848	6.815	6.720	7.802
Al	1.389	1.018	1.042	1.152	1.248	1.289	.173
Ti	.118	.100	.110	.142	.149	.111	-
Fe_t	1.518	1.286	1.273	1.755	1.848	1.864	2.143
Mn	-	-	-	.030	.047	.041	.109
Mg	3.214	3.462	3.450	3.016	2.891	2.976	2.773
Ca	1.833	1.864	1.973	1.815	1.748	1.805	1.557
Na	.638	.568	.496	.978	.655	.741	.372
K	.170	.097	.094	.243	.241	.230	.077

Table 5.3 contd.

Sample No.	FTC 65			M 11		
	1	2	3	1	2	3
SiO_2	39.452	39.618	39.864	38.394	37.830	37.998
Al_2O_3	11.780	11.467	10.769	11.635	11.294	11.960
TiO_2	3.868	3.804	3.393	.491	.925	.599
FeO*	16.915	15.679	15.669	27.572	27.041	26.134
MnO	.680	. 77	.591	.953	.681	.731
MgO	9.600	10.028	10.417	3.599	3.771	3.973
CaO	10.905	10.696	10.629	7.738	8.069	7.724
Na_2O	3.198	3.054	3.864	4.368	4.250	3.967
K_2O	1.852	1.905	1.993	2.484	2.344	2.471
Total	98.275	97.024	97.484	97.360	96.246	95.605
Mg/ Mg+Fe	50.3	53.3	54.2	18.9	19.9	21.3
structural formula based on 23 oxygen atoms						
Si	6.013	6.085	6.142	6.243	6.213	6.236
Al	2.117	2.076	1.955	2.230	2.186	2.314
Ti	.444	.440	.416	.06	.114	.074
Fe	2.157	2.014	2.018	3.749	3.714	3.587
Mn	.088	.088	.077	.131	.095	.102
Mg	2.182	2.296	2.392	.872	.923	.972
Ca	1.781	1.760	1.755	1.348	1.420	1.358
Na	.946	.909	1.154	1.372	1.353	1.262
K	.360	.374	.392	.515	.491	.517

Table 5.4 Chemical results of biotites.

sample No.	AP3	FTS 87		FTS 13		
	1	1	2	1	2	3
SiO_2	37.752	39.171	38.893	39.496	39.588	39.721
Al_2O_3	12.518	12.523	12.510	12.146	11.826	11.978
TiO_2	3.928	4.288	4.397	-	-	1.817
FeO*	14.299	10.859	11.352	12.520	12.430	12.138
MnO	-	.103	.143	-	-	-
MgO	15.678	17.917	17.656	17.638	17.892	18.212
CaO	-	-	-	-	-	-
Na_2O	-	-	-	-	-	-
K_2O	8.988	9.751	9.838	9.960	9.874	9.657
Total	94.548	95.111	95.743	93.979	93.762	94.538
Mg/ Mg+Fe	52.3	62.3	60.9	58.5	59.0	60.0

Structural formula based on 22 oxygen atoms.

Si	5.734	5.777	5.754	6.032	6.052	5.948
Al	2.241	2.177	2.182	2.187	2.131	2.115
Ti	.449	.473	.490	-	-	.205
Fe	1.817	1.339	1.404	1.599	1.589	1.520
Mn	-	.013	.018	-	-	-
Mg	3.550	3.939	3.894	4.016	4.077	4.066
Ca	-	-	-	-	-	-
Na	-	-	-	-	-	-
K	1.741	1.835	1.857	1.941	1.926	1.845

Table 5.4 contd.

sample no.	FTC9	FTC 65			
	1	1	2		
SiO_2	35.585	35.707	34.810	35.294	33.201	34.891
Al_2O_3	10.270	14.476	14.500	13.241	16.742	14.926
TiO_2	2.458	5.690	5.726	3.986	3.240	3.713
FeO^*	19.939	17.428	18.068	28.882	30.039	28.937
MnO	.398	.614	.567	.462	.289	.303
MgO	11.190	11.348	11.257	5.370	4.168	4.438
CaO	-	.227	-	.008	-	.048
Na_2O	.928	-	-	.221	.344	.191
K_2O	5.671	9.164	9.626	9.306	9.391	9.660
Total	86.658	95.143	94.664	97.100	97.611	97.105
Mg/ Mg+Fe	35.9	39.4	38.4	15.7	12.2	13.3

Structural formulae based on 22 oxygen atoms.

Si	5.955	5.453	5.376	5.593	5.260	5.513
Al	2.026	2.606	2.639	2.473	3.127	2.780
Ti	.309	.653	.666	.475	.386	.441
Fe	2.790	2.227	2.333	3.828	3.980	3.824
Mn	.056	.080	.074	.062	.039	.041
Mg	2.791	1.584	2.650	1.268	.984	1.045
Ca	-	.037	-	.001	-	.008
Na	.301	-	-	.068	.106	.058
K	1.211	1.787	2.591	1.881	1.898	1.947

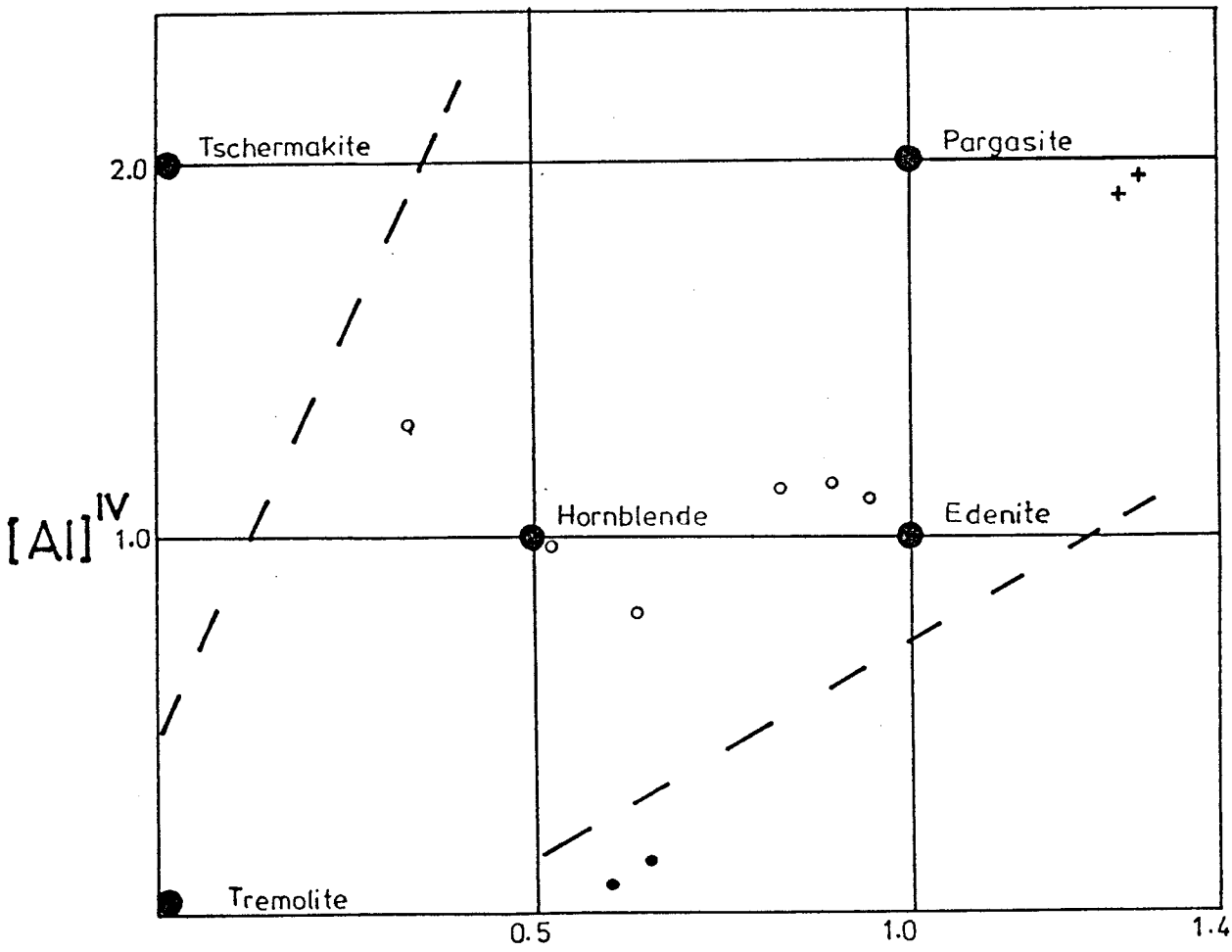

Fig. 5.6 Classification of the calcic amphiboles from the syenites (after Deer et al, 1962).

o–Sinda o– Lunkhwakwa + — Bandawe

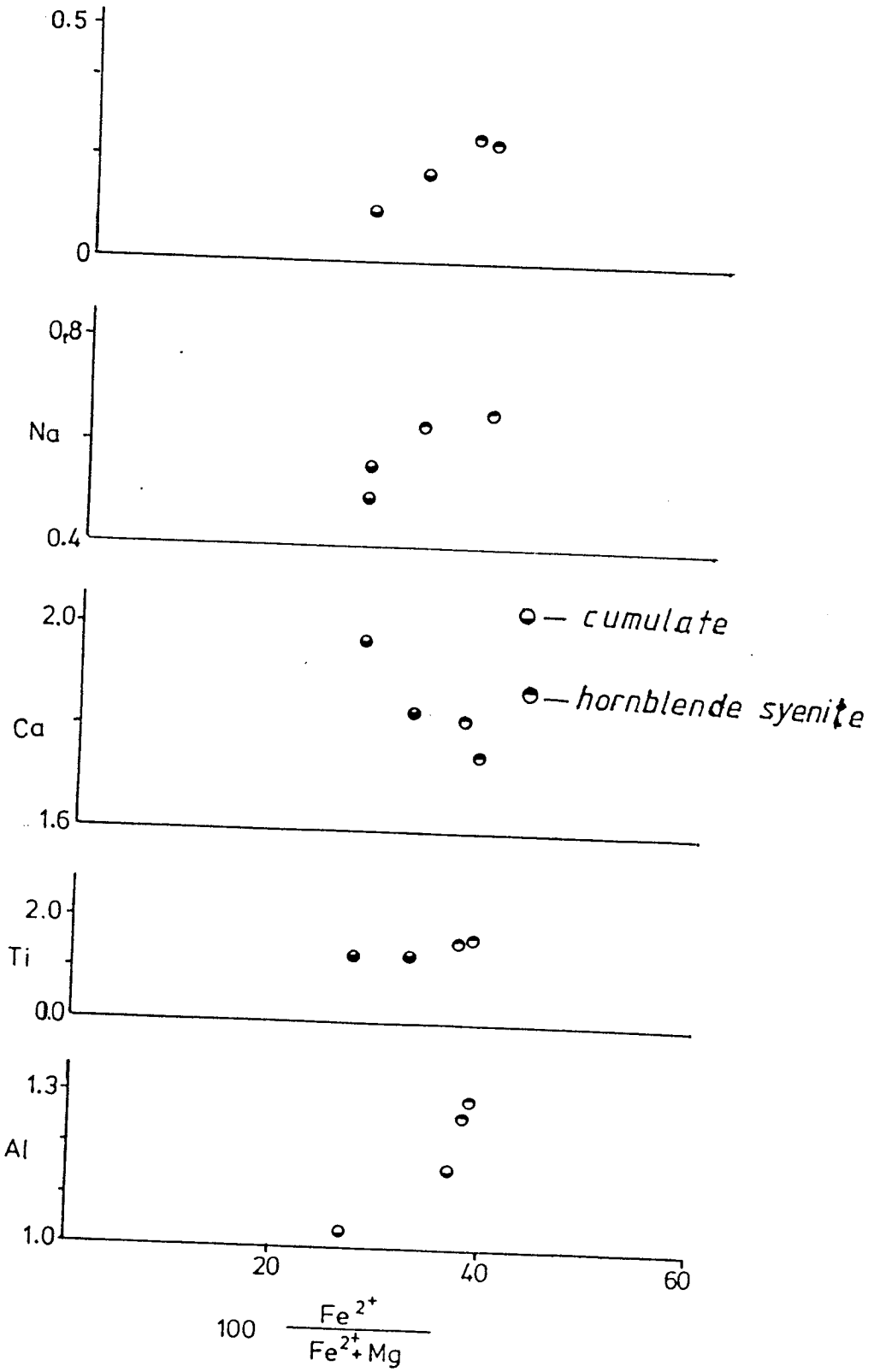

Fig. 5.7 Chemical variation in amphiboles from

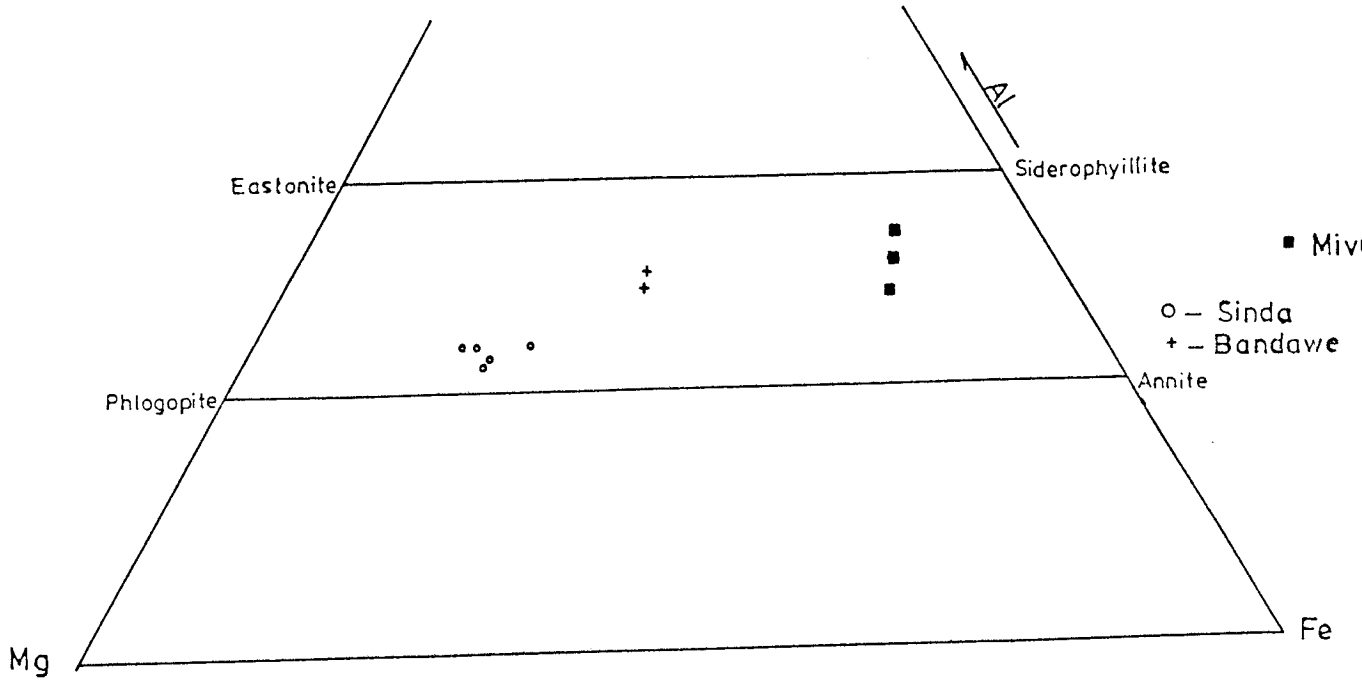

Fig. 5.8 Biotites from the syenites plotted on an Al-Mg-Fe diagram (after Deer et al, 1966).

Table 5.5 Chemical results of iron oxides and sphene.

Sample No.	AP 3		FTS 87					
	1		1	2		3		
SiO_2	.362	.468	.307	.262	-	.402	.312	.345
Al_2O_3	-	-	-	-	-	-	-	-
TiO_2	42.598	12.144	39.051	22.274	10.955	35.111	33.371	46.500
FeO*	49.415	78.484	56.771	68.448	79.484	59.698	59.939	50.015
MnO	.543	-	.383	.417	-	.395	-	.934
MgO	-	-	.442	.444	-	.416	.760	.753
CaO	-	-	-	-	-	-	-	-
Sum	93.579	92.657	97.209	92.324	91.216	96.034	95.051	98.666

Structural formulae based non 16 oxygen atoms.

Si	.058	.075	.016	.042	-	.062	.049	.051
Al	-	-	-	-	-	-	-	-
Ti	5.151	1.450	1.503	2.664	1.323	4.079	3.930	5.307
Fe^{3+}	-	4.886	1.013	2.590	5.346	-	-	-
Fe^{2+}	6.646	5.537	1.417	6.540	5.334	7.713	7.849	6.349
Mn	.065	-	.017	.560	-	.051	.120	.063
Mg	-	-	.034	.105	-	.096	.170	.202
Ca	-	-	-	-	-	-	-	-

Table 5.5 contd.

FTC 65

		1			2			3
SiO_2	.331	.224	-	.401	.429	2.008	.405	-
Al_2O_3	-	57.940	-	-	-	55.316	-	-
TiO_2	-	-	58.827	.267	51.042	.720	-	52.100
FeO*	87.209	25.178	33.730	90.855	36.213	24.000	92.775	38.513
MnO	-	2.266	12.838	-	11.036	1.664	-	9.639
MgO	-	6.136	-	-	-	6.184	-	.343
CaO	-	-	-	-	.296	-	-	-
Na_2O	.774	5.366	-	-	-	6.514	-	-
Sum	90.519	97.482	97.868	92.076	99.620	96.949	94.302	101.015

Structural formulae based on 16 oxygen atoms

Si	.052	.029	-	.063	.065	.217	.062	-
Al	-	7.373	-	-	-	7.044	-	-
Ti	-	-	5.932	.031	5.847	.059	-	5.872
Fe^{3+}	8.140	1.706	-	7.950	-	1.767	7.886	-
Fe^{2+}	3.568	.568	4.379	7.647	4.613	.401	11.933	4.828
Mn	-	.207	1.687	-	1.424	.152	-	1.224
Mg	-	.987	-	-	-	996	-	.976
Ca	-	-	-	-	.048	-	-	-
Na	.236	1.123	-	-	-	1.365	-	-

Table 5.5 cont'd

Sample No.	FTC 9			FTS 13		
	1		2	1		2
SiO_2	1.092	.262	.995	. 300	.390	.278
Al_2O_3	-	-	-	-	-	-
TiO_2	-	-	-	9.784	49.869	-
FeO*	87.538	91.152	87.465	81.885	45.514	91.102
MnO	-	-	-	-	-	-
Sum	89.511	92.019	89.084	92.293	99.552	92.029
STRUCTURAL FORMULA BASED ON 16 OXYGEN ATOMS						
Si	.176	.041	.164	.047	.060	.043
Al	-	-	-	-	-	-
Ti	-	-	-	1.160	5.793	-
Fe^{3+}	7.660	7.904	7.664	5.574	-	7.922
Fe^{2+}	4.158	4.062	4.182	5.224	5.880	4.030
Mn	-	-	-	-	.470	-

Table 5.5 contd.

sample No.	M11		FTS13	FTC 9		M 3	
	1	2	1	1	2	1	2
SiO_2	.302	.298	28.947	28.993	28.569	30.130	29.740
Al_2O_3	-	-	1.905	.949	.793	1.100	.912
TiO_2	51.156	50.236	32.113	34.288	35.093	36.353	36.842
FeO*	45.876	45.255	2.726	3.021	2.503	1.435	1.917
MnO	2.402	3.047	-	-	-	-	-
MgO	-	-	-	-	-	-	-
CaO	-	-	26.052	25.623	25.445	27.325	27.209
Sum	100.383	99.905	93.898	92.889	92.997	96.979	96.779
structural formulae based on 12 oxygen atoms							
Si	.041	.041	2.467	2.464	2.428	2.445	2.421
Al	-	-	.191	.095	.079	.105	.088
Ti	5.189	5.152	2.058	2.192	2.243	2.219	2.256
Fe^{3+}	-	-	-	-	-	-	-
Fe^{2+}	5.175	5.161	.194	.215	.184	.098	.130
Mn	.274	.352	-	-	-	-	-
Mg	-	-	-	-	-	-	-
Ca	-	-	2.379	2.333	2.317	2.376	2.373

Table 5.5 contd.

Structural formulae for iron oxides are based on 16 oxygen atoms whilst the forumale for sphene are based on 12 oxygens. The exsolved phases of single iron oxide grains have been analysed separately.

Chemical analyses of sphene from the Sinda, Lunkhwakwa and Mivula syenites are presented together with the iron oxide results. The only comment on the results on sphene is that they all have a low total oxide value, which most probably indicates unanalysed elements such as the REE, Zr and Nb.

Feldspar, Nepheline and Scapolite.
Chemical results of feldspars, nephelines and scapolite from the syenites are presented in table 5.6. The feldspars are calculated on the basis of 16 oxygen atoms whilst the nepheline formula is based on 8 oxygens.

The exsolved phases of the feldspars are plotted on an An-Ab-Or diagram shown as figure 5.9. A plagioclase feldspar from the pyroxene syenite of the Sinda area whose anorthite content was determined optically is also plotted on the diagram in order to show the trend in the feldspars of the Sinda syenites.

5.4 Discussion on the mineral chemistry of the syenites.
The chemical results presented in the previous section clearly indicate that there are significant differences in the chemistry of the syenites. Furthermore, the chemical composition of some of the minerals in some of the intrusions are atypical of igneous minerals and they probably reflect the metamorphic character of these intrusions.

5.4.1 Sinda syenites

The general chemical trends of the minerals from the apatite rich cumulate rocks and pyroxene syenite to the amphibole syenites (i.e. increasing Al,Na,K,Fe and

Table 5.6 Chemical results of feldspars, nepheline and scapolite

sample No.	AP 1		FTS 87					FTS 13	
	1	2	1	2		3		1	
SiO_2	62.885	63.181	64.497	64.123	63.222	63.051	63.020	64.632	65.504
Al_2O_3	18.983	19.338	19.665	19.095	22.562	22.926	18.482	18.730	20.237
CaO	-	-	1.180	.848	3.836	4.076	-	-	1.392
Na_2O	1.694	1.227	6.660	3.138	9.088	8.818	1.539	1.582	10.027
K_2O	13.377	13.894	6.503	10.368	.118	.262	13.156	14.600	1.705
BaO	2.524	1.989	.716	.896	-	-	1.105	.968	-
Sum	99.986	99.903	99.468	98.586	98.840	98.140	97.310	101.422	99.068
Structural formulae based on 16 oxygen atoms									
Si	5.886	5.889	5.858	5.929	5.640	5.600	5.612	5.940	5.848
Al	2.095	2.125	2.105	2.081	2.373	2.400	2.364	2.029	2.130
Ca	-	-	.115	.084	.367	.388	-	-	.065
Na	.299	.222	1.173	.564	1.572	1.519	.282	.282	1.736
K	1.598	1.652	.754	1.223	.013	.030	1.586	1.712	.194
Ba	.098	.072	.026	.032	-	-	.041	.035	-
An	-	-	5.60	4.40	18.80	20.00	-	-	6.4
Ab	15.00	11.40	56.72	29.60	80.50	78.40	14.80	14.00	84.00
Or	80.30	84.80	36.72	64.30	.70	1.50	83.10	84.00	9.40
Ca	4.70	3.80	1.26	1.70		-	2.10	2.00	-

Table 5.6 contd.

sample No	FTS 13				FTC 9			
	2		3		1		2	
SiO_2	64.782	63.119	64.957	62.902	63.182	67.752	67.862	63.170
Al_2O_3	20.889	17.857	21.502	18.081	18.133	19.311	19.386	18.070
CaO	2.191	-	2.452	-	-	.204	-	-
Na_2O	10.866	-	10.472	.852	.878	12.811	11.364	.042
K_2O	.175	14.866	.212	14.897	15.556	.207	-	14.626
BaO	-	.954	-	-	.501	-	-	.468
Sum	99.111	97.615	99.827	97.324	98.475	100.104	98.910	98.376
Si	5.771	5.998	5.741	5.973	5.942	5.951	5.989	5.958
Al	2.193	2.000	2.240	2.024	2.010	1.999	2.017	2.009
Ca	.209	-	.232	-	-	.019	-	-
Na	1.877	-	1.795	.157	.160	2.075	1.945	.191
K	.020	1.802	.024	1.802	1.866	.023	-	1.760
Ba		.036	-	-	.035	-	-	.033
An	9.9	-	11.3	-	-	.9	-	-
Ab	89.1	-	87.5	8.0	7.8	98.0	100.0	9.6
Or	1.0	98.0	1.2	92.0	90.5	1.1	-	88.7
Ca	-	2.0	-	-	1.7	-	-	1.7

Table 5.6 contd.

sample No	FTC 9		FTC 65					nepheline	
	3		1		2		3	4	5
SiO_2	68.159	63.328	63.840	64.474	65.261	63.733	63.043	43.761	45.010
Al_2O_3	19.227	18.284	18.963	19.874	20.071	18.878	19.246	33.413	33.533
CaO	-	-	-	.853	.994	.278	.608	.992	1.037
Na_2O	11.934	.805	2.836	5.913	7.962	2.899	3.480	15.818	16.043
K_2O	-	14.973	11.845	6.205	4.904	12.078	9.076	4.865	4.431
BaO	-	.386	.490	.393	.395	.455	.501	-	-
Sum	99.534	97.776	98.332	97.938	100.285	98.390	97.988	98.977	100.431
Si	5.989	5.953	5.918	5.877	5.833	5.915	5.866	2.107	2.131
Al	1.991	2.206	2.072	2.136	2.114	2.065	2.11	1.896	1.872
Ca	-	-	-	.083	.095	.028	.061	.051	.053
Na	2.033	.147	.510	1.045	1.380	.522	.628	1.477	1.473
K	-	1.796	1.401	.722	.559	1.431	1.298	.299	.268
Ba		.027	.034	.027	.027	.032	.035	-	-
An	-	-	-	4.4	4.6	1.4	3.0	Ne 70.0	69.1
Ab	100	7.5	26.2	55.7	67.0	25.9	31.0	Ks 14.3	12.6
Or	-	91.2	72.0	38.5	27.0	71.1	64.2	Qz 15.7	18.3
Cs	-	1.3	1.7	1.4	1.3	1.6	1.7		

Table 5.6 contd.

Sample No.	M 11					nepheline		
	1		2		3	4	5	6
SiO_2	64.714	64.007	63.835	64.293	69.751	43.883	43.668	44.139
Al_2O_3	18.445	19.766	18.695	18.362	19.399	33.779	32.707	34.340
TiO_2	-	.039	-	-	.116	-	-	-
FeO*	-	.059	.104	.034	-	.051	1.320	.048
MnO	-	-	-	-	.042	.046	.034	.068
gO	-	.183	-	-	-	-	-	-
CaO	-	-	-	-	.005	-	-	-
Na_2O	.543	10.092	.480	.279	11.727	16.562	16.374	16.504
K_2O	15.707	3.040	15.720	15.688	.023	6.195	5.887	6.057
BaO	1.149	.386	1.072	1.084	-	-	-	-
Sum	100.559	102.542	99.907	99.741	101.064	100.858	99.989	101.299
Si	5.984	5.962	5.948	5.988	6.020	2.098	2.105	2.089
Al	2.010	2.013	2.053	2.016	1.973	1.899	1.859	1.916
Ti	-	.003	-	-	.008	-	-	-
Fe	-	.004	.008	.003	-	.002	.053	.002
Mn	-	-	-	-	.003	.002	.001	.003
Mg	-	.024	-	-	-	-	-	-
Ca	-	-	-	-	-	-	-	-
Na	.097	1.691	.087	.050	1.962	1.532	1.531	1.515
K	1.853	.335	1.869	1.864	.003	.377	.362	.366
Ba	.042	.012	.039	.040	-	-	-	-

Table 5.6 contd.

Sample No	FTC 65 (scapolite)		
SiO_2	55.208	55.123	55.658
Al_2O_3	23.477	23.354	23.124
CaO	8.587	8.235	7.848
Na_2O	9.010	9.116	9.218
K_2O	.687	.734	.955
Sum	97.191	99.069	96.803
structural formulae based on 24 oxygen atoms			
Si	7.773	7.905	7.953
Al	3.896	3.948	3.895
Ti	-	-	-
Fe	-	-	-
Mn	-	-	-
Mg	-	-	-
Ca	1.295	1.265	1.202
Na	2.460	2.535	2.554
K	.123	.134	.174
Me%	32.2	32.2	30.5

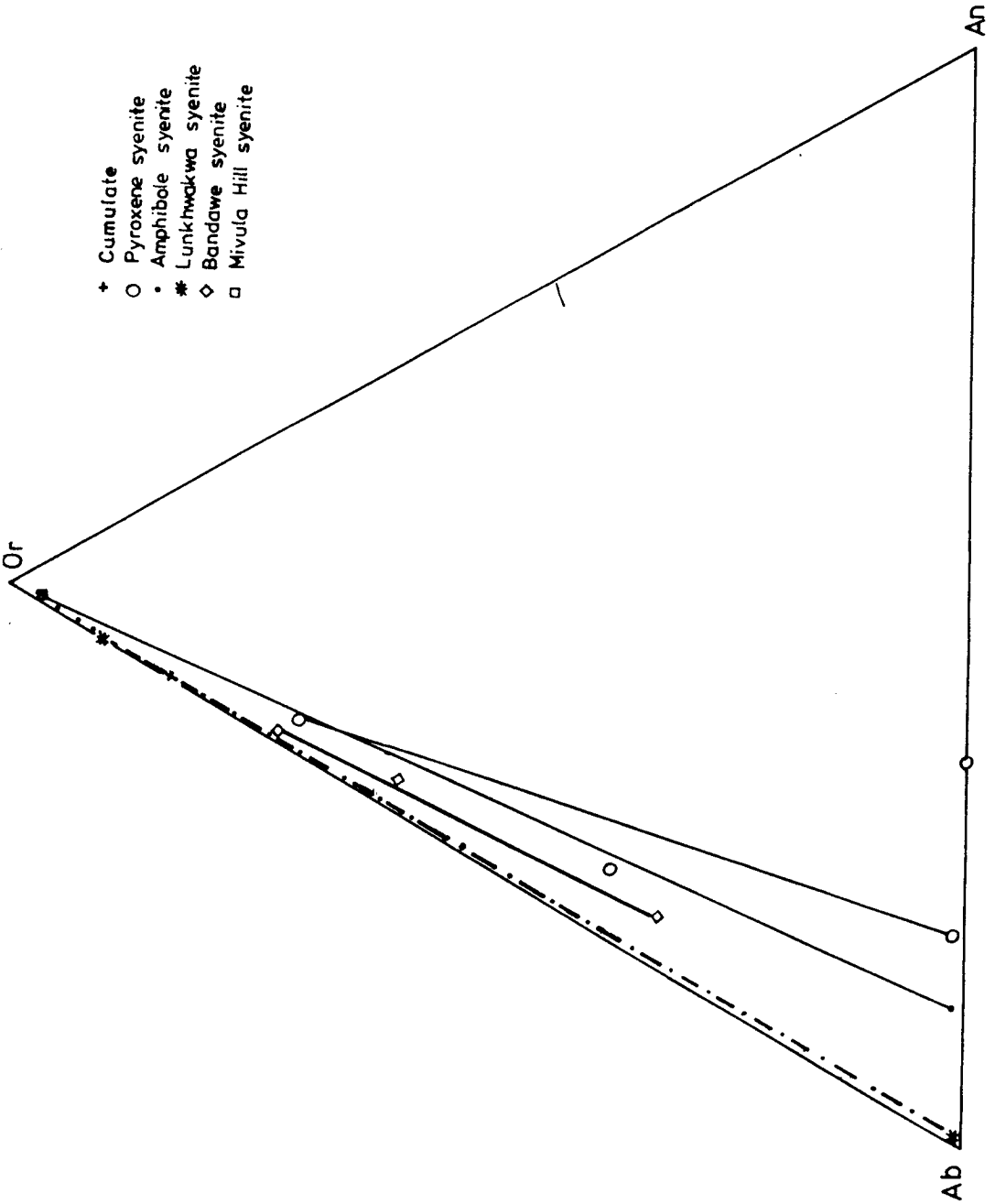

Fig. 5.9 Ab-Or-An plot of the feldpars from the syenites.

Ti and decreasing Mg and Ca(Fig. 5.5) are in agreement with the petrographic observations and they suggest a differentiation of a parent magma from a mafic one, from which the cumulates and the pyroxene syenite crystallized, to a more hydrous felsic one, from which the amphibole and leucocratic syenites crystallized.

The increasing Fe^{3+}/Fe^{2+} ratios with differentiation, and the exsolution of the Fe-Ti oxides are indicative of the increasing oxygen fugacities during differentiation. The conclusion is supported by the appearance of sphene in the mineral assemblage of the amphibole syenite. The presence of sphene in felsic igneous rocks has been shown to indicate oxidizing conditions during magmatic evolution (26).

The presence of microperthitic alkali feldspar in the pyroxene syenite as compared to mesoperthites in the hornblende and leucocratic syenites are interpreted as an indication of the increasing water contents of the magma with differentiation resulting in an increase in pH_2O (25). Exsolution of the alkali feldspar in the pyroxene syenite took place in a water deficient, solid state at relatively low temperature at which atomic migration was restricted whilst exsolution in the more differentiated syenites occurred at higher H_2O contents, supported by the presence of biotite and hornblende in these rocks.

5.4.2 Chipata syenites.

A. Lunkhwakwa syenite

The minerals of the Lunkhwakwa syenite reflect a chemistry which is consistent with its sodic nature. The feldspars and pyroxenes are characterized by higher Na relative to Ca and Mg.

The presence of an acmitic pyroxene (Fe^{3+}) and sphene as the main mafic phases indicates high oxygen fugacities during crystallization (26, 48). The low Mg/Mg+Fe ratios suggest that the liquid from which the syenite crystallized was in an advanced stage of fractional crystallization. Alternatively, the ratios may indicate a low degree of partial melting of the parent magma.

B. Bandawe syenite.

The chemistry and textures of the minerals from the Bandawe nepheline syenite, to a large extent, reflects the effects of metamorphism except for pyroxene which appears to have retained its original igneous composition. The presence of a diopsidic pyroxene in the syenite implies that it crystallized from an alkaline magma which had a miaskitic character, shown by the presence of biotite, diopsidic pyroxene and hornblende with accessory zircon and sphene. (74).

The mafic minerals are characterized by high Ti contents especially amphiboles and biotites. Amphiboles and biotites with high Ti contents are characteristic of high grade metamorphic rocks (34, 49). These amphiboles (34, 50) also have colours ranging from greenish-brown to reddish brown, the increasing brown colour being attributed to both the increasing metamorphic grade and Ti contents.

The iron-oxide is a complex solid solution of Fe-Mg-Ti-oxides which with metamorphism have exsolved into a spinel phase and an ilmenite phase. Spinel and ilmenite are typical minerals of high temperature metamorphism (50).

The chemical composition of scapolite has a high marialite component indicating that its composition was largely controlled by the presence of chlorine, hence its

occurrence as coronas around the main chlorine bearing mineral sodalite. The nepheline composition departs markedly from the ideal Morozevicz composition- $Ne_{75.0}Ks_{20.5}O_{4.5}$ and shows an incorporation of Si or loss of Na and K. From these features, it is concluded that the Bandawe syenite has suffered high grade metamorphism.

5.4.3 Mivula Hill syenite

The mineral chemistry of the Mivula Hill syenite is consistent with its undersaturated nature, having low Si and high alkalies. The amphibole is a sodium rich calcic type indicating relatively high calcium contents in the magma. The nepheline composition is within the normal range of nephelines from plutonic igneous rocks (50). The amount of excess SiO_2 in the nephelines indicates crystallization temperatures above $700^{o}C$ (51). The Mg/Mg+Fe ratios of the minerals are low, indicative of crystallization from a highly fractionated magma.

5.5.0 Comparison of the mineral chemistry of the syenites.

Table 5.7a.

Mineral	Sinda Syenites	Lunkhwakwa Syenite	Bandawe syenite	Mivula Hill syenite
Pyroxene	sodian salite	acmitic aegirine augite	Ti rich sodian salite	aegirine
Amphibole	edenite and hornblende	-	pargasite	ferro edenite
Biotite	Phlogopitic	-	intermediate between Phlogopite-Eastonite and Annite-Sidero-Phyllite	Annite-Sidero phyllite
Oxides	Ilmenite-magnetite	magnetite	Ilmenite-spinel	Ilmenite
Alkali Feldspar	appreciable anorthite contents, incomplete exsolution (high temp) of Na-K in pyx syenite, complete exsolution (low temp) in unexsolved in cumulate	No anorthite content complete exsolution (low temp) of Na-K Phases	little anorthite contents incomplete exsolution (met) of Na-K Phases	No anorthite contents, complete exsolution (low temp) of Na-K phases.
Nepheline	-	-	$Ne_{70}Ks_{143}$ $Qz_{15.7}$	$Ne_{73.2}Ks_{18.0}$ $Qz_{8.8}$

Table 5.7b

	Sinda Syenite	Lunkhwakwa Syenite	Bandawe Syenite	Mivula Hill Syenite
High	Si,Al,Ti,Mg and Ca	Na,Fe and Mn	Si,Ti,Mg and Ca	Al,Fe,Mn,Na and K
Low	Na,K,Fe and Mn	Si,Al,Ti, Mg and Ca	Al,Fe,Mn,Na and K	Si,Ti,Mg and Ca
Mg/Mg+Fe	60 - 78	32 - 36	40 - 70	12 - 20

It is clear from the results presented above that the chemistry of the minerals from the syenites is significantly different, thus indicating that the chemistries of their magmas were different.

Comparison of the pyroxene from the syenites with common trends of alkali pyroxenes (45) shows that the pyroxenes from the Lunkhwakwa and Bandawe syenites have an undersaturated trend whereas those from the Sinda syenites are unevolved. This suggests either chemical differences in their parent magmas or different degrees of evolution from a similar magma.

Another point of interest is the increasing Mg/Mg+Fe mineral ratios from the Sinda syenites through the Bandawe, Lunkhwakwa to the Mivula Hill syenites. This trend and the above chemical differences could be due to several reasons, some of which are: (1) different degrees of partial melting of chemically similar source regions (2) different degrees of fractional crystallization of related parent magmas and (3) different chemical compositions of the source regions. The possible mechanisms of the origin of the syenites will be discussed further in chapter 8.

CHAPTER 6

Petrochemistry

6.1 Analytical techniques.

Major elements were analysed by X-ray fluorescence analysis on glass discs prepared with a sodium tetraborate flux, except for Na and Mg, which were analysed by atomic absorption, and volatiles which were analysed as loss on ignition.

Trace elements were analysed on pressed powder pellets by X-ray fluorescence using a Phillips PW1400 spectrometer and the techniques of Norrish and Chappell. (52). Results were corrected for background interference from tube and sample spectral lines, and for matrix variation using the major element composition. USGS standards (G-2, GSP-1, W-1, BCR-1 and PCC-1) were used for calibration.

6.2 Presentation of results.

The major elements have been recalculated to 100 per cent on a water-free basis and are presented in tables 6.1-6.4 in order of increasing SiO_2. Means of chemically similar samples used in plotting the various graphs are also included in the tables.

6.3 Chemical classification.

The alkalis versus SiO_2 and alkalinity ratio versus SiO_2 diagrams (Fig. 6.1 and 6.2), (53, 54). i) show a general increase in alkalinity from the Sinda syenites to the Mivula Hill syenite and ii) classifies the Sinda syenites as alkaline with transitions into the calc-alkaline field, the Lunkhwakwa and Bandawe syenites as alkaline and the Mivula Hill syenite as peralkaline.

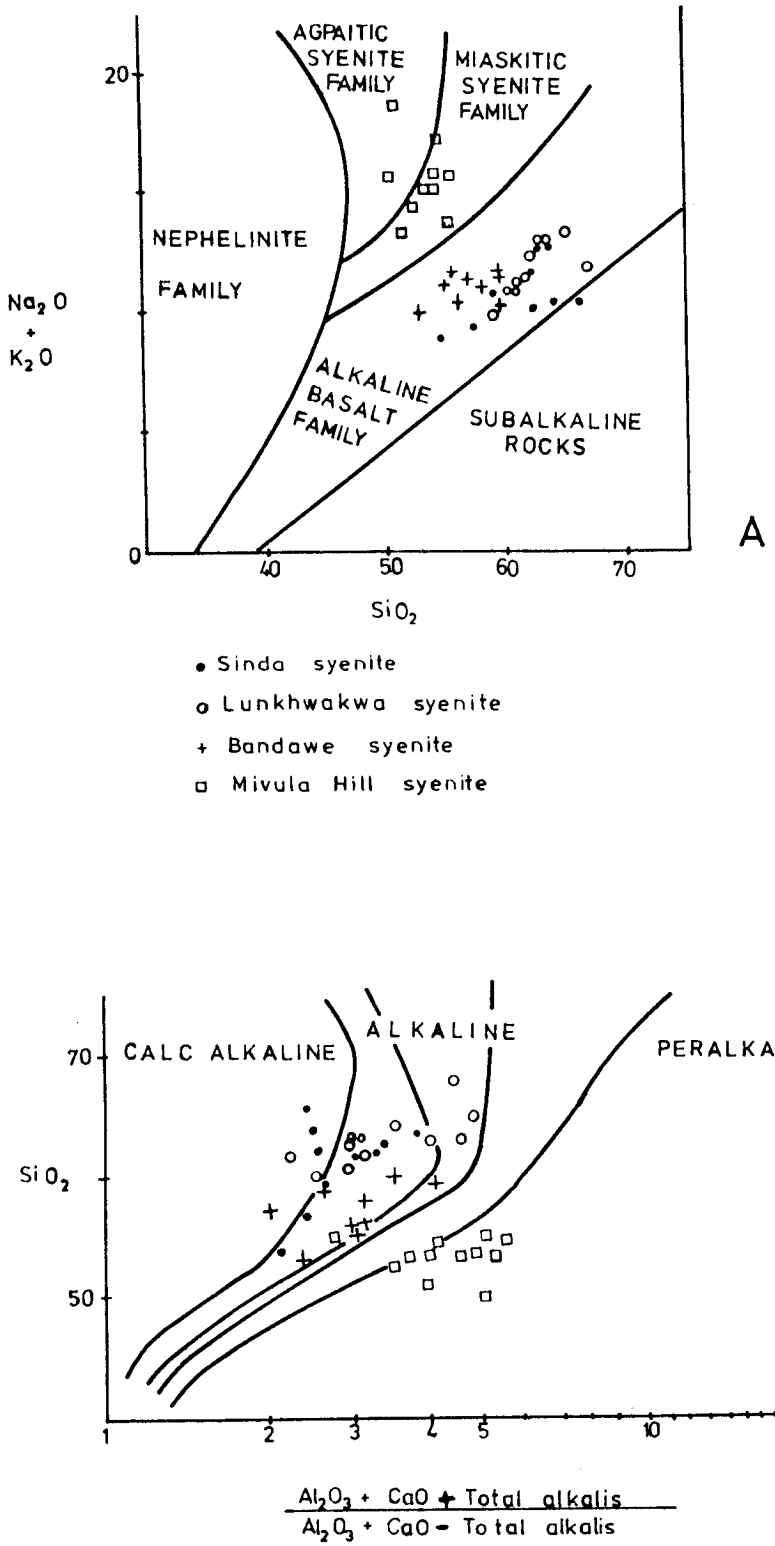

Fig. 6.1 Total alkalis vs SiO_2 and alkalinity ~~ratio~~ vs SiO_2 variation diagrams (after Currie , 1977 and Wright, 1969.

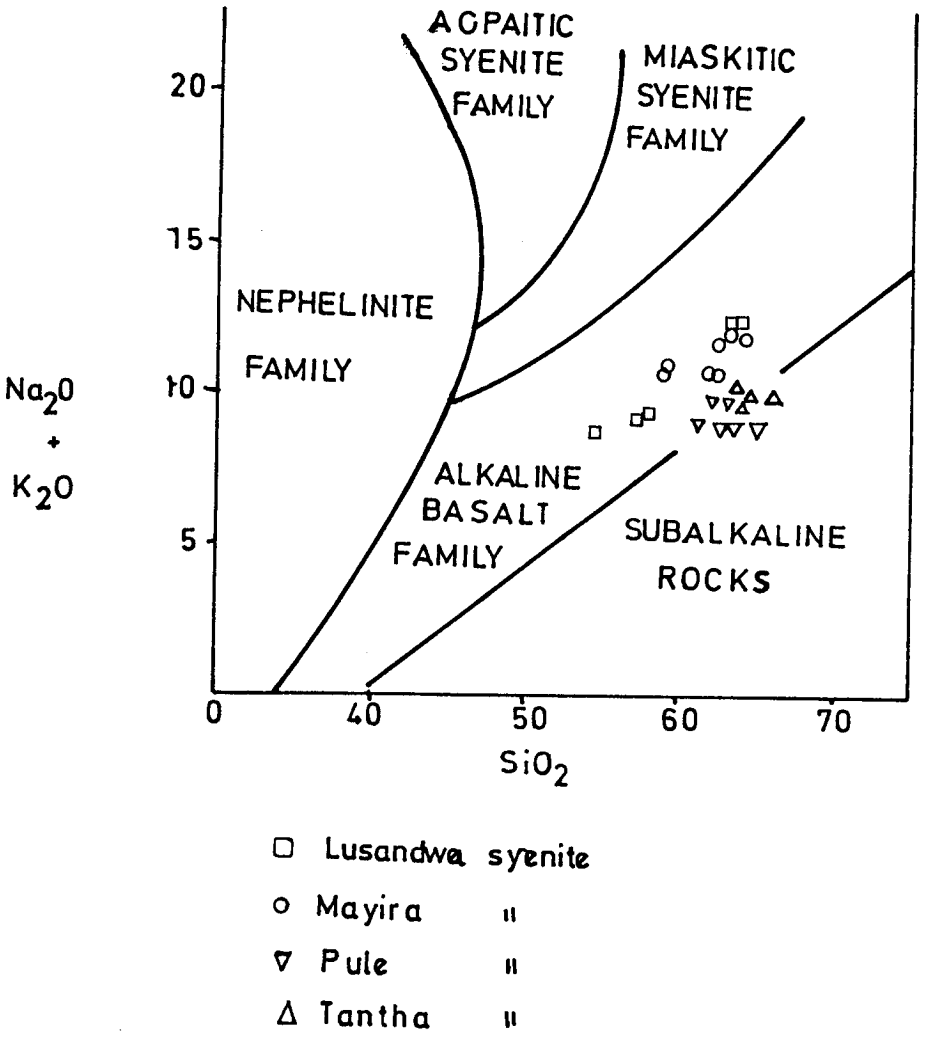

Fig. 6.2 Total alkalis vs SiO_2 variation diagram for the Sinda syenites.

The Bandawe and Mivula Hill nepheline syenites are both miaskitic types having agpaitic indices (Na+K/Al) between 0.53-0.67 and 0.64-1.0 respectively. Although both are miaskitic, only the Mivula Hill syenite has a peralkaline character because of its lower SiO_2 and higher alkali contents.

6.4 Chemical variation in the Sinda syenites.

6.4.1 Major elements.

The Harker diagrams (fig. 6.3) show element variation both between the intrusions and within a single pluton, in this case the Pule intrusion.

The insert depicting the chemical variation among the Pule samples shows that a) the majority of the samples cluster around a mean composition, thus warranting averaging of these analysis to simplify the diagrams and b) the odd samples from the Pule intrusion shows the same mode of variation as shown by the main series of the Pule and Tantha syenites, indicating that no information is lost by the use of the means.

Throughout these variation diagrams two trends are evident, one comprising the Lusandwa and Mayira intrusions and the other the Pule and Tantha intrusions.

Element variation in the Lusandwa and Mayira intrusions is characterized by a steady decrease in FeO, MgO, CaO, TiO_2 and P_2O_5 and a corresponding increase in Al_2O_3, Na_2O and K_2O from the pyroxene syenites through the hornblende syenites to the leucocratic syenites. The Pule and Tantha intrusions parallel these trends but at higher levels for CaO, MgO, FeO and P_2O_5 and at a lower level for K_2O,. but diverge with respect to Al_2O_3 and Na_2O which both decrease.

The triangular diagrams show that CaO, MgO and FeO remain in constant proportions with increasing Al_2O_3 (fig. 6.4) and that the K_2O: Na_2O ratio increases.

Table 6.1 Whole rock major and trace element analyses of the Sinda syenites.

	1	2	3	4	5	6	7	8
	AP3	AP2	AP1	FTS/12	/16	/39	Mean	/17
SiO_2	35.75	44.33	62.52	58.94	59.41	60.00	59.45	61.91
TiO_2	.29	.10	.33	.98	1.12	1.09	1.06	.82
Al_2O_3	1.44	1.38	8.16	16.03	16.90	16.28	16.40	17.56
Fe_2O_3	2.02	.74	2.17	2.96	3.57	3.26	3.26	2.74
FeO	3.95	1.06	-	2.56	1.82	2.21	2.20	1.13
MnO	.18	.08	.08	.10	.09	.09	.09	.08
MgO	10.30	2.30	.73	3.03	2.17	2.43	2.54	1.43
CaO	31.35	28.51	11.41	4.14	3.44	3.80	3.79	2.55
Na_2O	.60	.28	.55	4.27	4.65	4.30	4.41	4.94
K_2O	.12	.39	5.56	6.48	6.29	6.00	6.26	6.51
P_2O_5	14.00	20.82	8.48	.51	.55	.53	.54	.33
FeOT*	5.76	1.72	1.95	5.22	5.03	5.14	5.13	3.60
$\frac{FeOT}{FeOT+MgO}$	.36	.43	.73	.63	.70	.68	.67	.72
$\frac{Fe_2O_3}{FeO}$	.51	.70	-	1.16	1.96	1.48	1.53	2.42
LoI	1.05	.99	1.01	.88	.95	1.10	.98	.51
Tot	98.35	96.08	96.81	98.78	98.45	98.35	98.53	98.55
Rb	.6	8.1	105	230	209	257	232	256
Ba	78	1060	7180	3800	3350	3510	3553	3390
Sr	2050	1960	2480	1950	2020	1730	1900	2140
La	1980	4110	2700	217	259	288	255	353
Ce	3020	5700	3450	320	383	427	376	407
Nd	1140	1950	1080	121	129	146	132	136
Y	130	201	83	29	30	43	34	32
Zr	25	12	21	414	638	589	547	523
Nb	26	59	39	39	54	88	60	57
Cr	420	208	80	94	28	45	56	20
Ga	8	2	9	21	22	24	22	22

Table 6.1 contd.

	9	10	11	12	13	14
	FTS/99	/87	/86	/94	/93	Mean
SiO_2	54.83	57.46	58.11	63.52	63.64	63.58
TiO_2	1.42	1.18	1.22	.76	.77	.76
Al_2O_3	15.38	14.93	15.88	18.14	18.07	18.10
Fe_2O_3	7.68	3.05	3.25	2.75	2.76	2.75
FeO	-	3.07	2.71	.45	.46	.45
MnO	.11	.11	.09	.10	.11	.10
MgO	4.64	4.78	3.68	.50	.52	.51
CaO	6.28	5.54	4.86	1.21	1.02	1.11
Na_2O	3.62	3.54	3.82	5.63	5.70	5.67
K_2O	5.13	5.61	5.68	6.85	6.85	6.85
P_2O_5	.91	.74	.70	.08	.08	.08
FeOT	6.91	5.81	5.63	2.92	2.94	2.93
$\frac{FeOT^*}{FeOT+MgO}$	.60	.55	.60	.85	.85	.85
$\frac{Fe_2O_3}{FeO}$	-	.99	1.20	6.11	6.00	6.05
LoI	.67	.99	.75	.51	.66	.59
Tot.	98.51	98.14	98.19	98.64	98.68	98.66
Rb	138	186	177	126	128	127
Ba	6300	4260	4550	227	122	175
Sr	2800	1960	2150	83	50	67
La	156	168	167	386	360	373
Ce	245	268	269	552	523	538
Nd	113	107	108	183	188	186
Y	24	29	23	90	82	86
Zr	136	366	452	706	749	728
Nb	21	33	34	77	73	75
Cr	120	288	122	6	5	5
Ga	22	18	21	18	17	17

Table 6.1 contd.

	15 /30	16 /33	17 /26	18 /31	19 /22	20 /21	21 /32	22 /29	23 Mean
SiO_2	60.28	61.71	62.27	62.61	62.66	62.69	64.86	64.33	62.43
TiO_2	1.00	.97	.96	.98	.83	.93	.93	.75	.92
Al_2O_3	15.31	14.69	15.26	14.27	15.18	14.73	14.50	14.62	14.82
Fe_2O_3	3.30	3.02	3.26	3.71	3.51	2.81	3.06	2.99	3.21
FeO	2.26	2.33	1.81	1.65	1.48	1.99	2.33	1.42	1.91
MnO	.08	.10	.08	.08	.09	.07	.10	.06	.08
MgO	2.83	2.65	2.18	2.46	1.96	2.35	2.39	2.11	2.37
CaO	3.96	3.99	3.24	3.83	3.24	3.92	3.72	3.33	3.65
Na_2O	4.02	3.93	4.14	3.95	4.22	3.53	3.87	4.07	3.97
K_2O	6.24	5.87	6.13	5.71	6.26	6.28	5.91	5.82	6.03
P_2O_5	.70	.73	.66	.73	.56	.71	.70	.51	.66
FeOT	5.23	5.05	4.74	4.99	4.64	4.52	5.08	4.11	4.80
$\frac{FeOT}{FeOT+MgO}$	.65	.66	.68	.67	.70	.66	.68	.66	.67
$\frac{Fe_2O_3}{FeO}$	1.46	1.30	1.80	2.25	2.37	1.41	1.31	2.11	1.75
LoI	.81	.62	.62	.83	.82	.84	.80	1.29	.83
Tot	98.09	97.85	98.15	98.12	98.34	98.33	98.26	98.62	98.22
Rb	163	162	163	139	173	177	186	178	168
Ba	4460	4900	4700	4140	4390	4010	4230	3860	4336
Sr	2510	2350	2430	2380	2240	2050	2097	2020	2260
La	254	376	189	313	356	329	267	200	286
Ce	396	464	329	429	495	388	414	307	403
Nd	156	183	109	150	188	154	150	111	150
Y	35	43	25	31	54	44	33	27	37
Zr	469	370	405	360	433	359	377	382	394
Nb	49	39	43	35	40	50	54	46	45
Cr	56	55	38	47	38	39	54	40	46
Ga	22	23	21	20	21	20	23	21	21

Table 6.1 contd.

	24 /2	25 /5	26 /4	27 /7B	28 Mean(2,5)	29 Mean(4,7B)
SiO_2	61.77	62.64	62.71	63.80	62.20	63.26
TiO_2	.90	.65	.66	.65	.81	.65
Al_2O_3	16.08	16.02	18.35	17.92	16.10	18.13
Fe_2O_3	3.30	2.27	2.23	2.47	2.80	2.35
FeO	1.39	1.36	.79	.38	1.94	.59
MnO	.09	.10	.09	.04	.10	.07
MgO	2.00	.89	.60	.53	1.44	.56
CaO	3.15	3.61	1.63	1.57	3.38	1.60
Na_2O	4.62	5.68	5.07	5.40	5.15	5.23
K_2O	6.28	6.41	7.74	7.13	6.34	7.43
P_2O_5	.41	.37	.12	.10	.39	.11
FeOT	4.36	3.40	2.80	2.60	3.88	2.70
$\frac{FeOT}{FeOT+MgO}$	.69	.79	.82	.83	.74	.82
$\frac{Fe_2O_3}{FeO}$	2.37	1.67	2.82	6.5	2.02	4.66
LoI	.87	1.16	.49	.42	.88	.45
Tot.	98.68	98.31	98.66	98.72	98.50	98.69
Rb	269	102	255	291	186	273
Ba	3310	5040	2160	1350	4175	1755
Sr	1620	2410	1380	1010	2015	1195
La	344	229	215	349	287	282
Ce	464	393	418	342	429	380
Nd	147	170	118	130	156	124
Y	47	43	50	46	45	48
Zr	545	505	691	717	525	704
Nb	72	83	93	53	78	73
Cr	43	3	3	12	23	8
Ga	21	17	23	24	19	23

Table 6.1 contd.

	30 /44	31 /52	32 /50A	33 /46	34 Mean	35 /49
SiO_2	63.78	64.25	64.28	64.30	64.15	65.96
TiO_2	.86	.79	.76	.78	.80	.66
Al_2O_3	14.86	14.51	14.48	14.66	14.63	14.37
Fe_2O_3	2.74	2.51	2.70	3.05	2.75	2.20
FeO	1.71	1.80	1.69	1.23	1.60	1.32
MnO	.60	.06	.06	.07	.06	.05
MgO	1.57	1.68	1.58	1.59	1.61	1.58
CaO	2.97	3.48	3.69	3.13	3.32	3.01
Na_2O	3.98	3.85	3.52	3.87	3.81	3.59
K_2O	6.62	6.40	6.61	6.66	6.57	6.71
P_2O_5	.85	.66	.60	.65	.69	.54
FeOT	4.18	4.06	4.12	3.97	4.08	3.30
$\frac{FeOT}{FeOT+MgO}$	.73	.71	.72	.71	.72	.68
$\frac{Fe_2O_3}{FeO}$	1.60	1.39	1.60	2.48	1.78	1.67
LoI	.85	1.34	1.40	.57	1.04	1.05
Tot.	98.50	98.64	98.34	97.91	98.35	98.35
Rb	182	189	188	208	192	188
Ba	5540	4850	5130	5670	5298	5470
Sr	2150	2040	2130	2230	2138	2100
La	208	151	191	184	184	154
Ce	298	263	234	265	265	239
Nd	135	109	134	109	122	100
Y	33	28	39	23	31	20
Zr	442	446	406	366	415	371
Nb	21	41	39	34	34	30
Cr	25	24	26	25	25	22
Ga	21	22	22	21	22	21

Table 6.1 contd.

*FeO_t: Total iron as FeO

Analyses: 1-3 cumulate rocks, Mayira Hills intrusion
4-7 pyroxene syenite " " "
8 hornblende syenite, " " "
9-11 pyroxene syenite, Lusandwa intrusion
12-14 leuco syenite, " "
15-23 hornblende syenite, Pule intrusion
24-29 leuco syenite, Mayira satellite intrusion
30-35 hornblende syenite, Tantha intrusion

Analysis of the major elements were carried out by I. Sørensen, Geological Survey of Greenland, Denmark while trace element analysis were done by Dr. J.C. Bailey, Institute of Petrology, University of Copenhagen, Denmark.

Table 6.2 Major and trace element data used in the diagrams.

	1	2	3	4	5	6	7	8	9
SiO_2	35.75	44.33	62.52	59.45	61.91	54.83	57.46	58.11	63.58
TiO_2	.29	.10	.33	1.06	.82	1.42	1.18	1.22	.76
Al_2O_3	1.44	1.38	8.16	16.40	17.56	15.38	14.93	15.88	18.10
Fe_2O_3	2.02	.74	2.17	3.26	2.74	7.68	3.05	3.25	2.75
FeO	3.95	1.06	-	2.20	1.13	-	3.07	2.71	.45
MnO	.18	.08	.08	.09	.08	.11	.11	.09	.10
MgO	10.30	2.30	.73	2.54	1.43	4.64	4.78	3.68	.51
CaO	31.35	28.51	11.41	3.79	2.55	6.28	5.54	4.86	1.11
Na_2O	.60	.28	.55	4.41	4.94	3.62	3.54	3.82	5.67
K_2O	.12	.39	5.56	6.26	6.51	5.13	5.61	5.68	6.85
P_2O_5	14.00	20.82	8.48	.54	.33	.91	.74	.70	.08
FeO*T	5.76	1.72	1.95	5.13	3.60	6.91	5.81	5.63	2.93
$\frac{FeOT}{FeOT+MgO}$	.36	.43	.73	.76	.72	.60	.55	.60	.85
$\frac{Fe_2O_3}{FeO}$	.51	.70	-	1.53	2.42	-	.99	1.20	6.05
LoI	1.05	.99	1.01	.98	.51	.67	.99	.75	.59
ToT	98.35	96.08	96.81	98.53	98.55	98.51	98.14	98.19	98.66
Rb	.60	8.1	105	232	256	138	186	177	127
Ba	78	1060	7180	3553	3390	6300	4260	4550	175
Sr	2050	1960	2480	1900	2140	2860	1960	2150	67
La	1980	4110	2700	255	353	156	168	167	373
Ce	3020	5700	3450	376	407	245	268	269	538
Nd	1140	1950	1080	132	136	113	107	108	186
Y	130	201	83	34	32	24	29	23	86
Zr	25	12	21	547	523	136	366	452	728
Nb	26	59	39	60	57	21	33	34	75
Cr	420	208	8	56	20	120	288	122	5
Ga	8	2	9	22	22	22	18	21	17

Table 6.2 contd.

	10	11	12	13	14	15	16
SiO_2	62.20	63.26	64.15	65.96	62.43	64.33	62.35
TiO_2	.81	.65	.80	.66	.92	.75	.05
Al_2O_3	16.10	18.13	14.63	14.37	14.82	14.62	13.60
Fe_2O_3	2.80	2.35	2.75	2.20	3.21	2.99	-
FeO	1.94	.59	1.60	1.32	1.91	1.42	4.72
MnO	.10	.07	.06	.05	.08	.06	.12
MgO	1.44	.56	1.61	1.58	2.37	2.11	.96
CaO	3.38	1.60	3.32	3.01	3.65	3.33	2.52
Na_2O	5.15	5.23	3.81	3.59	3.97	4.07	5.44
K_2O	6.34	7.43	6.57	6.79	6.03	5.82	5.78
P_2O_5	.39	.11	.69	.54	.66	.51	.18
FeOT	3.88	2.70	4.08	3.30	4.80	4.11	4.72
$\frac{FeO}{FeOT+MgO}$	.74	.82	.72	.68	.67	.66	.83
$\frac{Fe_2O_3}{FeO}$	2.02	4.66	1.78	1.67	1.75	2.11	-
LoI	.88	.45	1.04	1.05	.83	1.29	-
Tot.	98.50	98.69	98.95	98.35	98.22	98.62	95.72
Rb	186	273	192	188	168	178	110
Ba	4175	1755	5298	5470	4336	3860	1600
Sr	2015	1195	2138	2100	2260	2020	200
La	287	282	184	154	286	200	70
Ce	429	380	265	239	403	307	161
Nd	156	124	122	100	150	111	65
Y	45	48	31	20	37	27	20
Zr	525	704	415	371	394	382	500
Nb	78	73	34	30	45	46	35
Cr	23	8	25	22	46	40	2
Ga	19	23	22	21	21	21	330

Table 6.2 contd.

*FeO_t: Total iron as FeO

Analyses:

1-3	apatite rich rocks
4	pyroxene syenite, Mayira intrusion
5	hornblende syenite " "
6-8	pyroxene syenite, Lusandwa intrusion
9	leuco syenite " "
10	hornblende syenite, Mayira satellite intrusion
11	leuco syenite " " "
12-13	hornblende syenite, Tantha intrusion
14-15	hornblende syenite, Pule intrusion
16	average syenite (57)

LEGEND FOR FIGURES 6.3 - 6.5

Lusandwa intrusion

□ pyroxene syenite (single analysis)

■ leuco syenite (mean of 2)

Mayira intrusion

● pyroxene syenite (mean of 3)

⊖ hornblende syenite (mean of 2)

○ hornblende syenite (single analysis)

⊖ leuco syenite (mean of 2)

◇ pyroxene apatite cumulate

Pule intrusion

▼ horblende syenite (mean of 7)

▽ hornblende syenite (single analysis)

Tantha intrusion

▲ hornblende syenite (mean of 5)

△ hornblende syenite (single analysis)

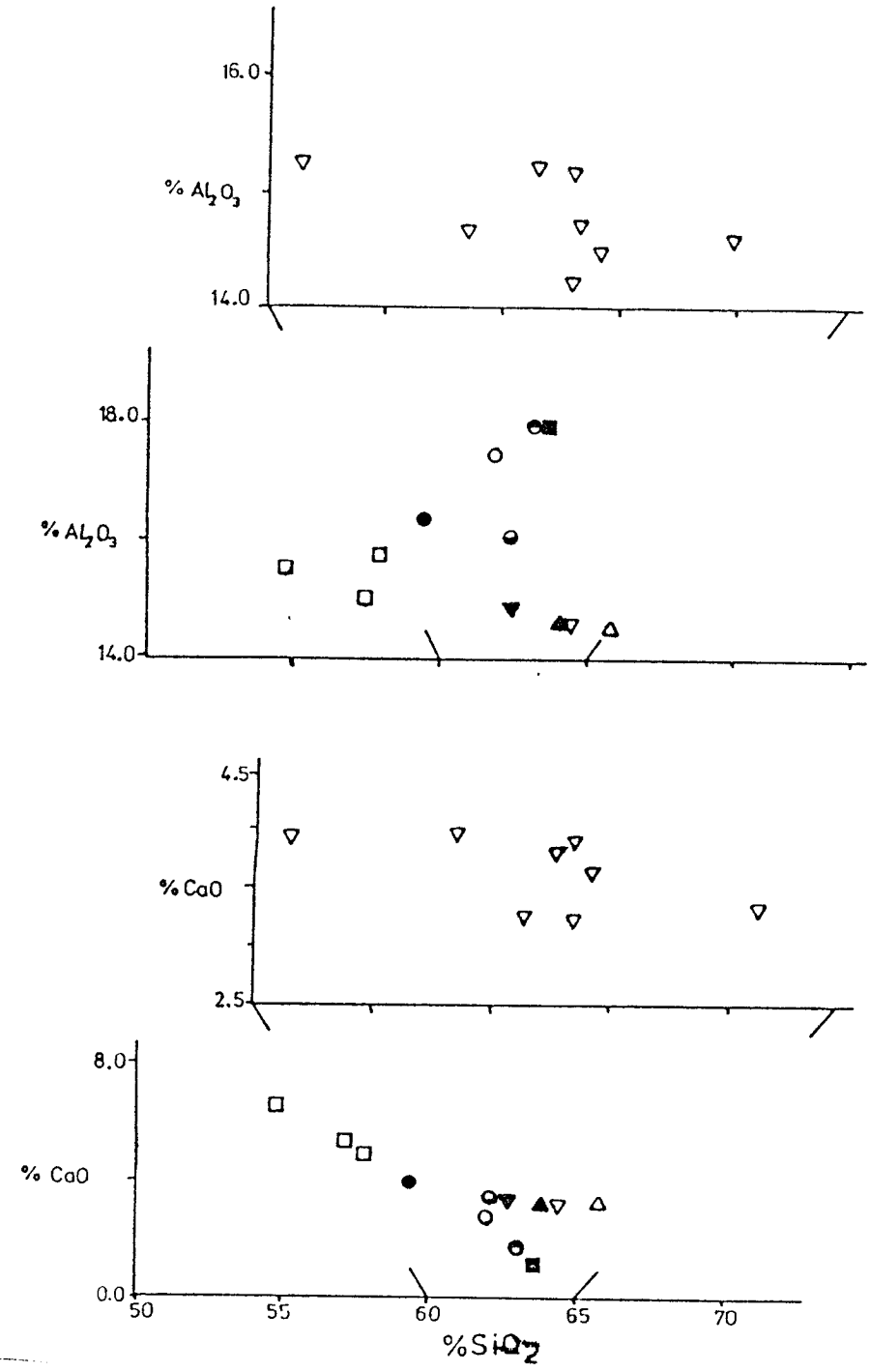

Fig. 6.3 Harker varition diagram for the Sinda syenites.

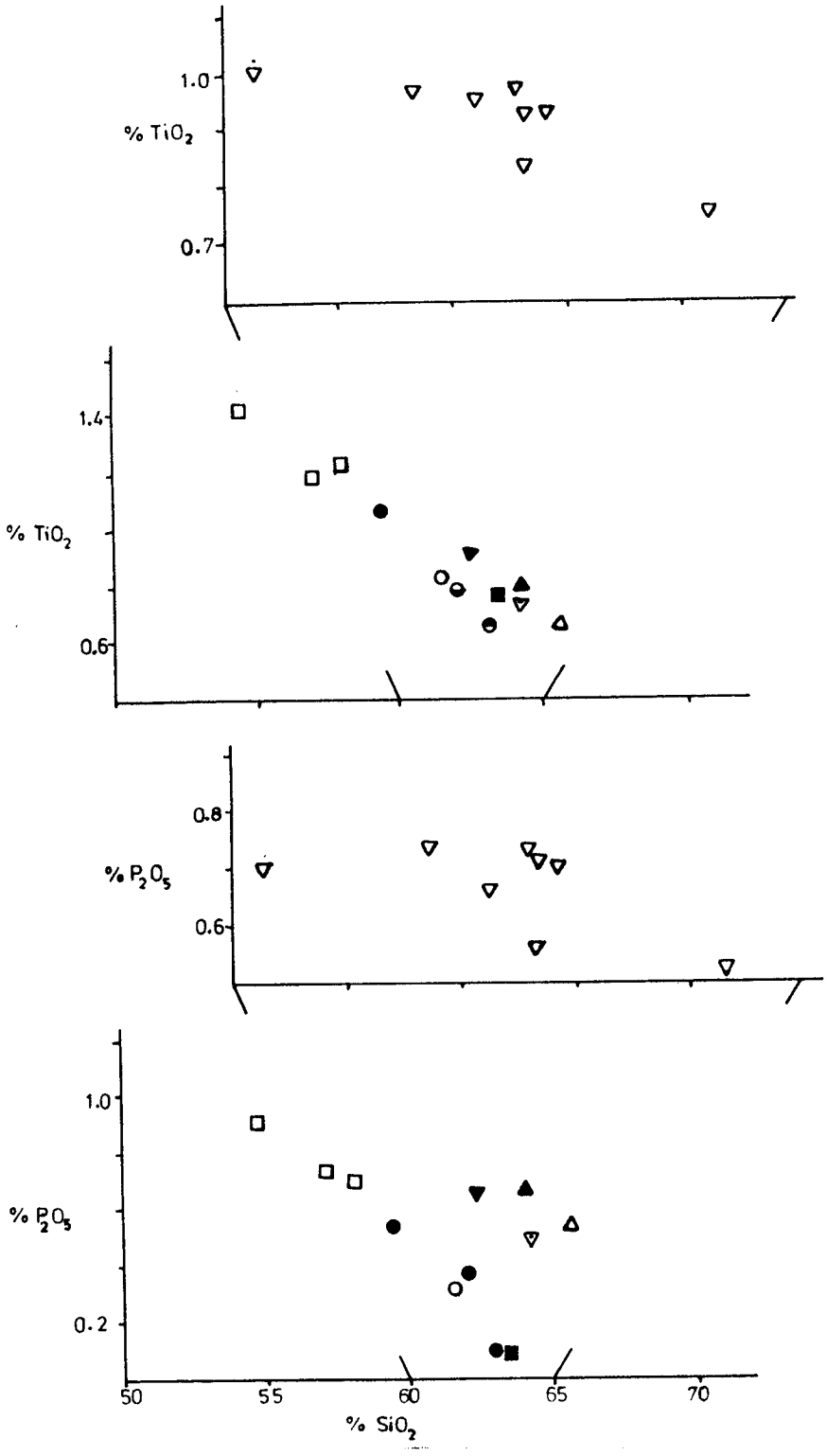

Fig. 6.3 Harker variation diagram for the Sinda syenites. (contd.)

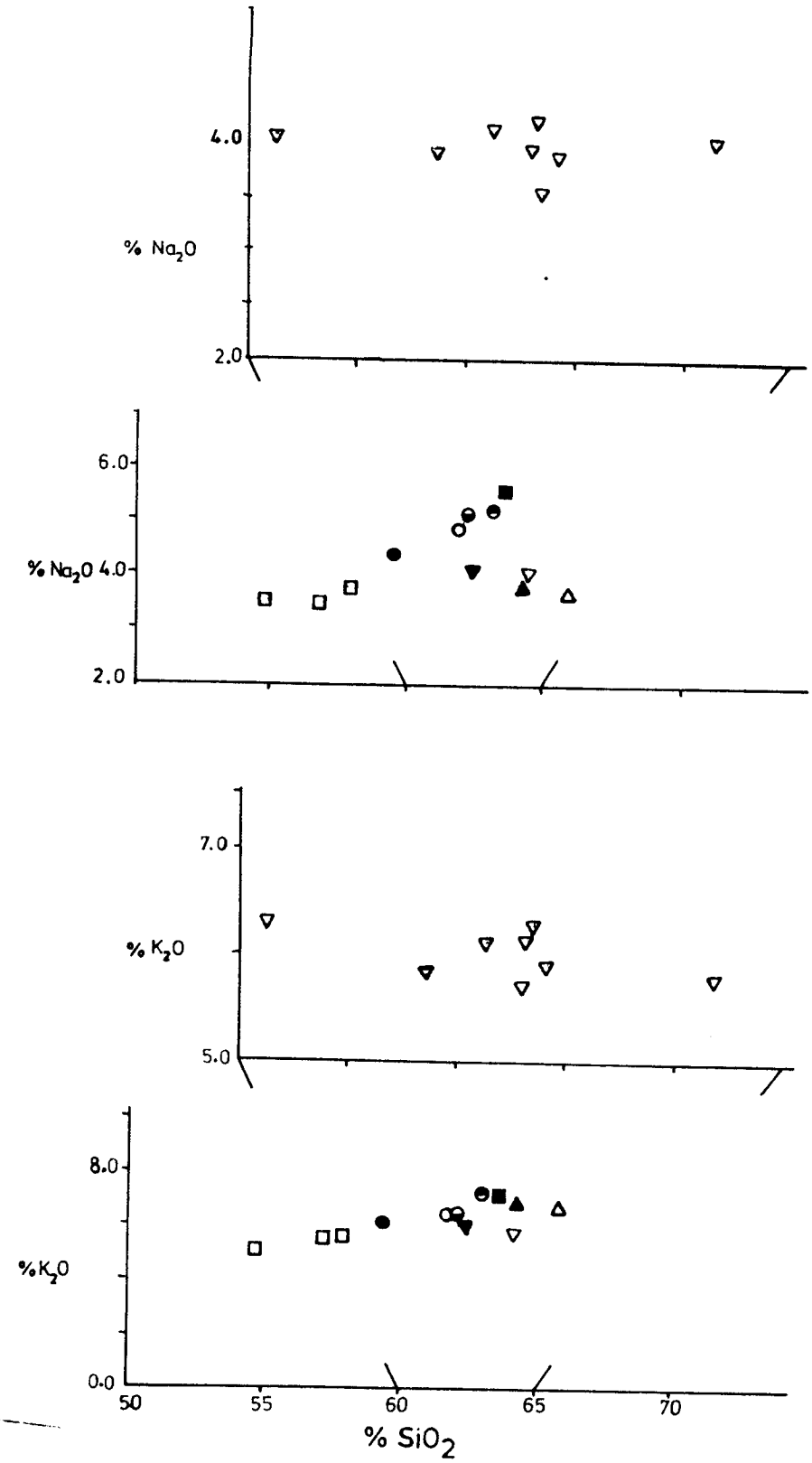

g. 6.3 Harker variation diagram for the Sinda syenites.
ontd.)

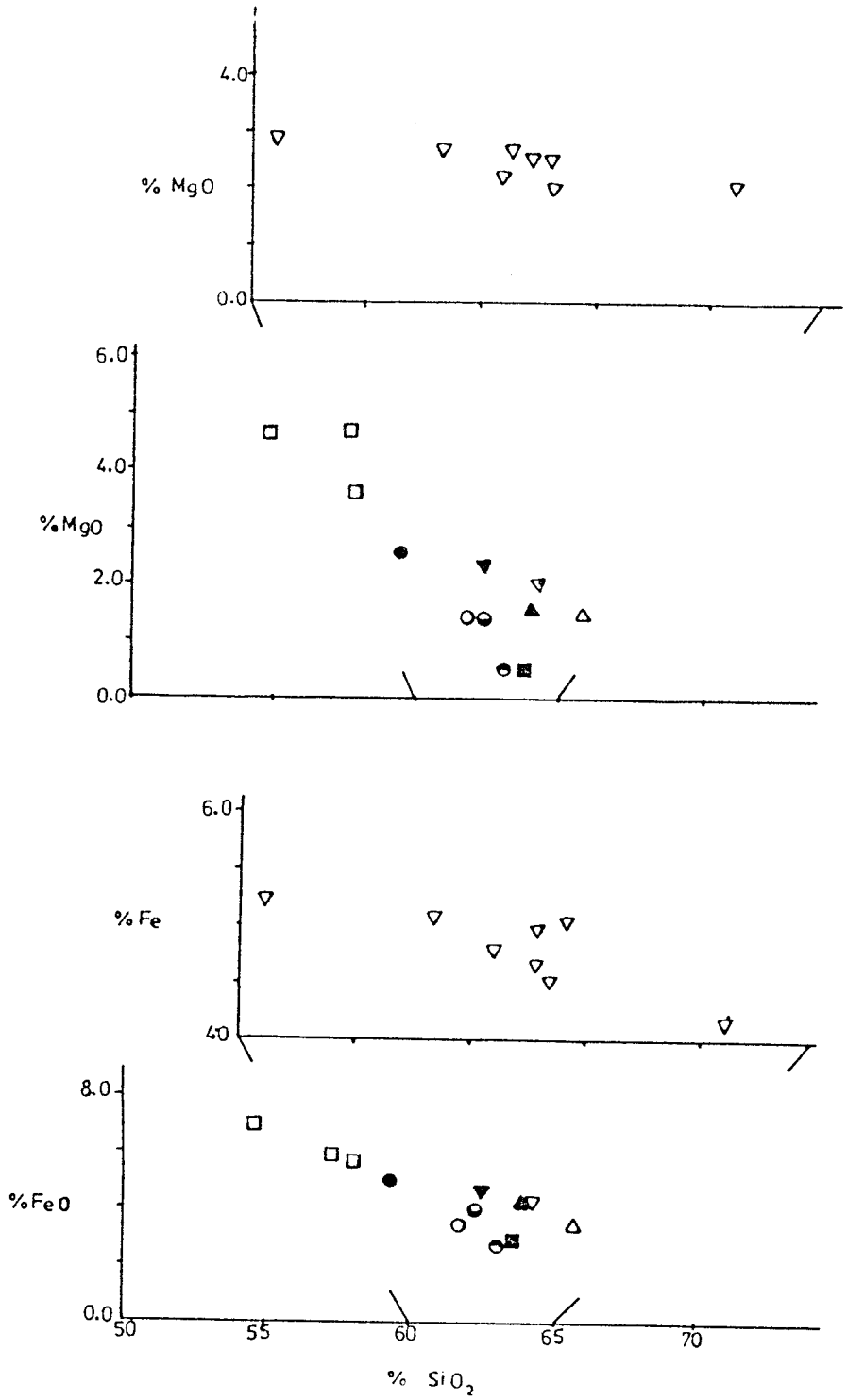

Fig. 6.3 Harker variation diagram for the Sinda syenites (contd.)

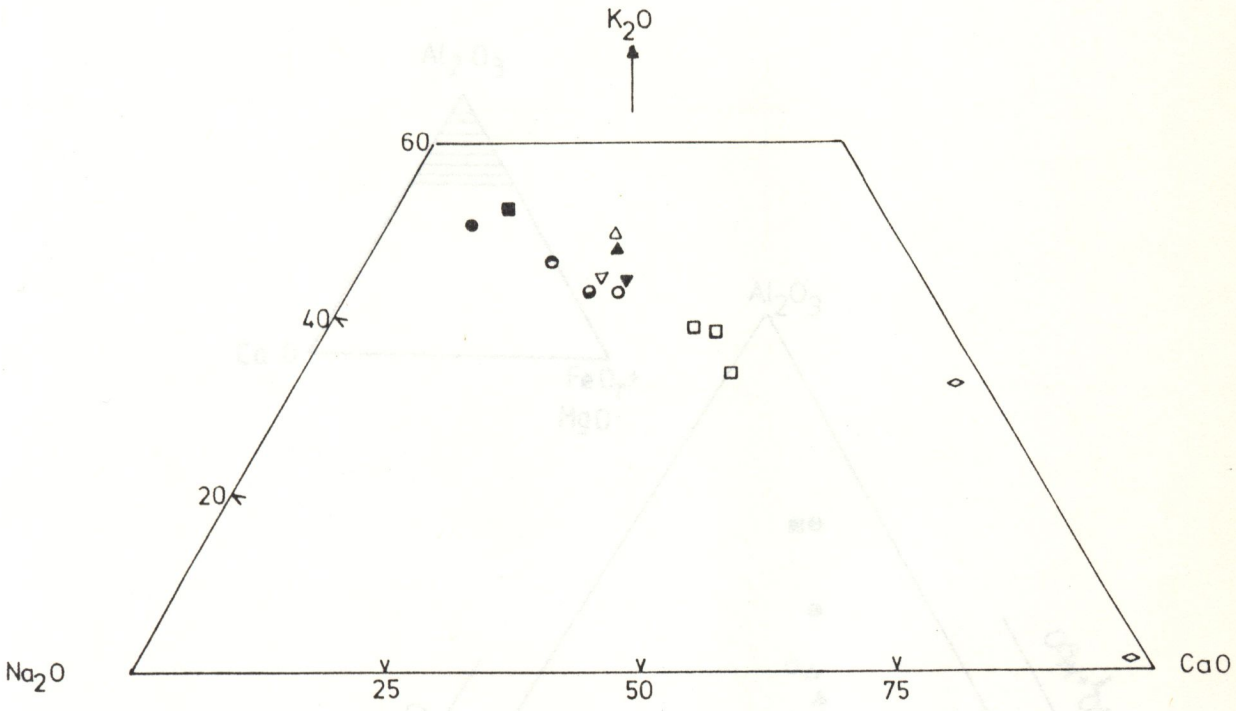

Fig. 6.4a. Triangular diagrams for the Sinda syenites using the parameters CaO, MgO, FeO, Al_2O_3, Na_2O and K_2O.

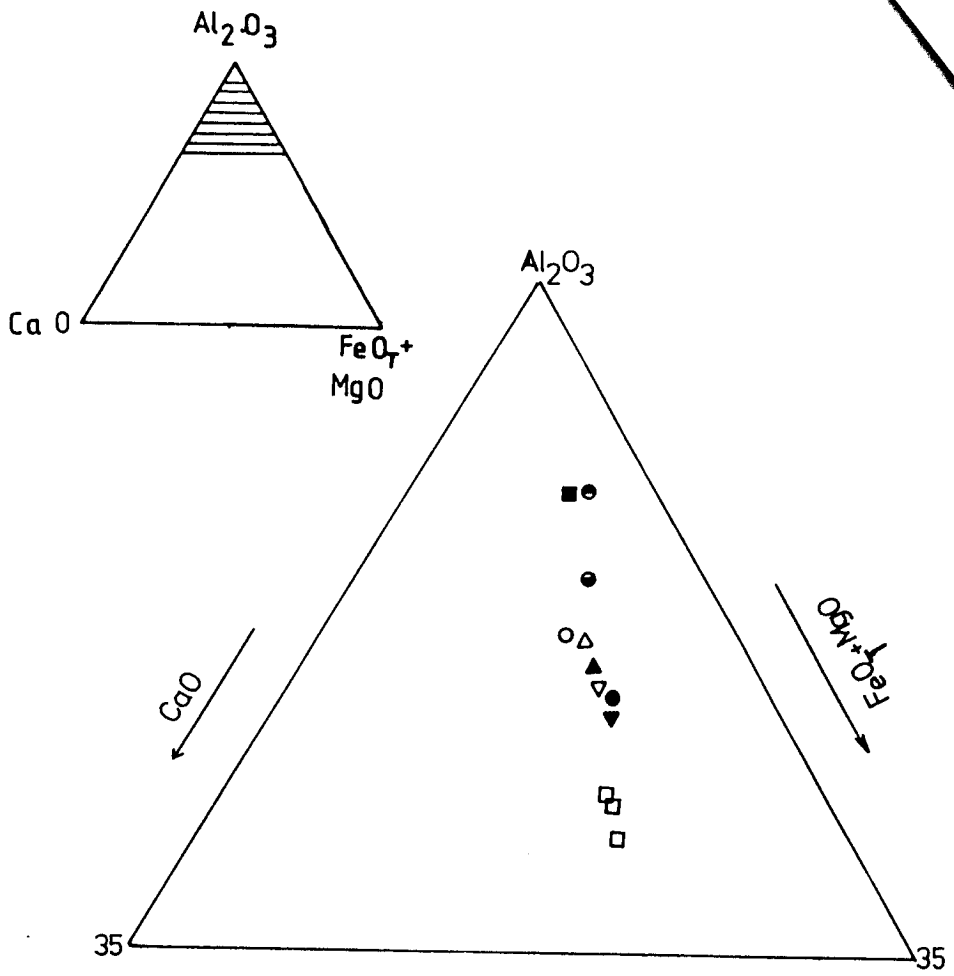

Fig. 6.4b. Triangular diagrams for the Sinda syenites using the parameters CaO, MgO, FeO, Al_2O_3, Na_2O and K_2O.

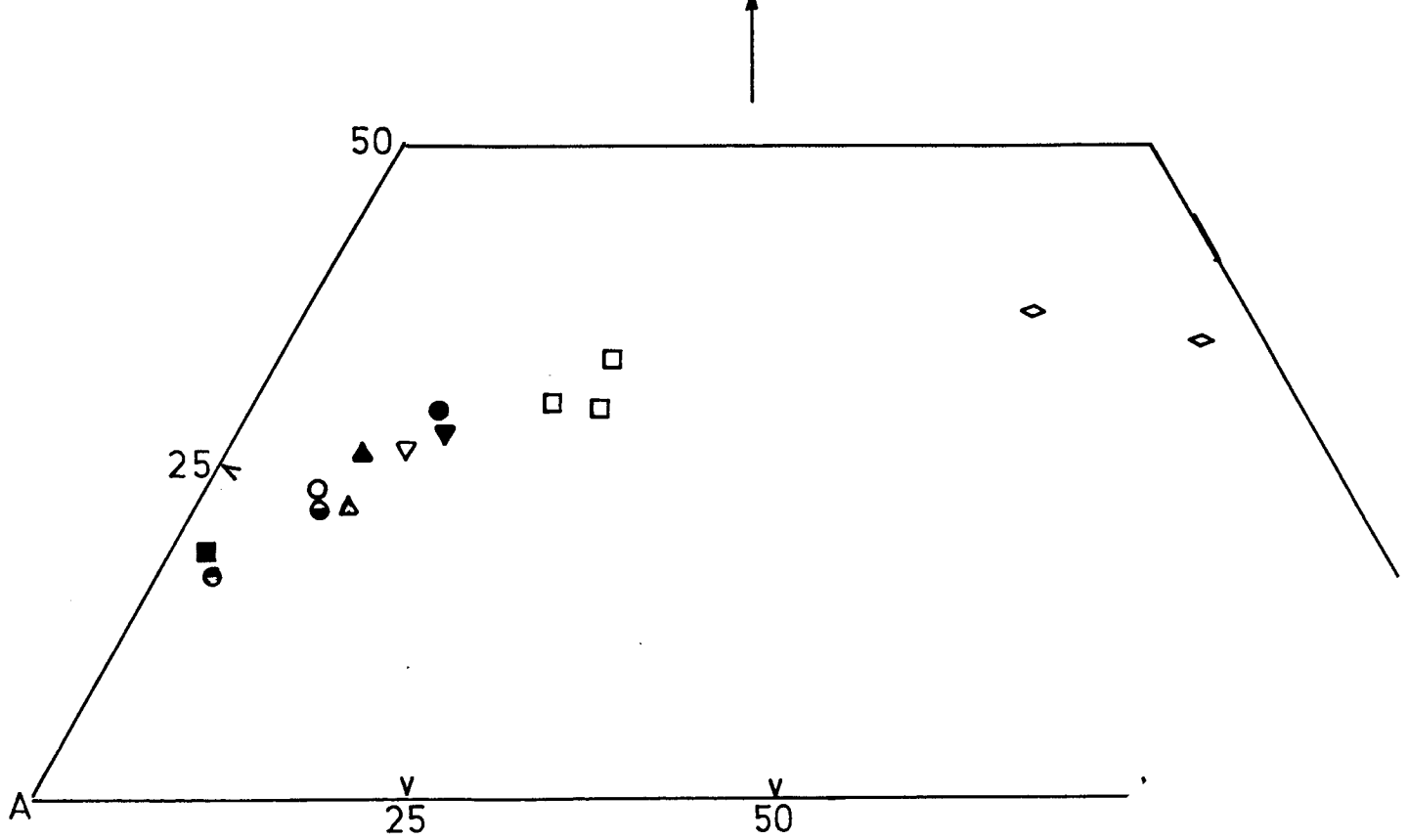

Fig. 6.4c. Triangular diagrams for t
the parameters CaO, M
K_2O.

The Harker and triangular diagrams both show regular variations in the chemistry of the rocks suggesting that they form a petrogenetic suite, whereas the divergence of the Tantha and Pule syenites suggest the existence of two series.

6.4.2 Trace elements

Except for the apatite rich rocks the trace elements in the syenites also show a regular variation with SiO_2 and (Fig. 6.5) define trends comparable with those shown by the major elements. Four groups of trace elements may be distinguished on the basis of their variation patterns and ionic properties.

There is a rapid exponential decrease in Cr from about 300 ppm in the pyroxene syenites to less than 20ppm in the leuco-syenites. The Pule and Tantha syenites have higher contents of Cr, which decreases less dramatically.

In both the Lusandwa and Mayira intrusions, both Ba and Sr show a rapid decrease from the pyroxene syenite, to the leuco-syenite with a kink at about 63% SiO_2. In contrast, the Pule and Tantha syenites show decreasing Ba contents, whilst Sr remains constant.

There is a general increase of Rb and the LREE (La, Ce and Nd) with increasing SiO_2 in both the Lusandwa and Mayira intrusions whereas in the Pule and Tantha intrusions, these elements have an opposite trend. The K/Rb ratios of the syenites is similar to that of the average syenite (57).

The chondrite normalised rare earth diagram (Fig 6.5) shows that the syenites have a fractionated REE pattern with a relative enrichment of the LREE.

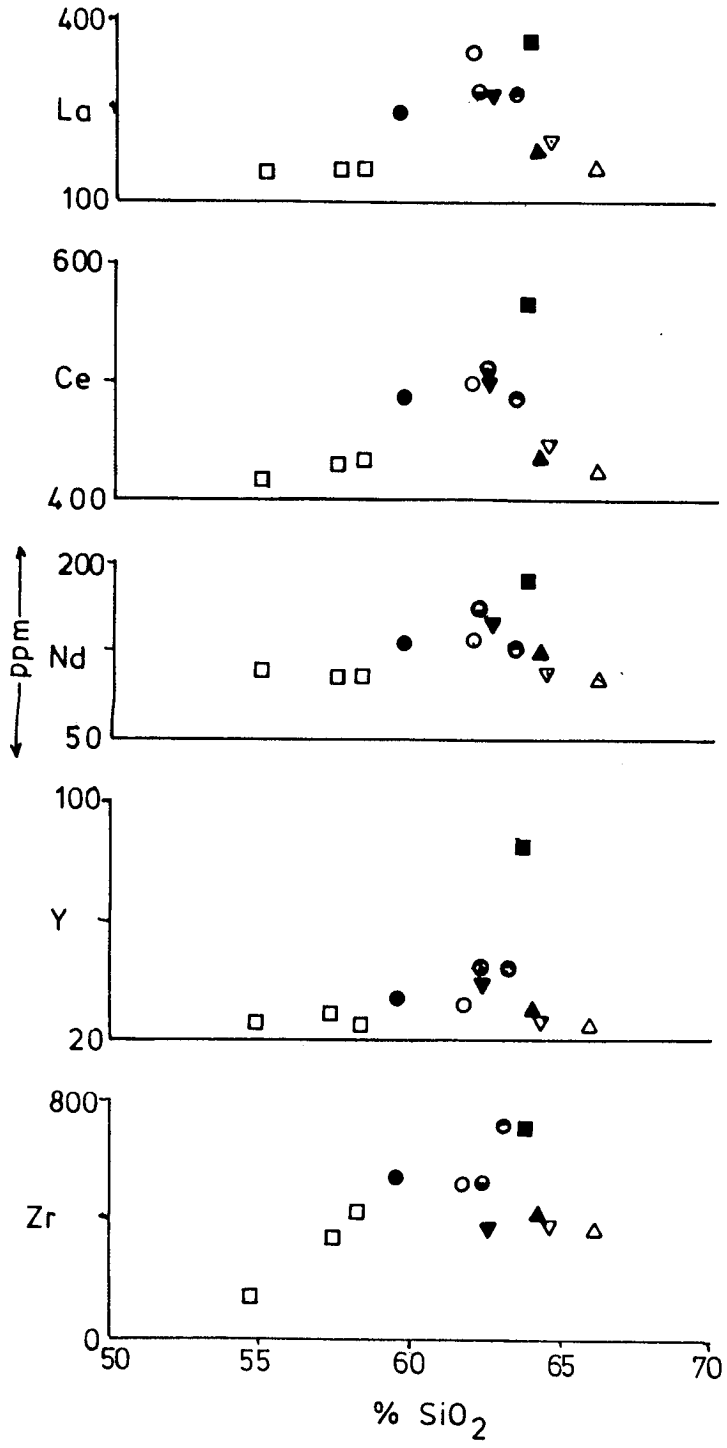

Fig. 6.5 Trace element variation in the Sinda syenites.

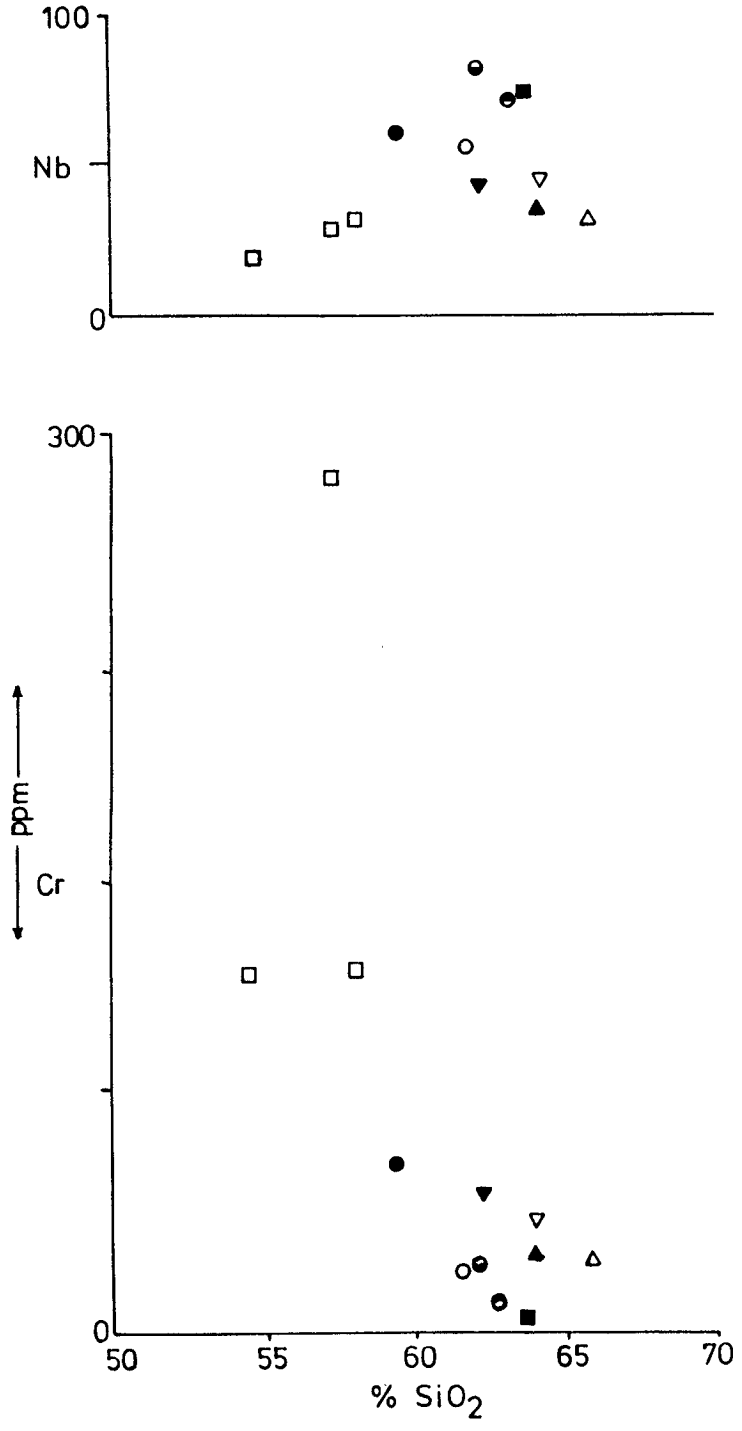

Fig. 6.5. Trace element variation in the Sinda syenites. (contd.)

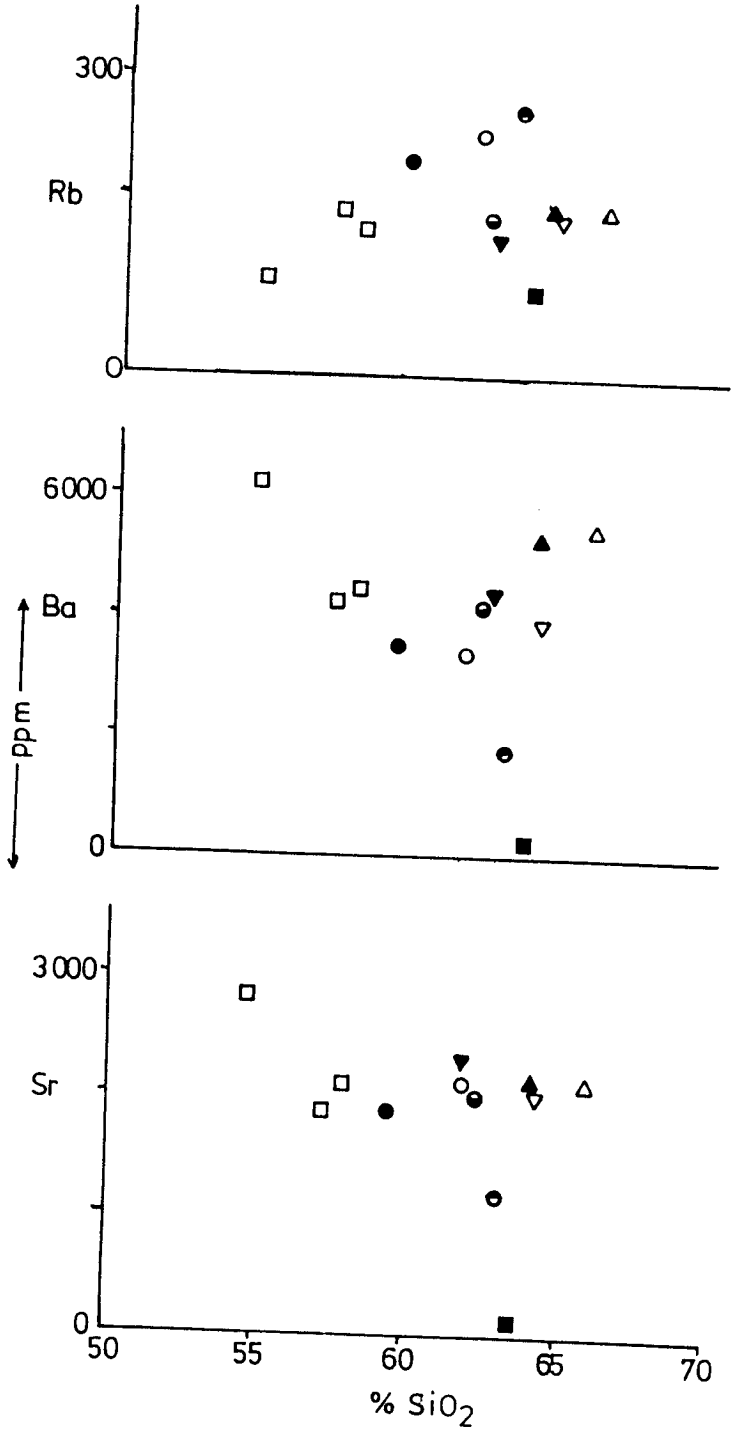

Fig. 6.5 Trace element variation in the Sinda syenites. (contd.)

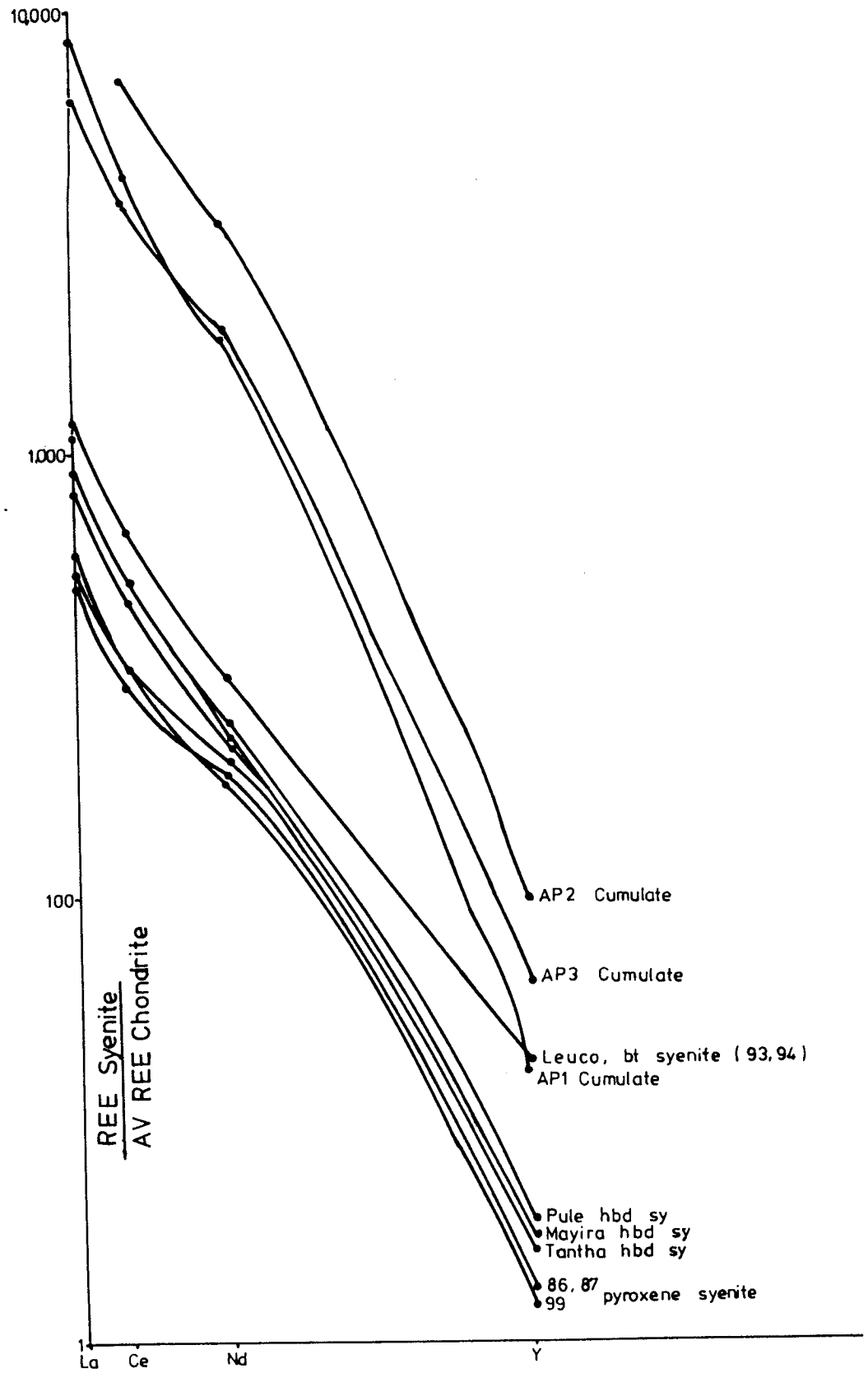

Fig. 6.6 Chondrite normalised REE diagram for the Sinda syenites

The high field strength elements (Zr, Nb and Y) show a positive correlation with each other increasing with higher SiO_2 contents except in the Pule and Tantha intrusions where they show the reverse. Zr, Nb and Y do not readily substitute for the major elements because of their relatively high ionic potentials, hence they usually concentrate in residual liquids (56). The opposite trend seen in the two southern intrusions requires attention.

6.5 Petrogenesis.

The Sinda syenites show systematic chemical variations which define smooth trends on variation diagrams (Figs.6.2-6.5) suggesting that the intrusions are related.

Chemical trends in igneous rocks are commonly considered to represent chemical evolution of magmas as they undergo differentiation, forming the well known liquid line of descent.

In plutonic igneous rocks, whose magmas are rarely completely liquid (74), variation trends do not necessarily represent a liquid line of descent, but rather reflect compositional changes in the magma as a result of a variety of processes. The three main processes which may lead to the development of variation trends in plutonic rocks are i) fractional crystallization ii) crystal-liquid mixing and iii) magma mixing or assimilation. In the case of fractional crystallization, the variation trends which develop may reflect evolution of the magma and resulting compositional changes in the crystalline assemblages in equilibrium with successive liquids. The successive rock compositions along the trends will therefore reflect different crystalline assemblages.

Where crystal-liquid processes dominate, the trends may represent a mixing line betwen the liquid and a crystalline assemblage in which case successive rock compositions reflect the mixture of liquid and crystals in different proportions.

Chemical trends which result from the processes of magma mixing or assimilation likewise represent a mixing line between the magmas which have mixed or between magma and assimilated material, whilst the rocks show the proportions of the mixed phases.

The presence of two trends, one defined by rocks from the Lusandwa and Mayira intrusions and the other by rocks from the Pule and Tantha intrusions, in the variation diagrams of the Sinda syenites may be due to the operation of any two of the above mentioned processes. However, the diverging trends and the sharp kinks which are notable in the trace element trends may also arise solely as a result of fractional crystallization due to changes in the crystallizing assemblages. In contrast, the development of diverging trends solely as a result of either mixing or assimilation is difficult to imagine.

In either case, the overlap of SiO_2 values for compositions above 62% SiO_2 comprising the entire range of the Pule and Tantha intrusions suggests that their magmas evolved separately. The two trends may therefore represent separate batches of magma or one batch of magma from which the Pule and Tantha magmas became separated.

In the Lusandwa and Mayira intrusions, both major and trace element chemistry favour an evolution by fractional crystallization.

Major element variation, characterized by a systematic decrease in the ferromagneisan elements - Mg, Fe, Ti and (Ca) and an increase in the alkali elements - Na, K and, (Al) with increasing SiO_2, is typical of fractional crystallization in which the most SiO_2 rich rocks are the most fractionated.

Trace element behaviour, especially the exponential decrease of Cr with increasing SiO_2 (Fig. 6.5), is a strong indicator of crystal liquid fractionation involving ferromagnesian minerals with high crystal-liquid partition coefficients for Cr such as spinel, olivine and pyroxene. Similarly the general increase in the incompatible elements Rb, La, Ce, Nd, Y, Nb and Zr (Fig. 6.5) is typical of magma undergoing fractional crystallization. These elements do not substitute readily for any major element because of the low or high field strength of their ions and therefore concentrate in the residual liquid during crystallization.

Despite being considered as LIL (Large Ionic Lithophile) patterns of Ba and Sr contrast sharply with the other incompatible elements. The rapid decrease with SiO_2 and the kinks shown by both elements (Fig. 6.5) is typical of fractional crystallization involving alkali feldspar. In most magmas, Ba and Sr concentrate in the residual liquid until when alkali feldspar begins to crystallize, and then decrease rapidly due to the high partition coefficient of these elements in alkali-feldspar (56). Typical KD values for Ba and Sr in K-feldspar in a ryholitic liquid are 2.7-12.9 for Ba and 3.6-26 for Sr (76).

Quantitatively, the average Ba and Sr contents of 3700 ppm and 1800 ppm respectively in all but the leucosyenites of the Lusandwa intrusion are substantially higher than the average concentration of 1600 ppm Ba and 200 ppm Sr in the average syenite (57). This indicates that the rock compositions reflect crystal-liquid equilibria and that the rocks mainly consist of the crystalline assemblage with a minor admixture of trapped liquid.

Chemical variation among the major elements in the Pule and Tantha intrusions may also be explained by fractional crystallization. The major element trends, characterized by decreasing Mg, Fe, Ti, Ca and P with increasing SiO_2 are comparable to

the Lusandwa and Mayira trends but with a slightly different crystallizing assemblage. The opposed trace element trends are however difficult to explain in terms of fractional crystallization although the decreasing Rb, La, Ce, and Nd may conceivably represent increasing KD values due to low crystallization temperatures (97). The decreasing Nb, V and Zr contents with differentiation may reflect crystallization of minor phases such as sphene and zircon which are ubiquitous in the syenites.

The increase of Ba and Sr, and their high absolute concentrations suggest alkali feldspar accumulation although this is difficult to reconcile with the decreasing Na and Al contents. However, the decrease in Na and Al may reflect the removal of albite, that is a change to crystallization of two feldspars, as seen in thin section.

In an attempt to determine the proportions of the crystallizing assemblages, inspection of the Harker diagrams shows that the initially crystallizing assemblage for the Lusandwa and Mayira trend must satisfy the following chemical requirements: SiO_2 - 55%, TiO_2 - 1.5%, Al_2O_3 - 15%, FeO - 8% , MgO - 5%, CaO - 7%, Na_2O - 3%, K_2O - 4% and P_2O_5 - 1%. For the more evolved rocks of the Lusandwa and Mayira intrusions and for the Pule and Tantha intrusions, the corresponding values are: SiO_2 - 58%, TiO_2 - 1.5%, Al_2O_3 - 16%, FeO - 6%, MgO - 3%, CaO - 4%, Na_2O - 5%, K_2O - 7% and P_2O_5 - 0.5%.

On the basis of these chemical constraints, possible crystallizing assemblages which may explain these trends can be calculated. The first composition corresponds to a crystallizing assemblage of 55% alkali feldspar, 35% clinopyroxene, 2.5% apatite and 0.5% magnetite (Fig. 6.7). /The Second composition may be modelled either by increasing the proportion of alkali feldspar to 75% and reducing clinopyroxene (20%), apatite (1.5%) and magnetite (0.3%) or by change in the crystallizing assemblage to alkali feldspar (70%), hornblende (25%),

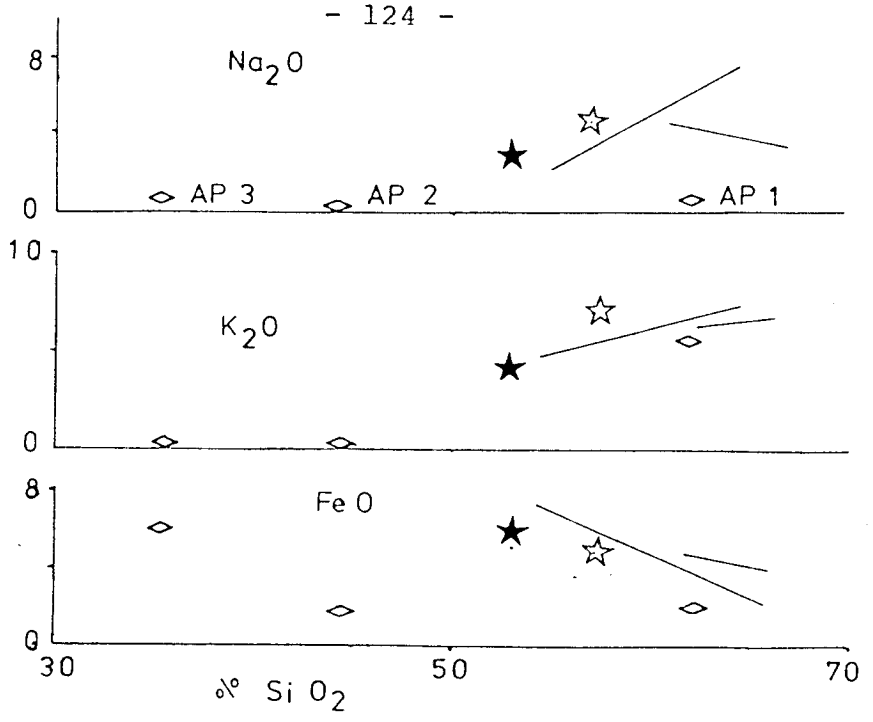

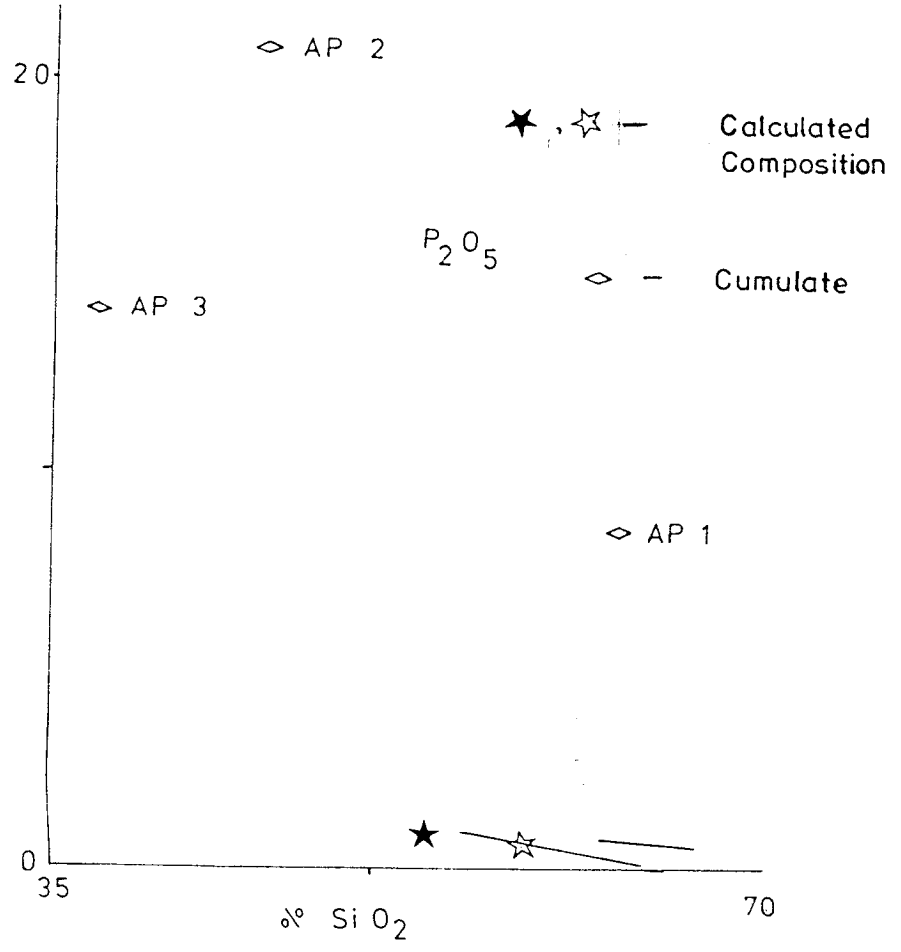

Fig. 6.7

Calculated chemical parameters to explain the variation trends observed in the Sinda syenites

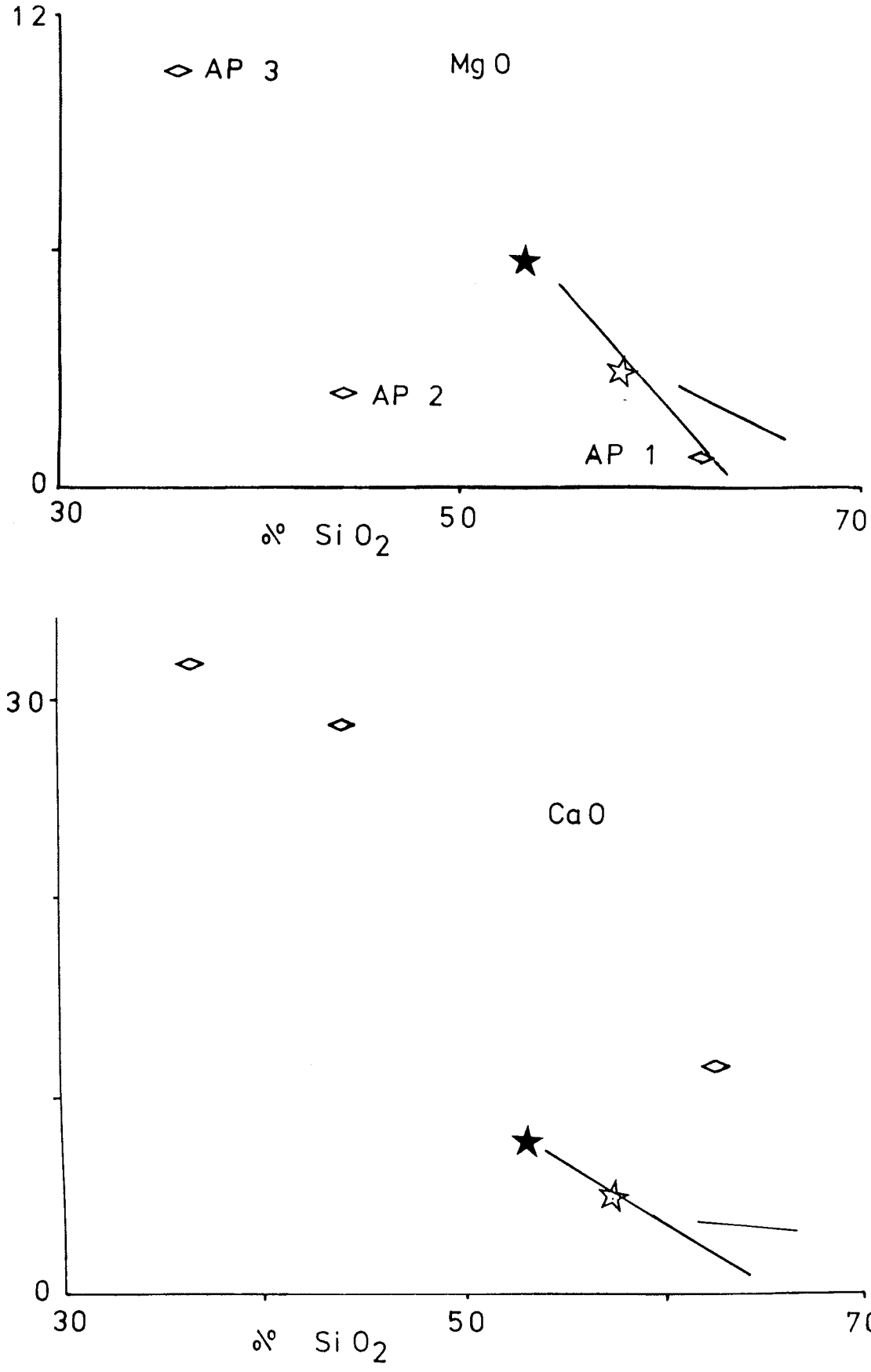

Fig. 6.7 (contd.) Calculated chemical parameters to explain the variation trends observed in the Sinda syenites.

apatite (0.3%) and sphene (3%) (fig. 6.7).

The trace element data for the Lusandwa and Mayira intrusions are consistent with fractional crystallization involving alkali feldspar, clinopyroxene, apatite and magnetite. The previously mentioned exponential decrease of Cr may be attributed to the crystallization of pyroxene and magnetite for which crystal/liquid K_D values of 90 and 50 respectively have been reported (76). The increase of the remaining trace elements reflect a bulk K_D of less than 1, consistent with apatite being the only crystallizing phase having high K_D values of any of the concerned elements.

The relatively slower decrease of Cr in the Pule and Tantha trend is explicable either by the crystallization of hornblende for which the K_D value is about 50 (77), or by a lower bulk K_D due to a smaller proportion of pyroxene and magnetite. The decreasing contents of the ferromagnesian elements remains difficult to explain although the decrease of REE, Zr, Nb and Y may be explained by crystallization of hornblende and sphene instead of pyroxene and apatite.

The apatite rich rocks were plotted onto the Harker diagrams to see how close they appproximate these compositions (Fig. 6.7) The two rocks AP2 and AP3 lie near the backward extension of the trends in accord with the previous conclusion that the trends represent crystallizing assemblages. Rock AP1 lies in the midst of the trends and is therefore an unlikely crystallizing assemblage to explain these trends.

From these diagrams, it is inferred that the apatite rich rocks, AP2 and AP3, do not in themselves represent the entire crystallizing assemblage but may form part of it. The interpretation of these rocks as part of the crystallizing assemblage and the layered nature of the rocks suggest that crystal sorting was involved in their formation and that they are cumulates resulting from gravitative differentiation of the

crystallizing assemblage. The low Fe^{2+}/Mg ratios and high Cr contents of the pyroxenes from these cumulates in comparison with the pyroxenes of the pyroxene syenites suggests that cumulation took place at an early stage of magma crystallization whilst the magma had a relatively low viscosity. Rock AP1 may represent a corresponding mixture of cumulate apatite and alkali feldspar formed by flow sorting of apatite and feldspar crystals or it may represent cumulate apatite in an evolved syenitic liquid. The high contents of Ba and Sr of 7,000 and 2,000 ppm respectively, low Rb(100 ppm) favour the former process.

The application of a crystal-liquid mixing model to explain the evolution of the Lusandwa and Mayira intrusions is rather difficult, firstly due to the kinks seen in the trends of Ba and Sr. Secondly the low Ba (1,700 ppm) and Sr (1,000 ppm) and high Rb (270 ppm) contents of the SiO_2 rich members suggests that the end members of this trend are dominated by residual liquid rather than accumulation of alkali feldspar. However, the relatively high Na_2O (3.62%), Ba (6,000 ppm) and Sr (3,000 ppm), and low Rb (140 ppm) of the most mafic pyroxene syenite (FTS99), suggests that this rock contains a high proportion of alkali feldspar to trapped liquid and that the scatter along the trends may be due to a limited degree of crystal-liquid mixing.

Whilst the crystal-liquid mixing model is unlikely to account for the element trends observed in the Lusandwa and Mayira intrusions, it can be considered a strong possibility to explain chemical variation in the Pule and Tantha intrusions.

Evidence for this is mainly provided by the unusual trace element trends. The inverse relationship with SiO_2 for most of the trace elements and the increasing Ba and Sr may reflect the mixing of a liquid rich in the incompatible elements and poor in Ba and Sr and a crystalline phase rich in Ba and Sr

but poor in the incompatible elements. Inspection of the Harker diagrams shows that alkali feldspar is the most likely mineral. However the analysed K-feldspar does not lie at the termination of this trend suggesting that a more SiO_2 rich phase is also involved. The only possible mineral is quartz, but its presence in the rocks as an interstitial mineral suggests that it crystallized from the liquid instead of being part of the crystalline phase interacting with trapped liquid.

Consideration of the magma mixing model for the Pule and Tantha trends shows that it may explain most of the element variations, but the Harker diagrams show that the mixing granitic liquid or crustal material would need to have practically no Al, La, Ce, Nd, Y and Nb at 74% SiO_2, a chemistry which would be unusual for a granite.

From a consideration of the three models, it is apparent that the magma mixing or assimilation model is least likely to have caused the chemical trends observed in the Sinda intrusions.

The crystal-liquid mixing model explains the aberrant variation observed in the Lusandwa and Mayira trend, and the chemical variation seen in the Pule and Tantha syenites. However, it does not adequately account for some element variations in the latter, namely the decreasing Al_2O_3 and Na_2O contents, both of which are major elements in alkali feldspar.

It thus appears that despite a few anomalies, the fractional crystallization model explain best most of the chemical variations observed in the Sinda syenite suite. It can also be concluded that crystal-liquid mixing was operative during crystallization but was subordinate to fractional crystallization.

If fractional crystallization is accepted to have been the main cause of element variation in the syenites, then both chemical and petrographic data indicate that the presence of two trends in the suite is due to different crystallizing mineral assemblages caused by changes in the conditions of crystallization. The Lusandwa and Mayira syenites both have an anhydrous high temperature mineralogy whilst both the Pule and Tantha syenites have a hydrous low temperature assemblage, suggesting different physical conditions during their crystallization.

To explain this, it may be of significance to note that both the Lusandwa and Mayira intrusions are diapiric, plug-like intrusions, the Lusandwa intrusion more so than the Mayira intrusion, whilst both the Pule and Tantha intrusions are sills. This implies emplacement of the Pule and Tantha magmas at higher structural levels which would have the tendency of reducing the total load pressure but increasing the H_2O pressure relative to the total pressure hence promoting the crystallization of hydrous phases.

The strong petrological relationship between the intrusions suggests that their parental magma evolved within a single, slowly crystallizing, magma chamber which was possibly located in the lower crust (Fig. 6.8). Tectonic disturbances related to regional metamorphism or orogenesis caused its remobilisation with most of its mass being emplaced as a diapir at a relatively high structural level whilst smaller batches of magma separated from it and were intruded along high level fractures as sills.

The disturbance of the crystallisation of the parental Sinda syenite magma may possibly have been caused by the influx of SiO_2 rich volatiles released during the solidification of the batholithic Sinda granites, thus explaining the hydrous crystallisation within the Pule and Tantha intrusions and the high SiO_2 required to satisfy the crystal-liquid mixing model.

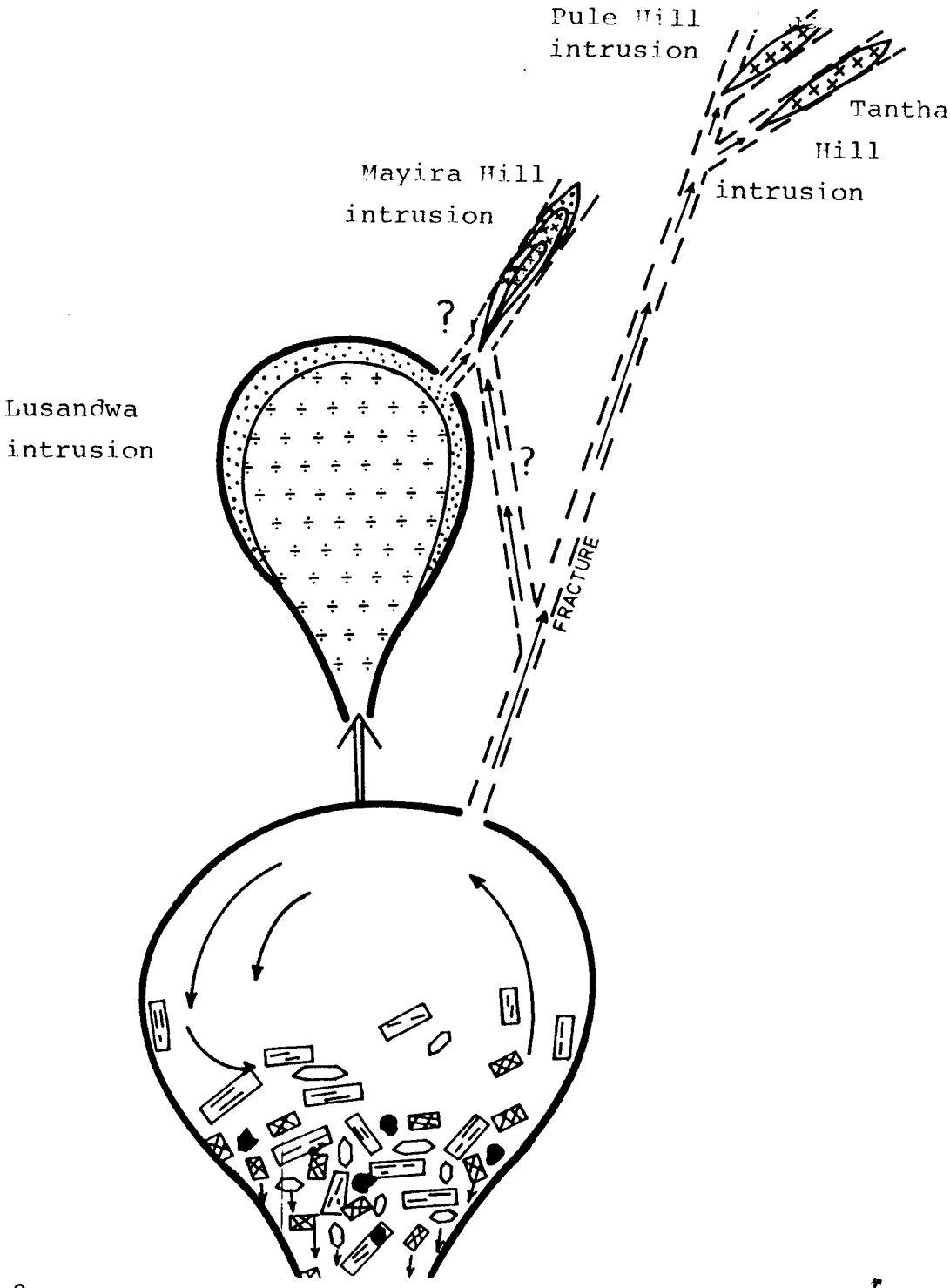

Fig. 6.8 Possible mechanism of emplacement of the Sinda syenites

6.6 Chemical variation in the Lunkhwakwa and Bandawe syenites.

Chemically, the Lunkhwakwa and Bandawe intrusions consist of mildly potassic oversaturated syenite and a sodi-potassic undersaturated syenite. The two intrusions display smooth, well defined chemical trends the Bandawe syenite more so than the Lunkhwakwa syenite in which the individual data points show some scatter along a general trend (Fig. 6.9).

The most notable difference between the two intrusions is the range in their SiO_2 contents. The Bandawe syenite has SiO_2 contents between 52% and 60% whilst the SiO_2 range of the Lunkhwakwa syenite is from 60% - 65%. Apart from the difference in SiO_2, the Bandawe syenite is notably higher in Al_2O_3, Na_2O and TiO_2 and lower in MgO, FeO, CaO, K_2O and P_2O_5 at 60% SiO_2 (Fig. 7.3). However, the two intrusions have comparable trace element contents except for Sr, Cr and Nb which are higher in the Lunkhwakwa syenite. These chemical features do not provide any immediate reason to consider the intrusions related and accordingly, they will be treated separately.

Lunkhwakwa syenite

6.1 Major elements

Major element variation in the Lunkhwakwa syenite is characterized by a systematic decrease in MgO, FeO and CaO up to about 63% SiO_2 after which they remain constant with increasing SiO_2.

TiO_2 shows a similar variation as the other ferromagnesian elements except for three analyses which have very low contents. P_2O_5 shows a scattered decrease with increasing SiO_2, (Fig. 6.9). The alkali elements Na_2O and K_2O

Table 6.3 Whole rock major and trace element analyses of the Chipata syenites.

	1	2	3	4	5	6	7	8	9
	FTS/29	/2	/37	/16	/13	/5	/30	/44	/6
SiO_2	59.10	60.28	60.63	61.64	61.73	62.43	62.86	62.88	63.24
TiO_2	.60	.22	.22	1.06	.14	.70	.67	.41	.38
Al_2O_3	11.60	13.30	16.75	15.33	16.00	18.29	17.15	17.39	18.47
Fe_2O_3	3.89	3.90	2.73	1.98	2.06	1.96	1.73	2.40	3.15
FeO	3.99	3.10	2.46	1.60	1.37	1.27	1.16	.52	.47
MnO	.41	.39	.11	.14	.09	.09	.09	.07	.11
MgO	2.25	1.81	1.85	2.15	1.12	.67	.80	.85	.23
CaO	7.42	5.78	3.14	5.03	4.36	2.06	2.71	2.38	1.24
Na_2O	3.99	3.89	4.66	3.78	5.11	4.88	4.69	4.85	5.93
K_2O	5.96	6.90	6.13	7.76	6.54	7.56	8.08	7.87	6.75
P_2O_5	.79	.43	.47	.44	.54	.12	.31	.32	.04
FeOT	7.49	6.61	4.92	3.38	3.22	3.03	2.72	2.68	3.30
$\frac{FeOT}{FeOT+MgO}$	.77	.79	.73	.61	.74	.82	.77	.76	.93
$\frac{FeO}{Fe_2O_3}$	.97	1.26	1.11	1.24	1.50	1.54	1.49	4.62	6.70
LoI	.56	.60	.70	.51	1.96	.80	.34	.47	.33
Tot	98.88	98.76	98.69	97.68	98.11	98.51	98.49	98.09	98.55
Rb	135	101	250	112	93	240	113	132	128
Ba	2580	2110	3040	14000	6000	2360	5460	6770	1710
Sr	737	1890	1710	2920	4900	1350	5630	5530	2730
La	937	228	337	68	267	251	153	155	421
Ce	1210	382	448	104	457	387	291	260	461
Nd	576	197	150	108	179	123	128	129	130
Y	175	84	42	23	39	42	24	25	51
Zr	225	553	610	30	330	677	148	233	923
Nb	253	86	78	19	95	81	78	62	101
Cr	20	8	26	7	3	11	8	7	6
Ga	22	24	23	15	19	22	17	22	17

Table 6.3 contd.

	10	11	12	13	14	15	16	17
	/40	/29B	/4B	/47	Mean	/72	/70	/69
SiO_2	63.39	64.06	64.97	68.20	62.88	52.72	54.96	55.65
TiO_2	.53	.46	.43	.04	.59	1.81	1.30	1.23
Al_2O_3	16.06	17.00	17.31	15.28	16.99	17.46	18.80	18.90
Fe_2O_3	2.32	1.59	1.58	1.88	2.05	4.45	2.89	2.64
FeO	1.29	1.04	.89	.61	1.25	3.55	3.24	3.30
MnO	.09	.07	.09	.13	.09	.14	.14	.15
MgO	.85	.65	.50	.51	.91	3.12	2.19	2.02
CaO	2.49	2.19	1.30	1.26	2.58	5.33	4.11	3.74
Na_2O	5.93	5.27	6.05	5.21	5.18	4.53	5.59	5.39
K_2O	6.74	7.50	6.82	6.71	7.16	5.40	5.78	6.10
P_2O_5	.29	.16	.07	.17	.29	1.48	.99	.86
FeOT	3.38	2.47	2.31	2.30	3.09	7.55	5.84	5.68
$\frac{FeOT}{FeOT+MgO}$	.80	.79	.82	.82	.78	.71	.73	.74
$\frac{Fe_2O_3}{FeO}$	1.80	1.53	1.78	3.08	1.88	1.25	.89	.80
LoI	.23	.37	.52	.47	.67	1.20	.93	.77
Tot.	98.85	98.22	98.52	98.92	98.43	98.60	98.72	98.11
Rb	123	117	106	145	147	121	134	177
Ba	3090	5340	1640	1710	4213	5300	4450	3380
Sr	1330	2220	1480	485	3019	3200	3060	2600
La	113	124	210	151	201	207	221	218
Ce	193	213	260	159	314	342	333	337
Nd	79	104	132	93	128	142	126	121
Y	28	27	47	33	34	29	29	31
Zr	290	453	290	54	380	218	415	510
Nb	79	52	122	22	81	33	70	90
Cr	10	5	7	8	10	8	10	7
Ga	24	17	22	22	21	20	22	21

Table 6.3 contd.

	18	19	20	21	22	23	24
	FTS/62	/73	/63	/66	/58	/61	Mean
SiO_2	55.96	56.98	57.75	59.28	59.72	59.70	56.62
TiO_2	1.49	1.42	1.45	1.20	.38	1.29	1.40
Al_2O_3	18.94	17.56	17.84	17.73	17.28	17.58	18.10
Fe_2O_3	2.85	3.12	3.29	2.55	1.61	2.53	3.04
FeO	3.06	2.70	2.57	2.06	1.39	2.38	2.86
MnO	.14	.16	.16	.14	.17	.15	.14
MgO	2.21	2.14	2.12	1.63	2.48	1.69	2.14
CaO	4.37	3.76	3.12	3.00	5.98	2.90	3.79
Na_2O	5.92	5.38	5.41	6.24	5.09	5.58	5.50
K_2O	4.28	5.96	5.59	5.64	5.25	5.65	5.60
P_2O_5	.79	.80	.68	.54	.65	.55	.84
FeOT	5.62	5.51	5.53	4.35	2.84	4.66	5.59
$\frac{FeOT}{FeOT+MgO}$	.72	.72	.72	.73	.53	.73	.72
$\frac{Fe_2O_3}{FeO}$	.93	1.16	1.28	1.24	1.16	1.06	1.08
LoI	.65	.80	.67	.86	1.64	.76	.83
Tot.	98.69	98.90	98.57	99.28	99.04	98.64	98.69
Rb	79	194	119	138	64	131	137
Ba	6300	3160	5080	4010	2980	4250	4491
Sr	2090	1770	1230	1180	1640	1200	2041
La	164	255	174	159	150	165	195
Ce	263	415	279	267	243	256	311
Nd	128	156	126	109	114	111	127
Y	37	44	39	39	36	43	36
Zr	143	534	239	352	75	469	360
Nb	34	85	48	66	66	43	59
Cr	3	7	5	7	5	3	6
Ga	21	22	20	19	18	21	21

Analyses:

1 - 9,	Pyroxene syenite, Lunkhwakwa syenite
10-12,	leucocratic syenite, "
13 ,	average composition of the syenite
15-23,	nepheline syenite, Bandawe syenite
24 ,	average composition of the syenite.

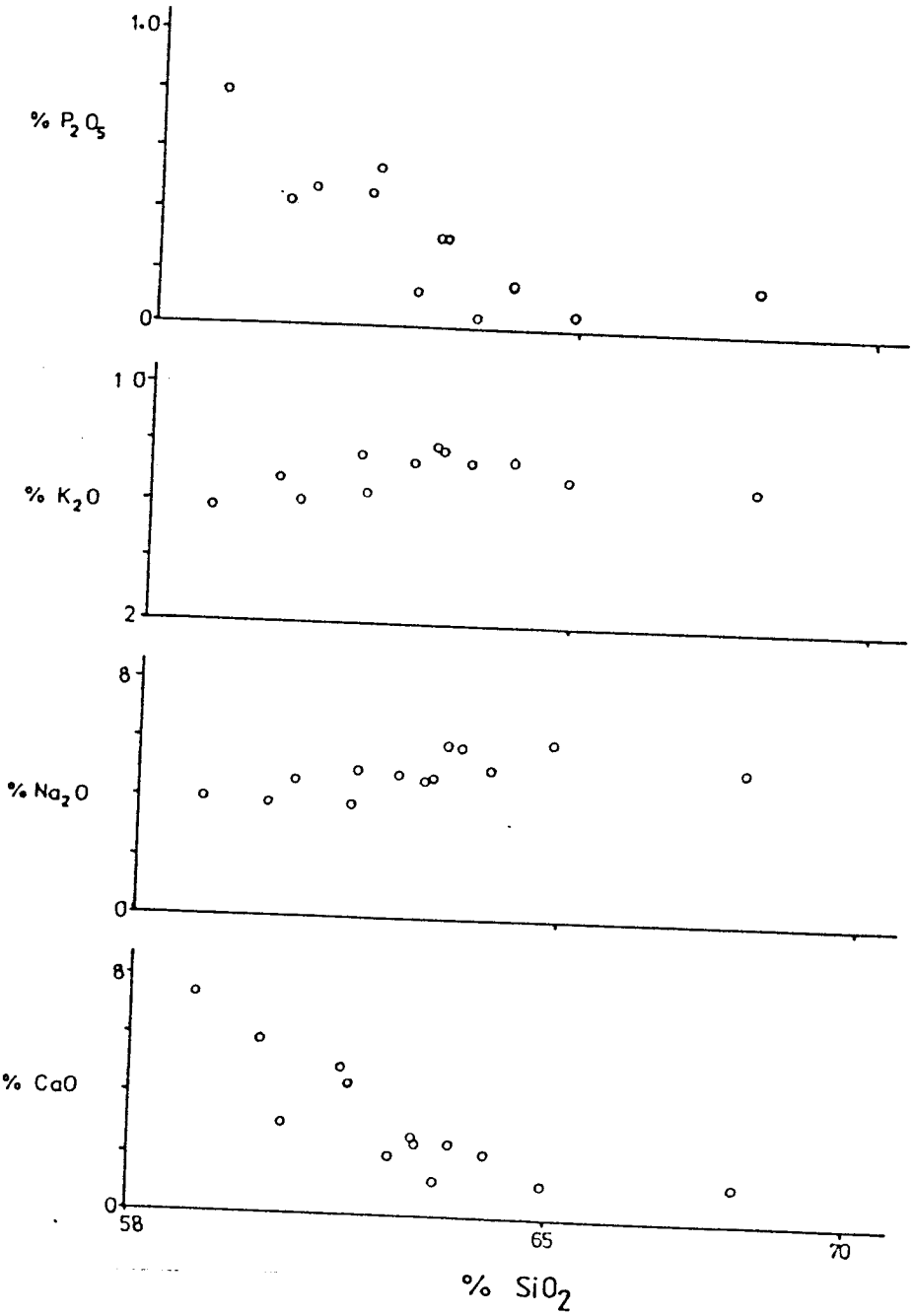

Fig. 6.9a. Harker variation diagrams for the Lunkhwakwa syenite . Circle;syenite.

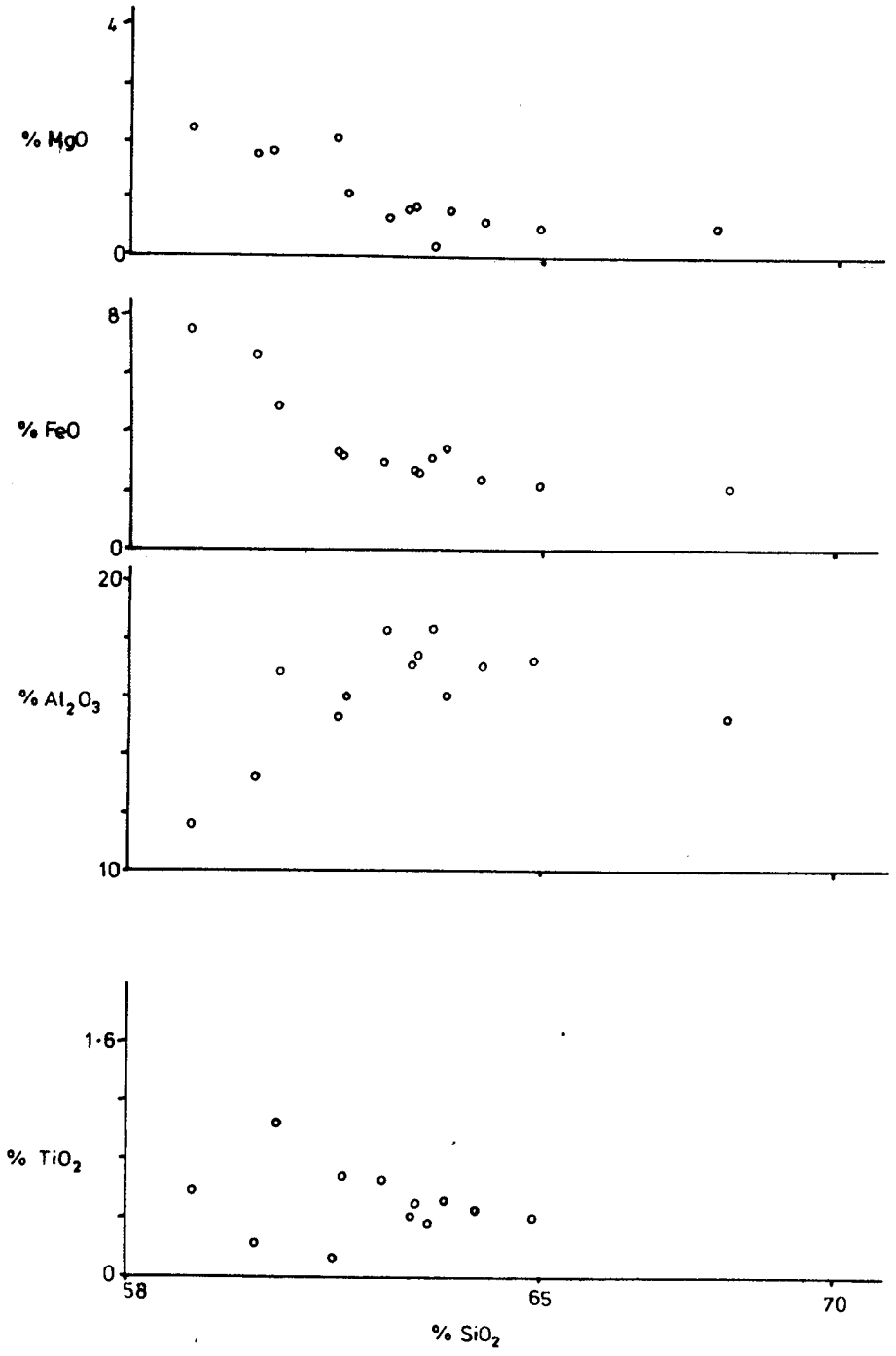

Fig. 6.9a. (contd.) Harker variation diagrams for the Lunkhwakwa syenite.

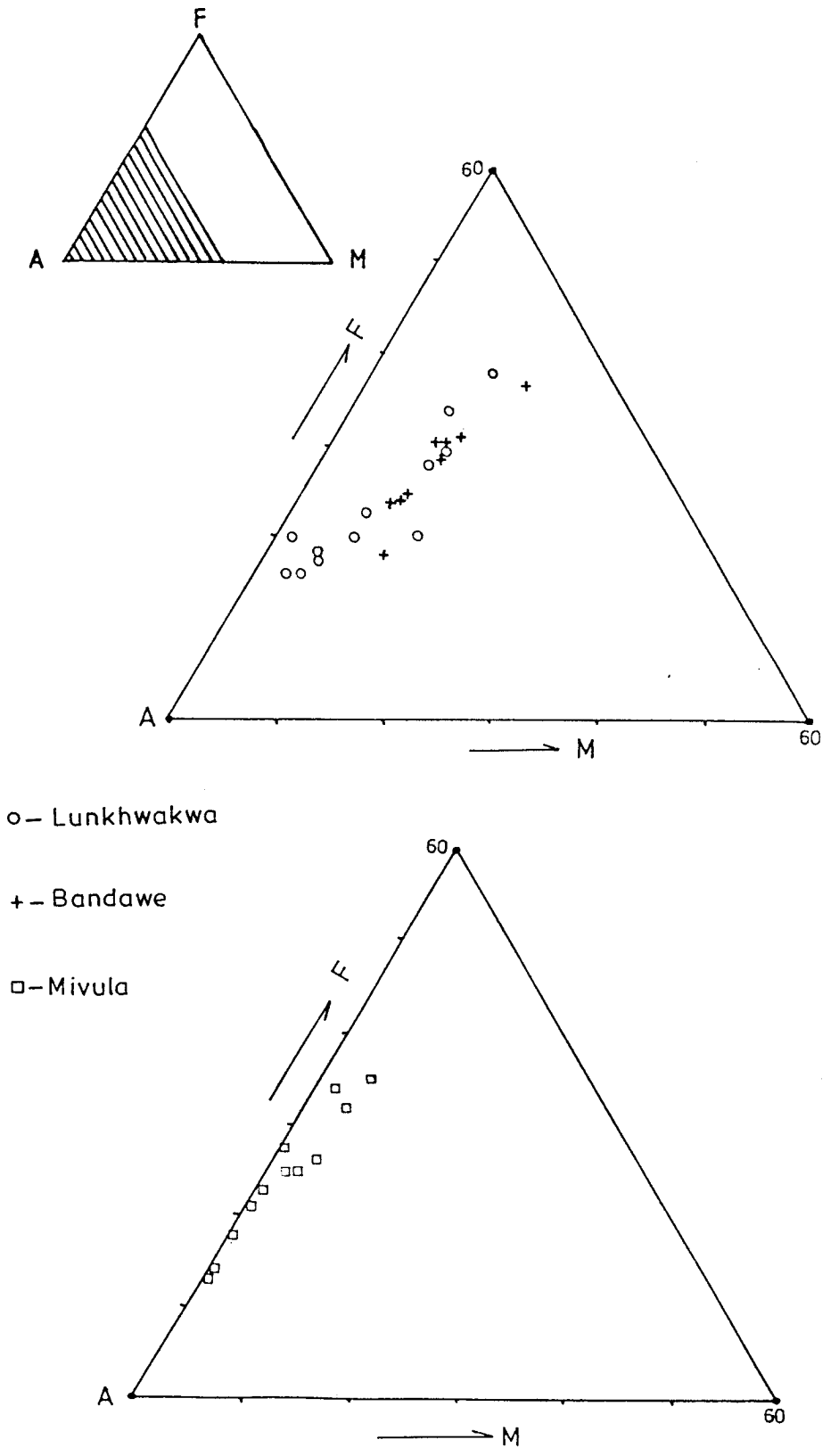

Fig. 7.0 Triangular diagrams for the Lunkhwakwa, Mivula and Bandawe syenites.

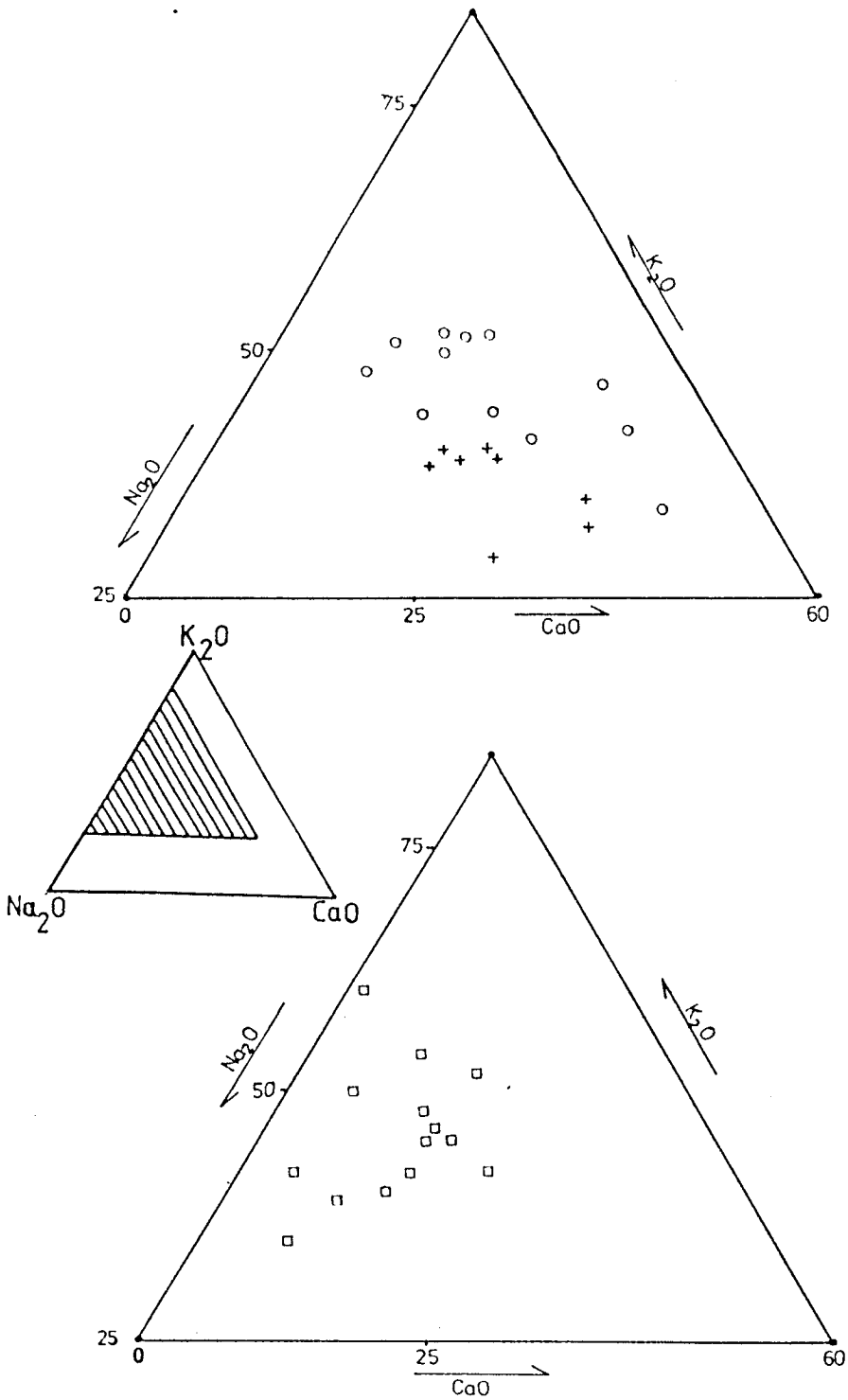

Fig. 7.0 Triangular diagrams for the Lunkhwakwa, Mivula and
(contd.) Bandawe syenites

show a corresponding systematic increase until at SiO_2 63% after which they decrease whilst Al_2O_3 behaves similarly but with scatter at the inflection point. The Na_2O - K_2O - CaO diagram shows some scatter but suggests a trend which swings towards Na-enrichment. (Fig. 7.0)

6.6.2 Trace elements.

Throughout most of the SiO_2 range, there is little variation in most trace elements except for Ba, Sr and Zr (Fig. 7.1a).

The chromium content of the Lunkhwakwa syenite is relatively constant at about 8 ppm except for samples 29 and 37 which contain higher concentrations of 20 ppm and 26 ppm respectively (Table 6.3).

Most analysis define a smooth decreasing trend of the LIL elements Ba and Sr except for six samples - 13, 16, 29B, 30, 40 and 44 which are anomalously high in these elements. These samples have Ba and Sr contents higher by a factor of 3 than the other the samples.

Among the other group of LIL elements, Rb shows little variation with SiO_2 (Fig. 7.1a) whilst the LREE and Y define a slightly decreasing trend with little scatter in the individual data points. Exceptions are samples 5 and 37 which are high in Rb and sample 29 which is high in the LREE and Y. A chondrite normalised REE plot (Fig. 7.2) shows that the syenite has a fractionated REE pattern.

Despite having similar chemical properties, the two high field strength elements Nb and Zr differ markedly in their behaviour. Nb shows the same slightly decreasing

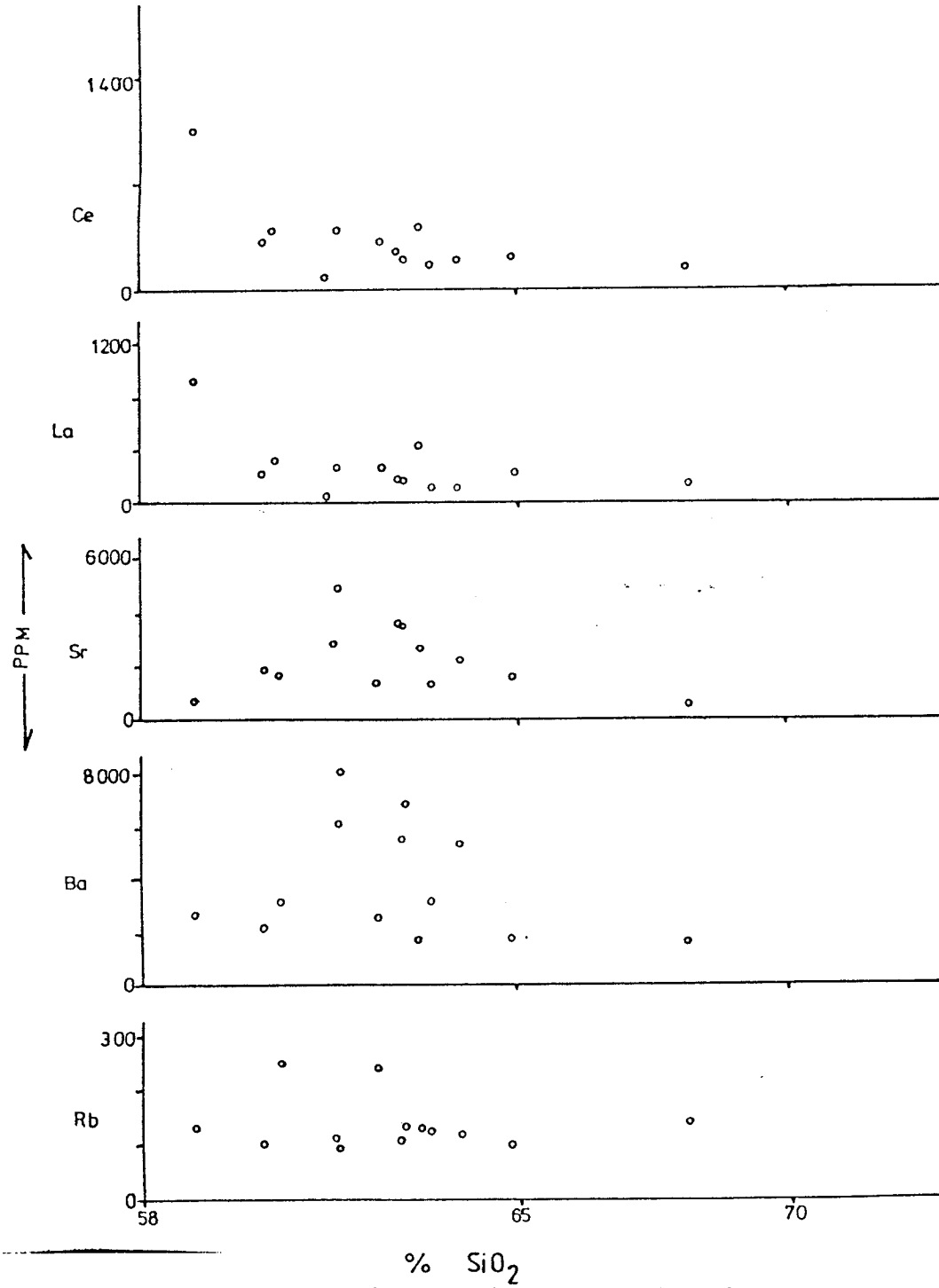

Fig. 7.1a. Trace element variation in the Lunkhwakwa syenite . o — Syenite.

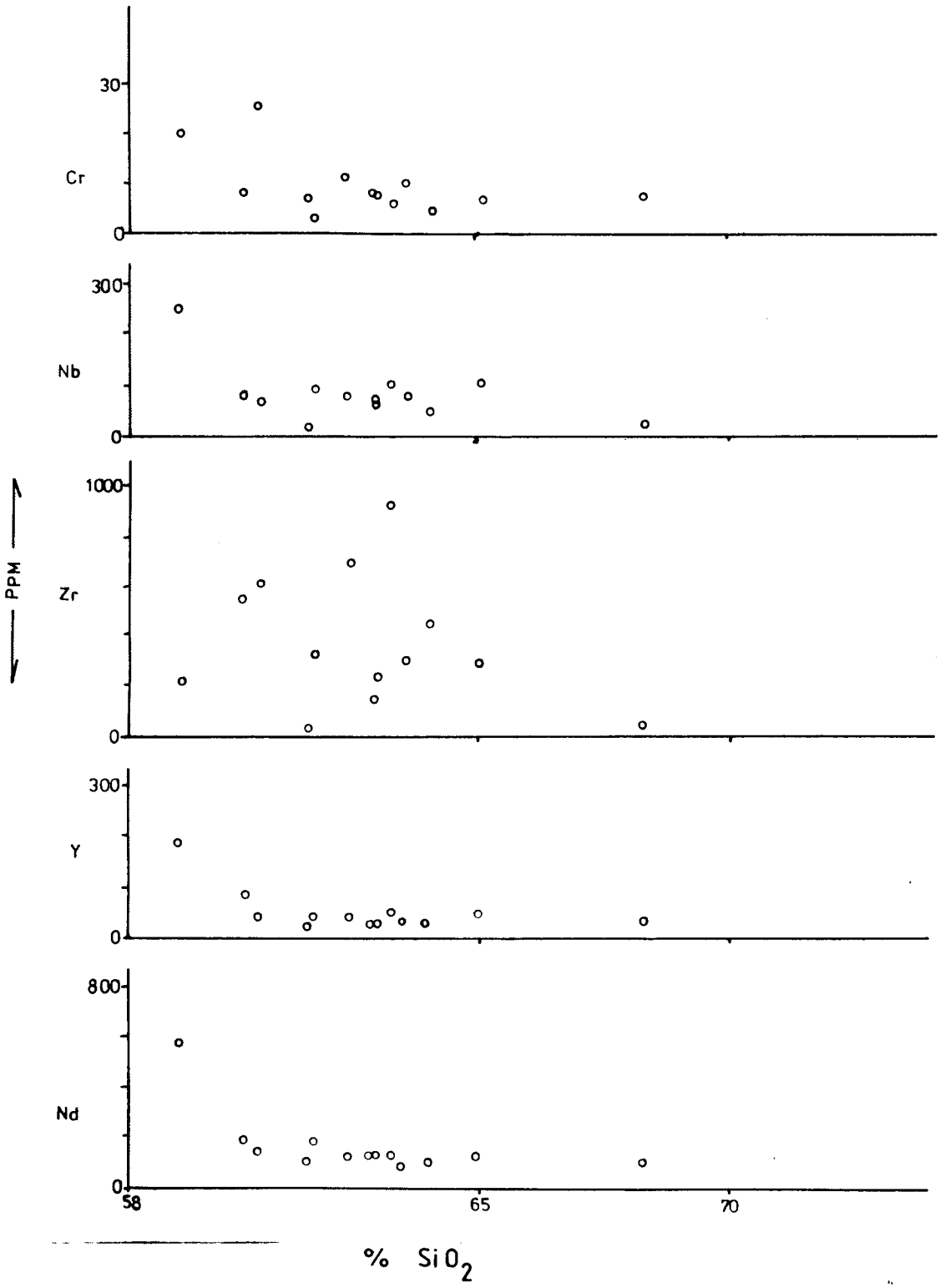

Fig. 7.1a.Trace element variation in the Lunkhwakwa syenite . (contd.)

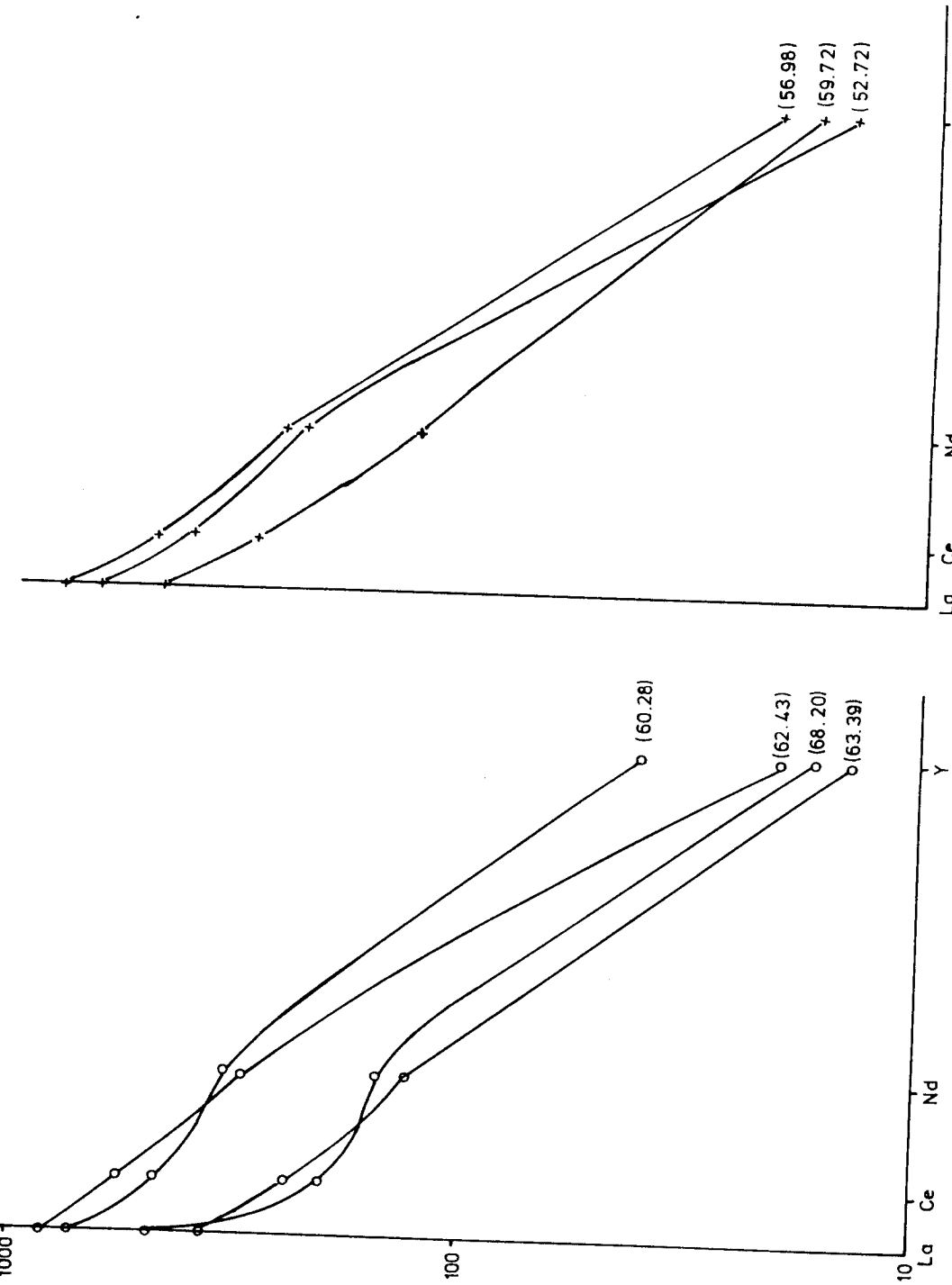

Fig. 7.2 Chondrite normalised REE diagrams for the Lunkhwakwa and Bandawe syenites.

trend with SiO_2 as the LREE whilst Zr shows a wide scatter and a poor correlation with SiO_2. The spread shown by Zr is however correlatable with the variation of Ba and Sr with samples high in Zr being low in both Ba and Sr and vice versa.

Bandawe syenite

6.6.3 Major elements

Chemical variation in the Bandawe syenite is characterized by a regular decrease in the major elements MgO, FeO, TiO_2, CaO and the minor element P_2O_5 with increasing SiO_2. However, one sample (FTC58) plots away from this trend being high in MgO, CaO and P_2O_5 and low in FeO and TiO_2. The alkali elements Na_2O, K_2O and (Al_2O_3) show a systematic increase up to about SiO_2 56% after which they decrease. Sample FTC58 is lower in Na_2O and K_2O and therefore plots slightly below these trends.

When plotted on the Na_2O - K_2O - CaO diagram, the analyses cluster in the centre of the diagram except for three samples which are higher in CaO.

6.6.4 Trace elements.

There is a slight variation in trace element contents within the SiO_2 range of the analysed samples except for Rb, Ba, Zr and to a lesser extent Nb and Cr. Sample FTC58 has lower contents of Rb, Ba and Zr than the rest.

Chromium shows a generally flat, decreasing trend with a slight scatter in the individual data points.

The LIL element Sr shows a systematic decrease whilst Ba and Rb both show a wide scatter with SiO_2. In general, the samples can be grouped into two, the first group which has relatively low SiO_2 contents has low Ba

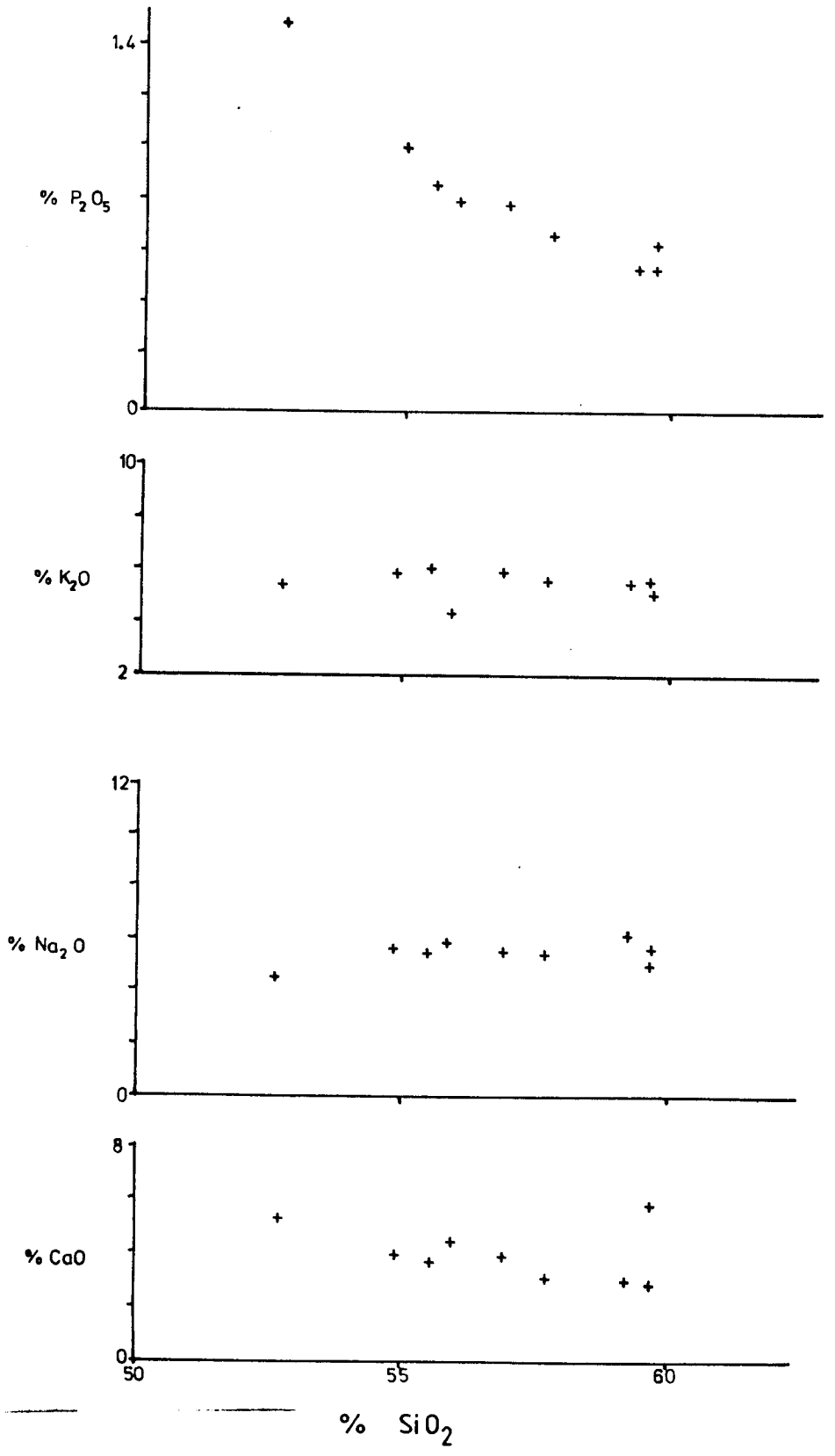

Fig. 6.9b. Harker variation diagrams for the Bandawe syenite. Cross; syenite.

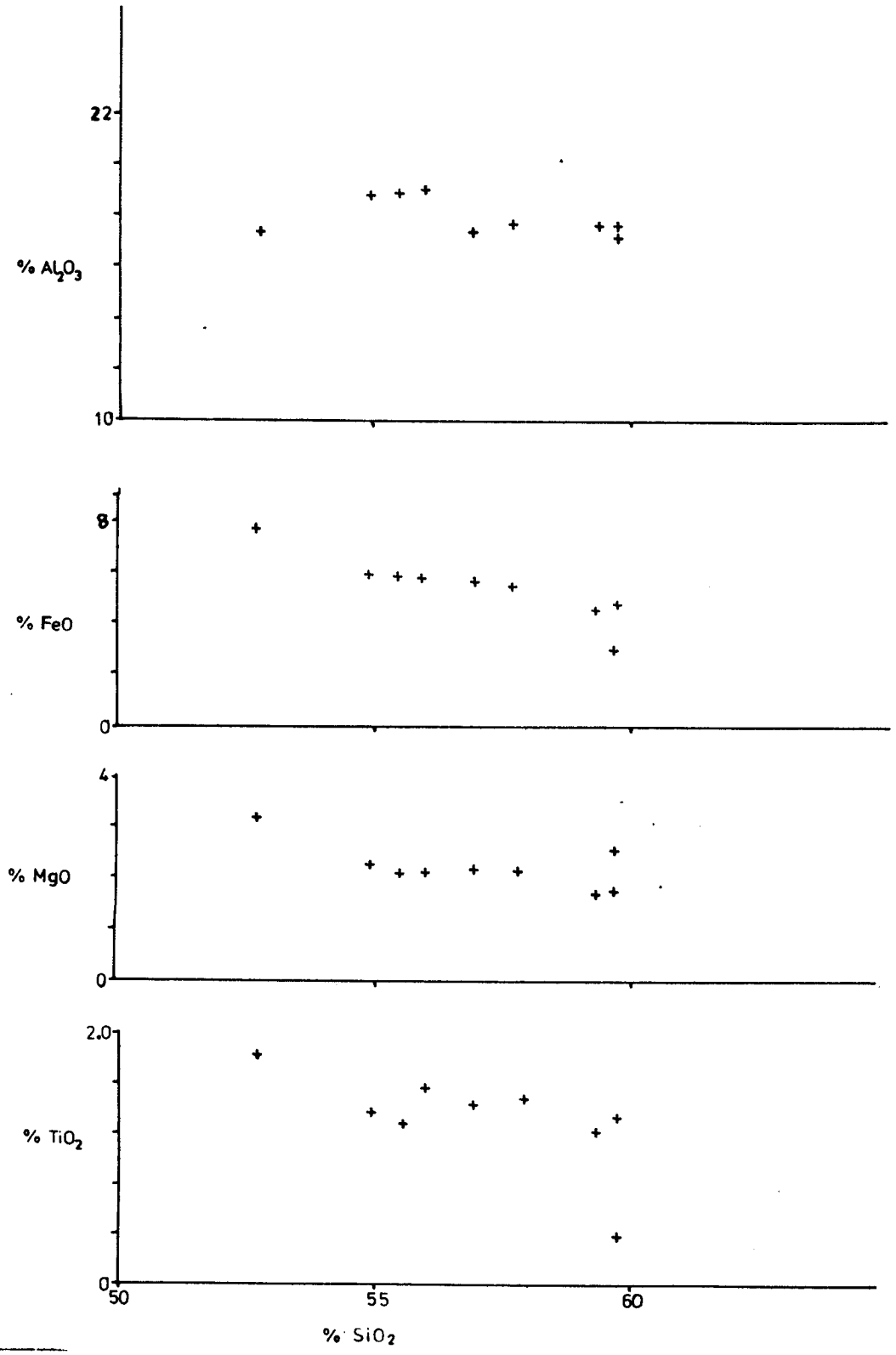

Fig. 6.9b. (contd.) Harker variation diagrams for and Bandawe syenite.

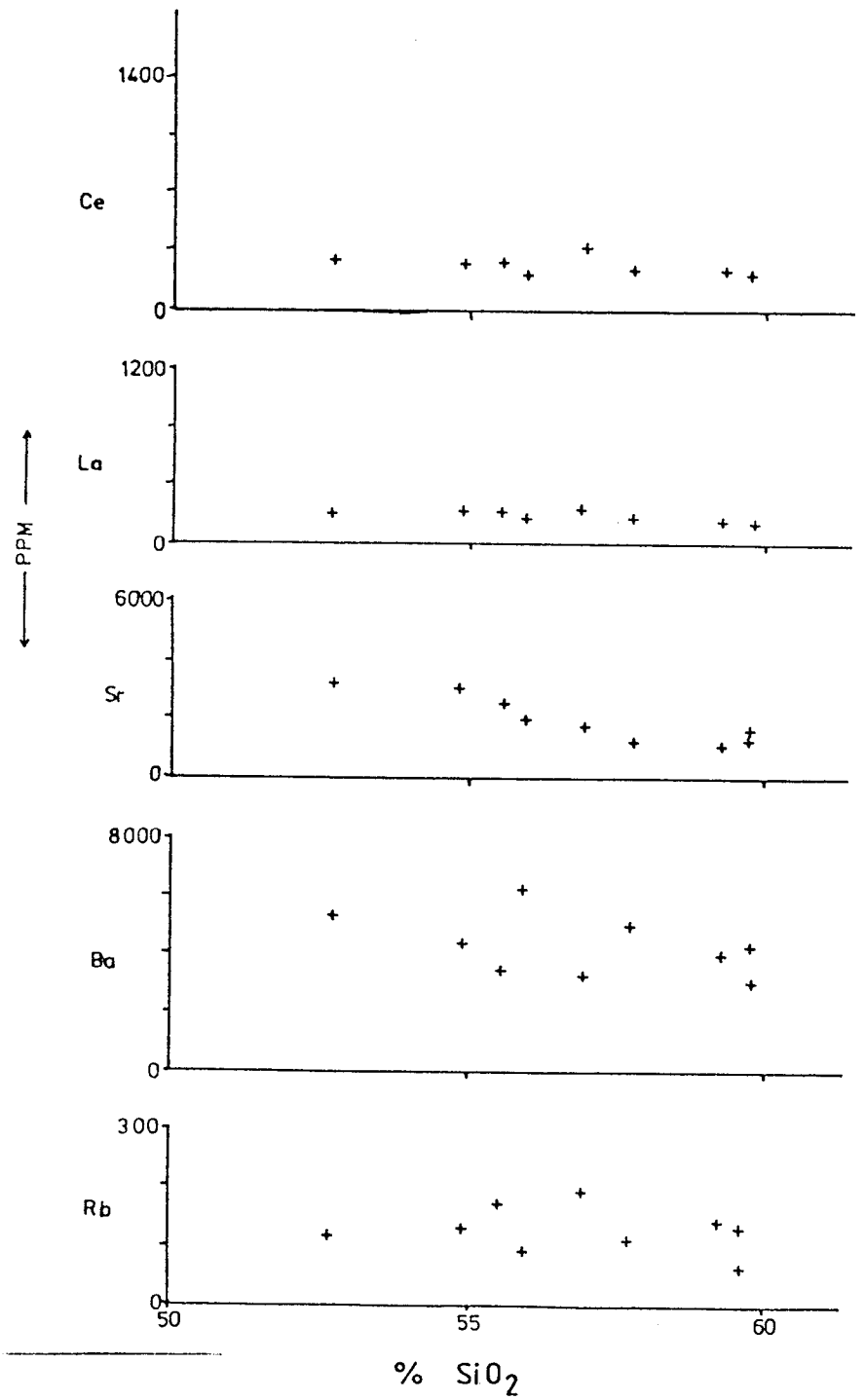

Fig. 7.1b Trace element variation in the Bandawe syenite. + — Syenite.

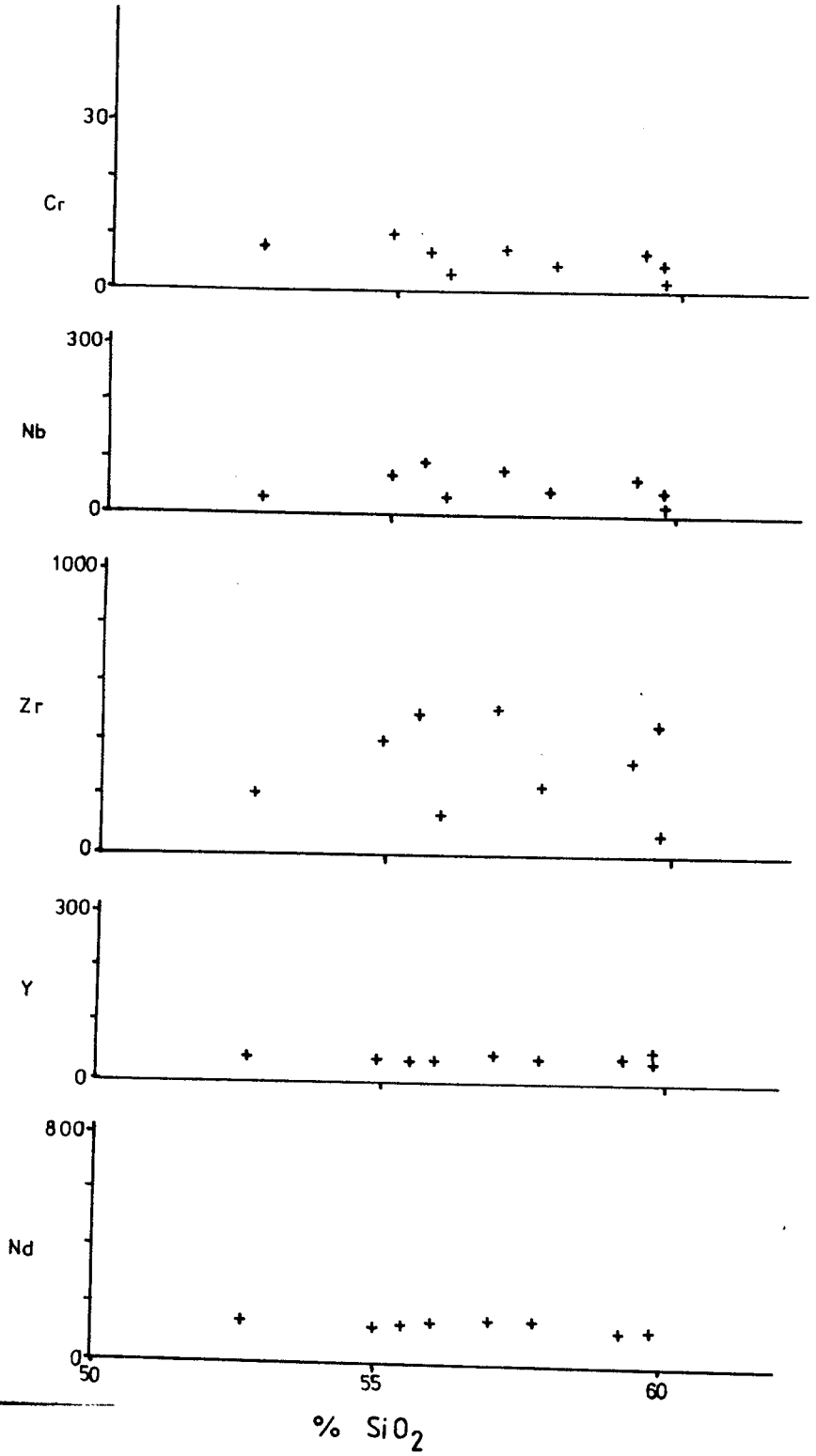

Fig. 7.1b. (contd.) Trace element variation in the Bandawe syenite.

and high Rb, the second group which is higher in SiO_2 has high Ba and low Rb contents. (Fig. 7.1B).

The LREE and Yttrium generally show a flat trend with little variation between the data points. A chondrite normalised plot (Fig. 7.2) shows that the syenite has a fractionated REE pattern.

The high field strength elements Zr and Nb show a scatter, Nb less so than Zr. The distribution of both Zr and Nb can be correlated with Ba and Rb. Samples high in Ba are generally lower in Zr and Nb than those which are low in Ba.

.7 Petrogenesis.

The Lunkhwakwa and Bandawe intrusions show systematic variations in their chemistry suggesting that crystal-liquid equilibria may have played a major role in their genesis. The two intrusions exhibit similar chemical trends (Fig. 6.9) suggesting that similar processes operated within them during crystallization. However, the slopes of these trends suggest that the degree to which these processes operated in the two intrusions was different. (Fig. 7.3).

.1 Lunkhwakwa syenite.

The major element patterns of the Lunkhwakwa syenite characterized by a systematic decrease in the ferro-magnesian elements, Mg, Fe, Ti, and (Ca) and a corresponding increase in the alkalis, Na, K and (Al), with a change of slope in some of these trends (Fig. 6.9A), are typical of fractional crystallization.

The variation patterns shown by the trace elements may also be attributed to fractional crystallization. The decreasing Ba and Sr concentrations with SiO_2 (Fig. 6.7)

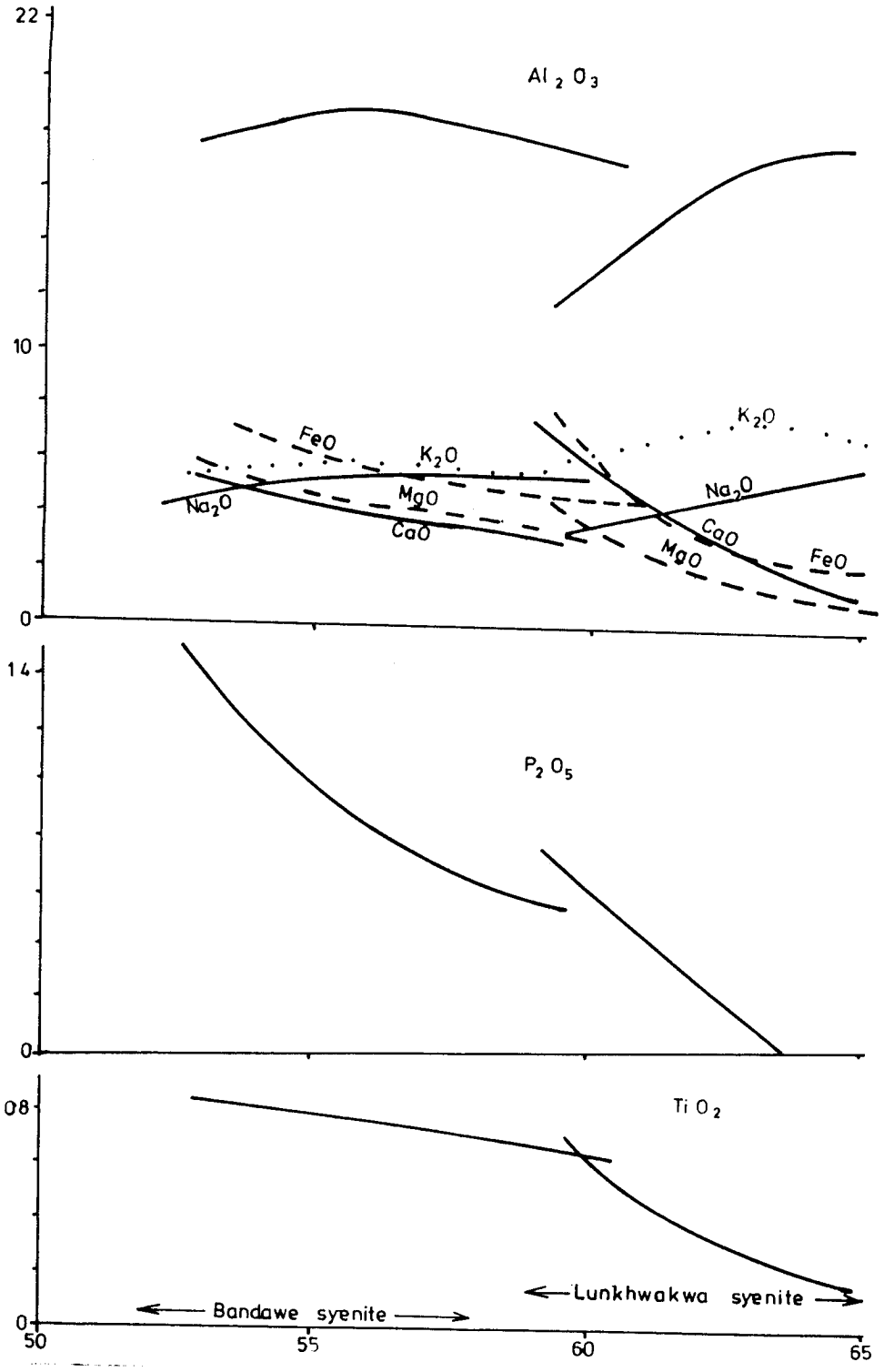

7.3 Chemical comparison of the Lunkhwakwa and Bandawe syenites.

suggests continuous crystallization of alkali feldspar whilst the unusually high concentrations of these elements in samples 13, 16,29B, 30, 40 and 44, some samples containing up to 14,000ppm Ba and 6,000ppm Sr, suggest substantial accumulation of alkali feldspar. These samples undoubtedly represent rocks chiefly consisting of alkali feldspar (refer to petrographic decriptions, chapter 4) accumulated by either settling, flotation or in situ 'cumulus' growth with little interstitial liquid. (75).

The negative correlation of Zr with both Ba and Sr is attributed to accumulation processes involving alkali feldspar. The relatively low contents of Zr in samples with the high Ba and Sr is taken to indicate the dilution of Zr by alkali feldspar. The relatively constant concentration of Rb may indicate that crystallization of the intrusion was at a relatively low temperature at which the partition coefficient between the main Rb incorporating phase, alkali feldspar and the liquid was close to unity. (76) The progressive decrease in the incompatible elements La, Ce, Nd, Y, and Nb indicates that their bulk liquid/crystal partition coefficient was greater than 1 and suggests that their distribution was largely controlled by the crystallization of alkali feldspar and the minor phase sphene.

This conclusion is supported by the observed high concentrations of these elements in sample FTC29 which has more than 5% modal sphene.

Consideration of the major element trends assuming that the most mafic sample represents the early crystallizing assemblage shows that the trends may be explained by crystallization in the proportions 60% alkali feldspar, 38% clinopyroxene and 2% sphene whilst the kink at 63% SiO_2 corresponds to an increase proportion of alkali

/d

feldspar (75%), sphene (3%) and a decrease in clinopyroxene (16%).

6.7.2 Bandawe syenite.

The general decrease in the ferromagnesian major elements MgO, FeO, TiO_2, (CaO) and (P_2O_5) and the increase in the alkalis Na_2O, K_2O and Al_2O_3, with a change in slope in the trend, favours an origin of the Bandawe syenite by fractional crystallization as well.

The general decrease in Sr and Cr with increasing SiO_2 is also in agreement with fractional crystallization involving ferromagnesian phases and possibly feldspar.

The relative scatter of Ba contents in the range 3000ppm-6000ppm and the negative correlation of Ba with Rb, Nb and Zr suggest crystal accumulation involving alkali feldspar (C.f. average syenite Table 6.2).

The generally constant concentrations maintained by the LREE and yttrium with increasing SiO_2 suggest continuous crystallization of a phase(s) with a bulk liquid/crystal partition coefficient close to 1 for these elements. A possible mineral which can account for the REE distribution patterns is amphibole which has liquid/crystal KD values of between 0.85-3.2 for the LREE and between 2.4-13 for the HREE (Dy) (76).

Thus, the chemical trends in the Bandawe syenite may be attributed to crystallization of 50% alkali feldspar, 15% nepheline, 20% clinopyroxene and 15% amphibole, assuming that the most mafic rock represents the early crystallizing assemblage.

In summary, the chemical data shows that despite having been dominated by similar processes during crystallization, the two syenite intrusions of the Chipata area have chemical characteristics which indicate that they originated from different magmas. Apart from being undersaturated, the Bandawe syenite is distinctly more mafic in character. The total alkali contents and the trace element data however show that in spite of its mafic character, the Bandawe syenite is relatively more fractionated.

These features suggest that the Bandawe syenite crystallized from a fractionated basic alkaline magma which may have had a mantle origin, whilst the siliceous nature of the Lunkhwakwa syenite suggests a partly crustal origin.

.8 Chemical variation in the Mivula Hill syenite.

The Mivula Hill syenite contrasts with the previously described intrusions by its lack of obvious systematic chemical variation in the Harker diagram (Fig. 7.4). However, the SiO_2 range of the analyses is limited, between 50-55%, thus reducing the possibility for any trends to be revealed.

An alternative variation diagram employing the FeO*/ FeO* + MgO ratio as a possible fractionation index also fails to reveal any systematic variation despite the relatively larger range, 0.87-0.98 (Fig.7.5).

.1 Major elements.

In general, there is a tendency for the major elements to cluster due to the low SiO_2 range, (Fig. 7.4) but the distribution of Al_2O_3, FeO, MgO and K_2O in most samples suggests that there may be a systematic variation. Inspection of the Harker diagrams for these elements shows that three sample, M1, M8 and M23 stand

Table 6.4 Whole rock major and trace element analyses of the Mivula Hill syenite

	1	2	3	4	5	6	7	8	9
	M13	M8	M4	M1	M23	M21	M7	M16	M2
SiO_2	50.28	51.11	53.35	53.87	54.05	54.35	54.62	55.12	55.24
TiO_2	.90	.29	.58	.36	.30	1.06	.43	.48	.92
Al_2O_3	19.52	24.86	20.86	23.70	23.07	21.18	21.64	21.26	21.38
Fe_2O_3	8.99	3.19	6.51	4.22	1.57	5.92	4.62	5.19	5.32
FeO	-	-	-	-	1.50	-	-	-	-
MnO	.17	.09	.18	.08	.14	.11	.15	.20	.12
MgO	1.00	.12	.17	.11	.15	.52	.12	.17	.57
CaO	3.55	1.55	3.17	.95	1.88	1.10	2.77	1.92	2.62
Na_2O	7.90	11.65	6.84	9.20	9.76	7.28	7.36	7.79	5.30
K_2O	7.62	7.12	8.25	7.49	7.52	8.42	8.23	7.87	8.43
P_2O_5	.05	.01	.08	.01	.04	.05	.04	.01	.09
FeOT	8.09	2.87	5.86	3.80	2.91	5.33	4.16	4.67	4.79
$\frac{FeOT}{FeOT+MgO}$	.89	.96	.97	.97	.89	.91	.97	.96	.89
$\frac{Fe_2O_3}{FeO}$	-	-	-	-	1.05	-	-	-	-
LoI	2.38	2.25	2.87	1.74	1.59	2.30	2.34	.84	1.93
Tot.	99.99	100.26	98.62	99.33	99.39	99.09	98.69	98.98	97.68
Rb	283	210	184	210	236	145	222	271	135
Ba	3580	737	2210	966	517	4560	1920	309	6870
Sr	1500	1630	1960	1570	1170	2190	2310	1120	2170
La	2	12	20	6	50	29	36	19	23
Ce	5	34	49	21	97	51	66	39	43
Nd	13	13	27	11	38	37	34	16	42
Y	3.8	6.8	10	4.7	17	10	12	10	11
Zr	79	196	149	124	222	75	166	219	144
Nb	35	68	72	66	91	91	114	107	106
Cr	3	3	4	4	5	3	30	3	3
Ga	29	23	16	21	23	21	17	23	23

Table 6.4 contd.

	10	11	12	13	14	15	16	17	18	19
	M11	M3	M9	MM6	M10	M24	M15	M17	M20	Mean
SiO_2	55.43	51.05	52.87	53.45	53.63	60.74	61.28	62.48	63.08	53.74
TiO_2	1.15	1.52	1.04	.74	1.00	.20	.22	.84	.79	.65
Al_2O_3	21.13	19.66	19.95	21.12	20.20	20.23	21.00	15.87	15.73	21.86
Fe_2O_3	5.87	8.89	8.91	5.83	6.40	1.12	3.14	5.41	6.49	5.14
FeO	-	-	-	-	-	1.49	-	-	-	-
MnO	.12	.23	.15	.14	.15	.10	.02	.14	.13	.14
MgO	.64	1.22	.56	.59	.89	.10	.10	1.78	1.66	.36
CaO	.35	3.84	1.66	2.77	2.33	.64	.02	3.40	1.57	2.00
Na_2O	5.87	6.20	5.94	7.67	6.75	7.01	3.01	7.65	6.28	7.90
K_2O	9.40	7.14	8.86	7.53	8.44	8.34	11.19	2.24	4.13	8.03
P_2O_5	.04	.25	.05	.17	.18	.01	.01	.19	.15	.04
FeOT	5.28	8.00	8.02	5.24	5.76	2.50	2.82	4.87	5.84	4.78
$\frac{FeOT}{FeOT+MgO}$	.89	.87	.93	.90	.87	.96	.97	.73	.78	.94
$\frac{Fe_2O_3}{FeO}$	-	-	-	-	-	.75	-	-	-	-
LoI	1.11	2.40	1.10	3.86	.72	2.47	1.14	1.10	.71	1.93
Tot.	98.42	98.26	99.19	98.85	98.77	98.73	99.12	98.85	98.83	99.04
Rb	195	184	245	229	231	271	445	49	190	210
Ba	5080	4360	2370	2520	3540	542	518	747	853	2675
Sr	1450	796	1400	1830	1460	586	483	568	502	1707
La	2	19	7	28	10	45	23	174	162	21
Ce	10	38	22	58	34	114	25	203	246	42
Nd	19	37	10	34	24	40	11	74	101	24
Y	3.8	15	6.9	13	9.7	16	90	53	62	8
Zr	84	437	137	367	257	4600	329	259	717	146
Nb	143	207	131	178	136	1260	62	31	185	89
Cr	3	25	5	18	47	3	18	55	65	6
Ga	23	25	24	20	24	29	23	20	20	22

Analyses:-

1 - 10,	nepheline sodalite syenite, Mivula Hill syenite
11- 14,	nepheline syenite dykes, Mivula Hill syenite
15 ,	vein "
16- 18,	Fenite "
19 ,	Average of Mivula syenite (analyses 1-10).

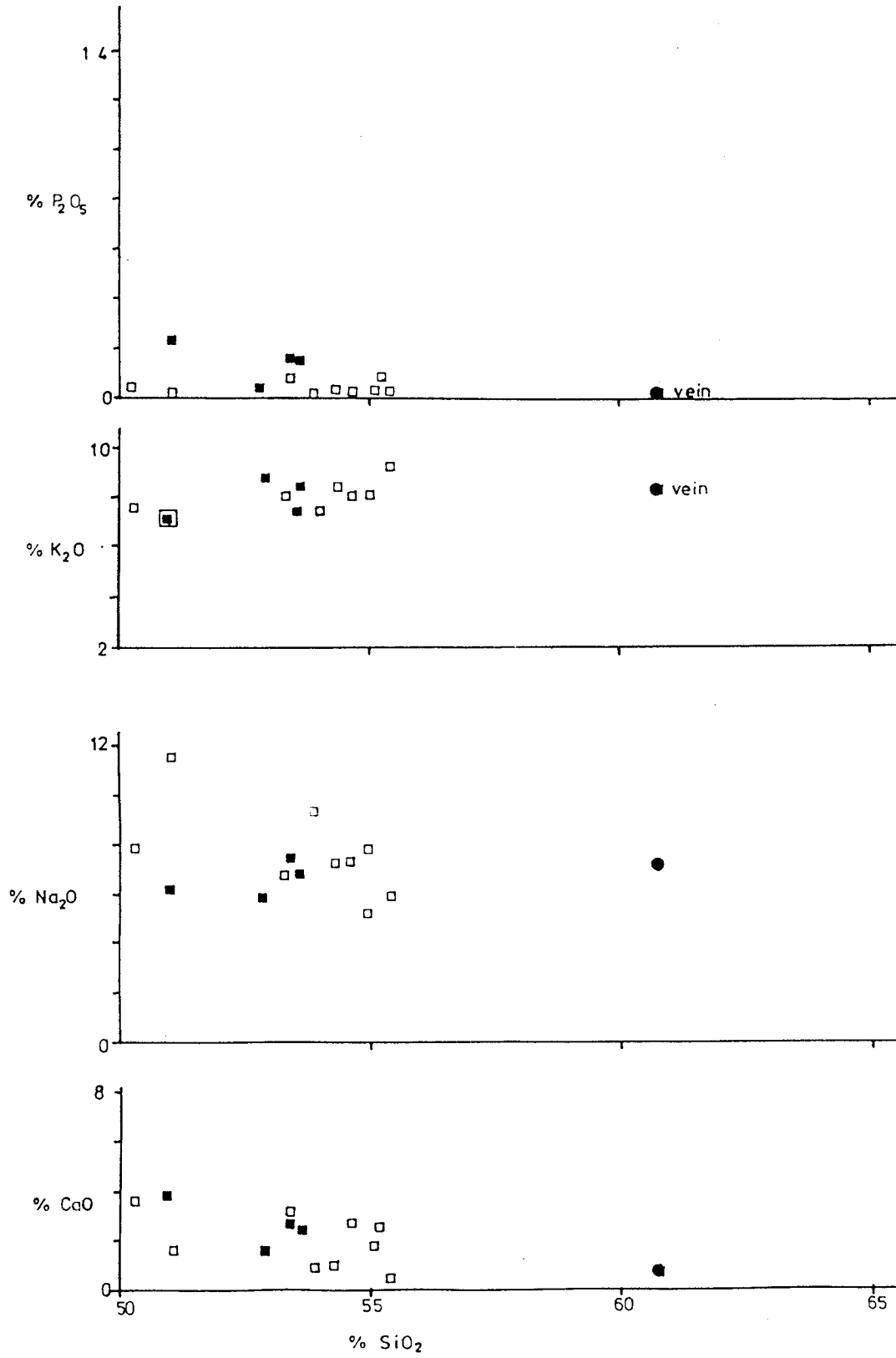

Fig. 7.4 Harker variation diagram for the Mivula Hill syenite.

□ — Syenite ■ — Dyke ● — Vein

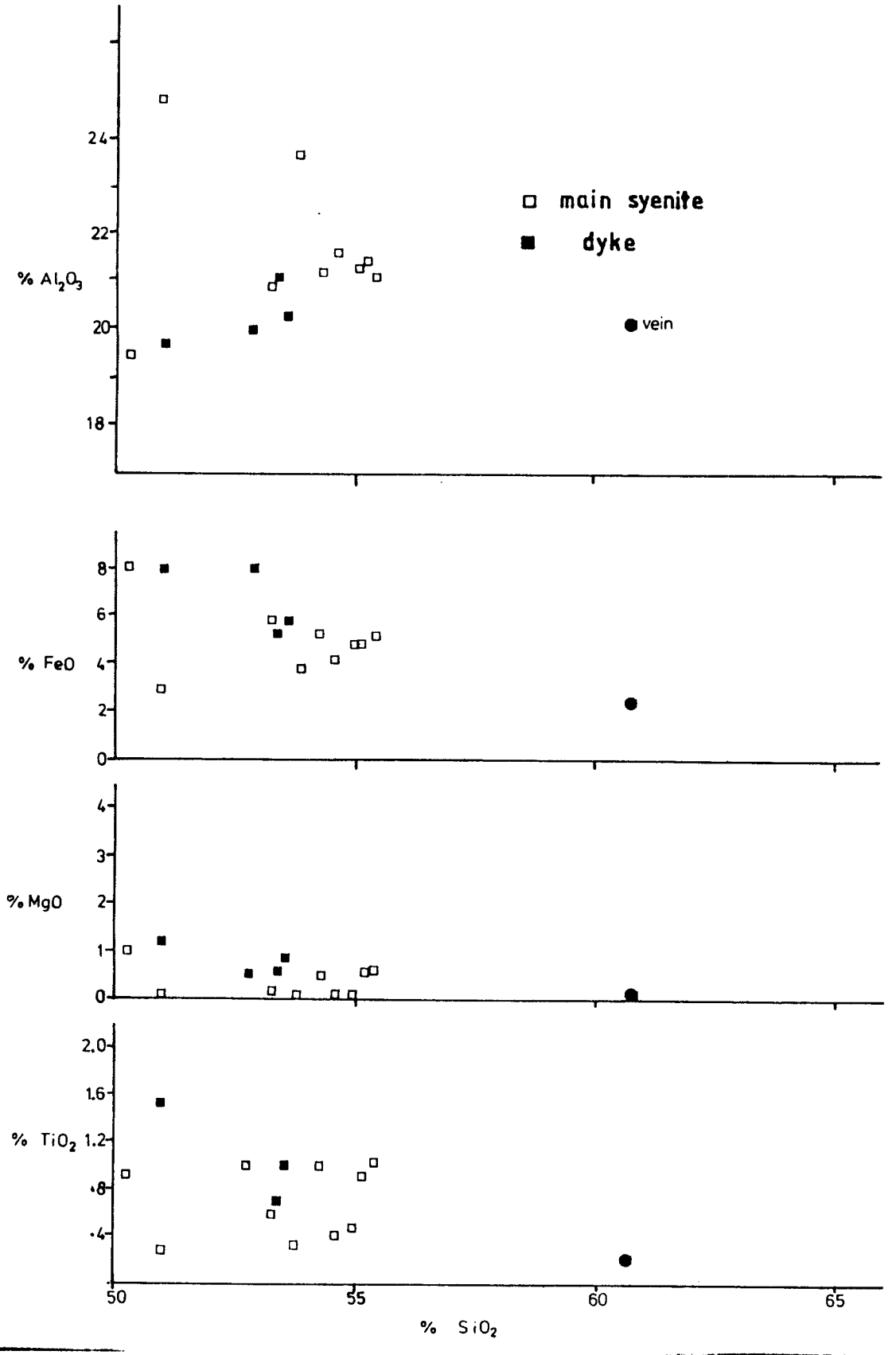

Fig. 7.4 (contd.) Harker variation diagram for the Mivula Hill syenite.

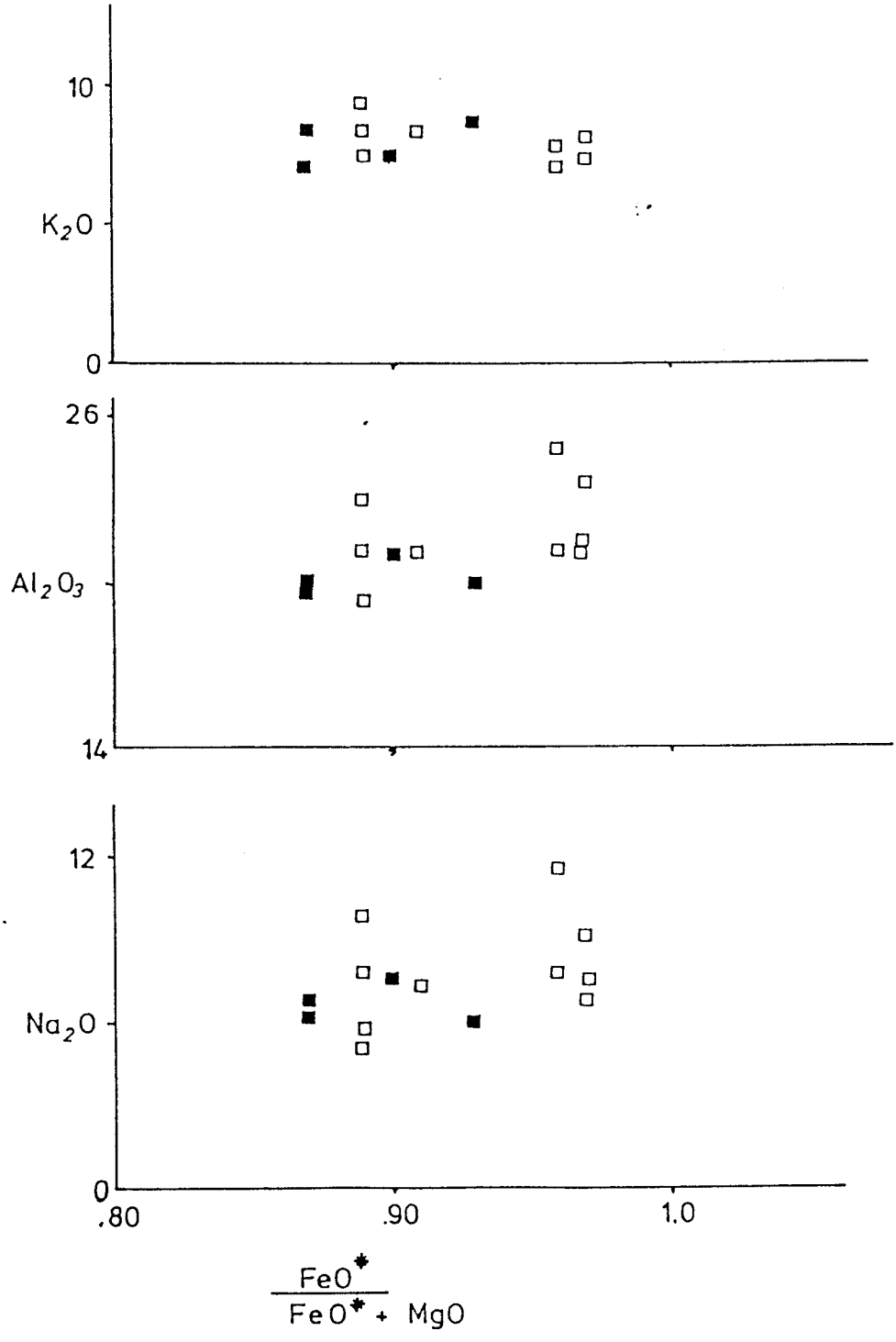

Fig. 7.5 Element variation in the Mivula Hill syenite using the FeO*/FeO*+MgO ratio as differentiation index.

out from the rest. These have very high Al_2O_3 and Na_2O contents and low MgO, FeO, TiO_2 and CaO. Consideration of the variation of these elements minus these three samples suggests that there is an increase in Al_2O_3 and K_2O and a decrease in MgO, FeO and CaO whilst Na_2O and P_2O_5 are fairly constant.

In the FeO^*/FeO^*+MgO diagram (Fig. 7.5) the analyses cluster into two groups, the analyses plotting as vertical lines in both groups. The first group consists of samples with an FeO^*/FeO^*+MgO index of 0.89 whilst samples of the second group are those with an index of 0.97.

6.8.2 Trace elements.

Trace element variation is characterized by a constancy in Cr contents and a scatter in Ba, La, Ce and Nd whilst Sr, Rb, Zr and Y cluster at about 55% SiO_2. Nb is exceptional in that it shows a regular increase with increasing SiO_2 (Fig. 7.6). When plotted against the FeO^*/MgO ratio, the high field strength element Zr increases with an increasing FeO^*/MgO whilst Nb shows much more scatter.

Despite the poor correlation with SiO_2, some of the trace elements show some coherence when plotted against each other (Fig. 7.7)

The absolute concentrations of Ba (2,700 ppm) and Sr (1,700ppm), are similar to the syn-orogenic alkaline intrusions of Malawi (41) and to those of Northern Norway (71, 93).

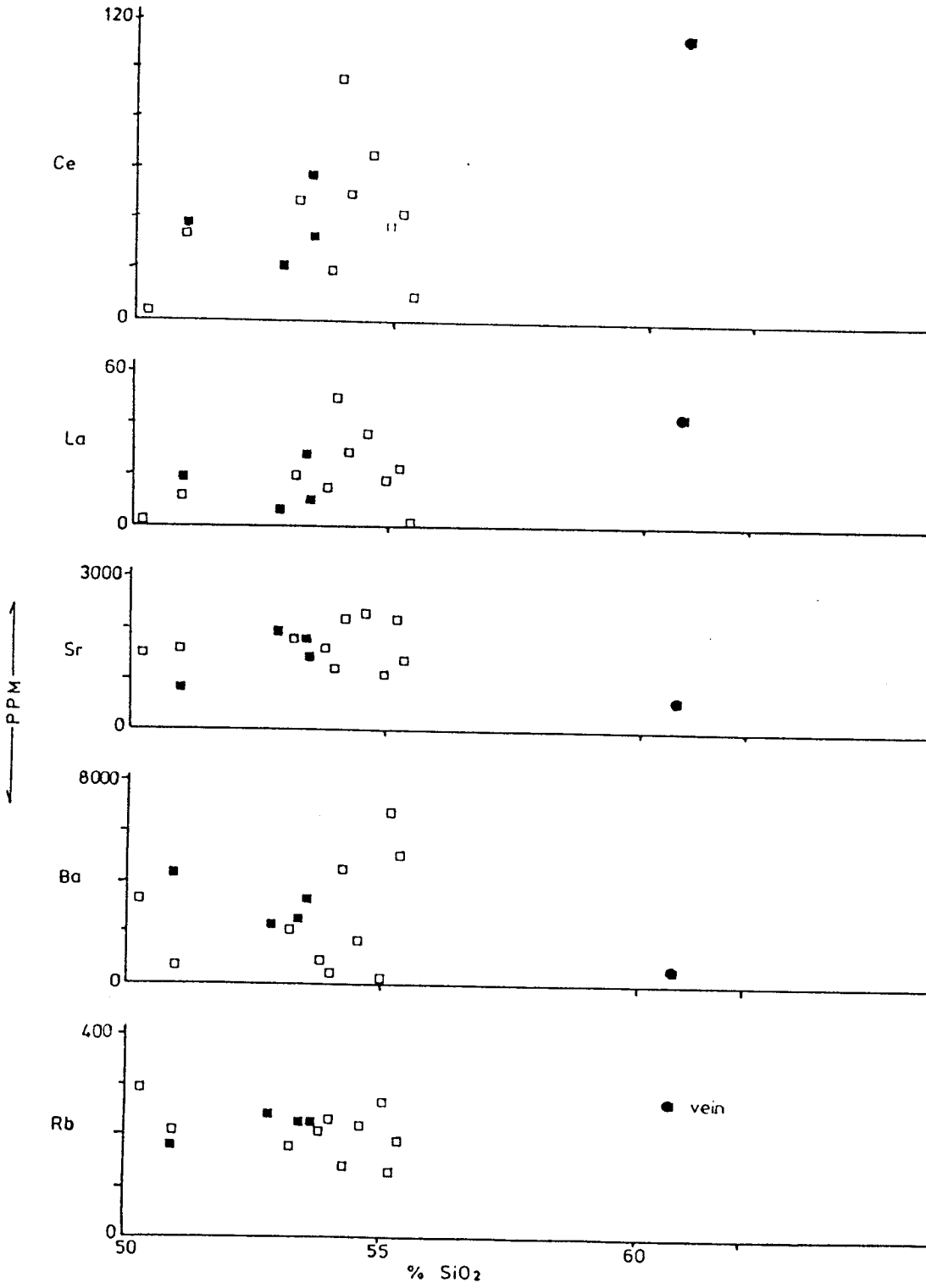

Fig. 7.6 Trace element variation in the Mivula Hill syenite.

□—*syenite* ■— *dyke* ●—*vein*

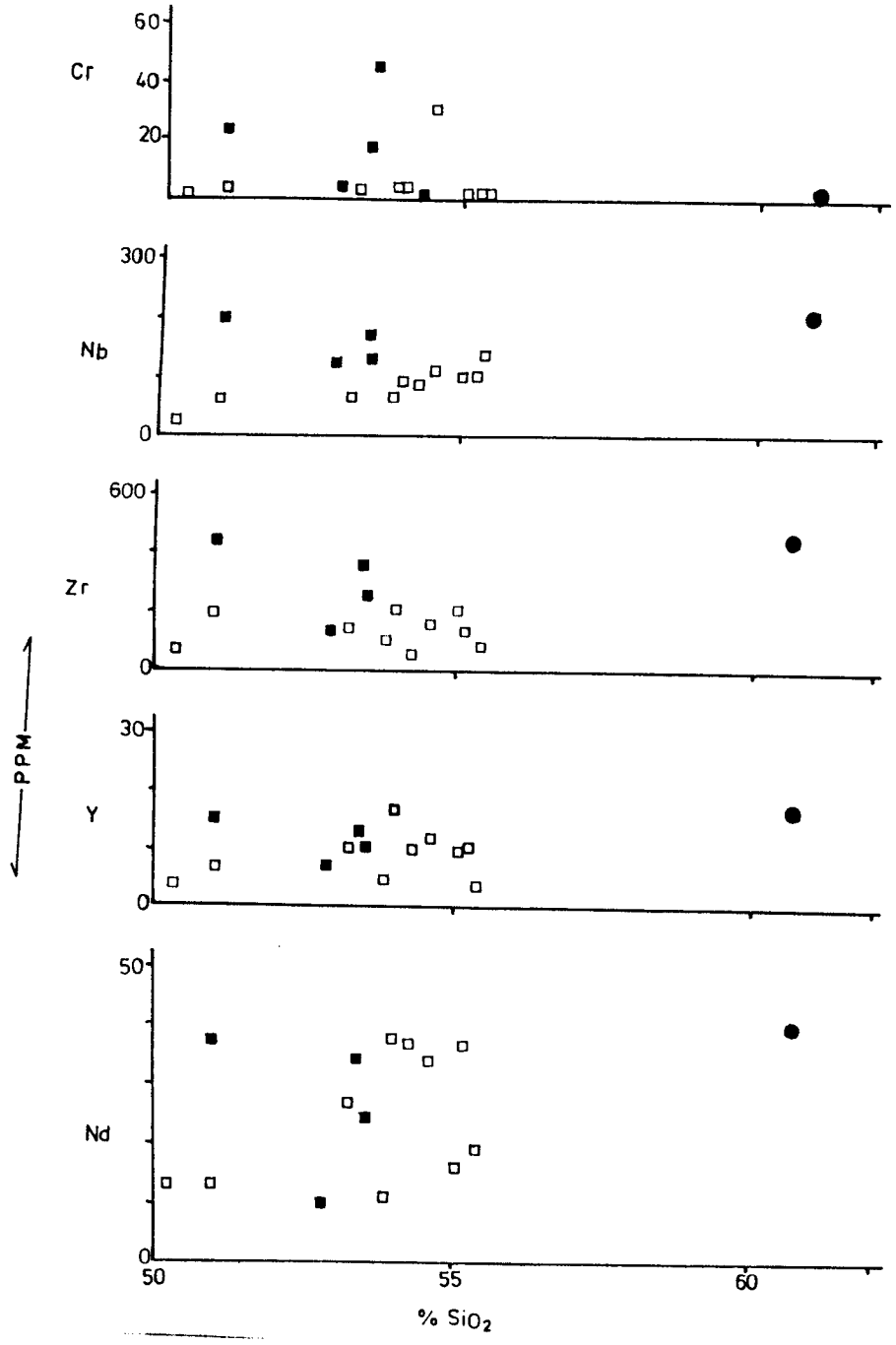

Fig. 7.6 (contd.) Trace element variation in the Mivula Hill syenite.

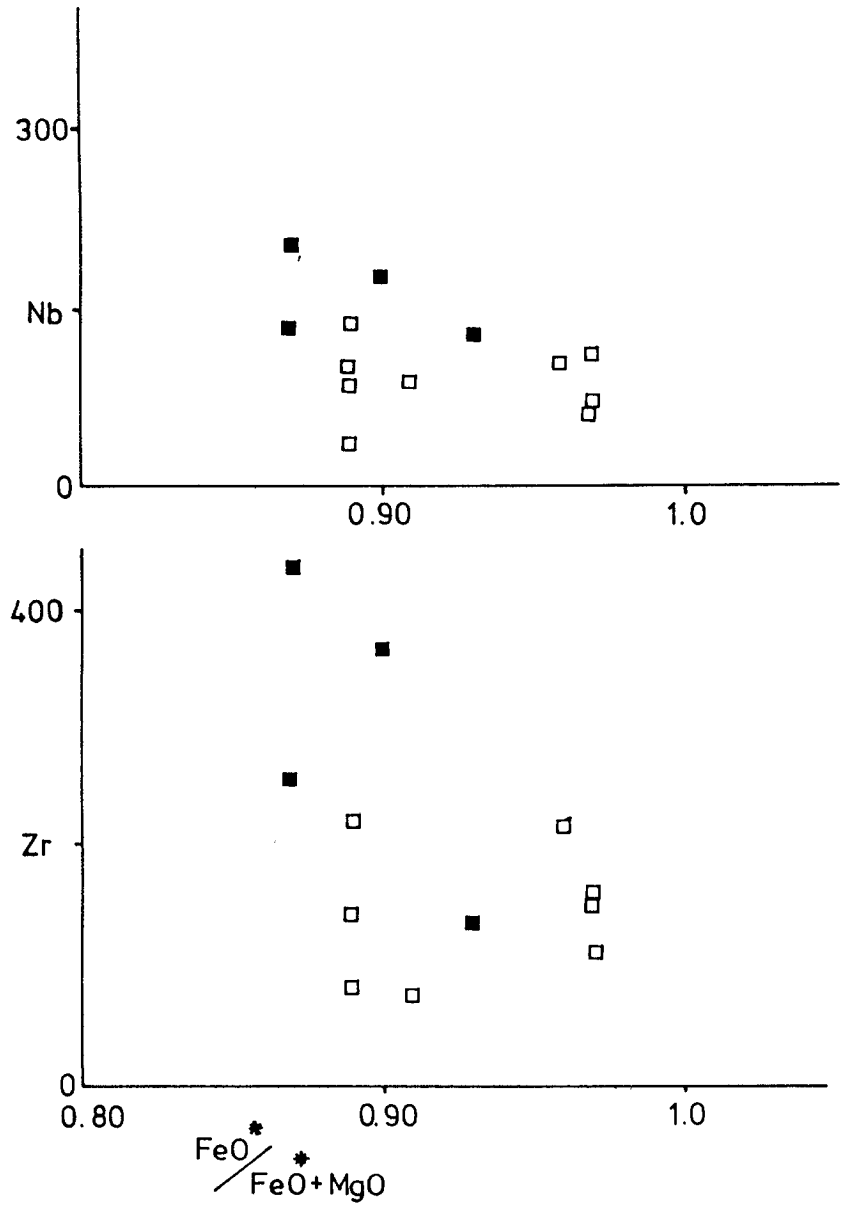

Fig. 7.6 (contd.) Trace element varition in the Mivula Hill syenite.

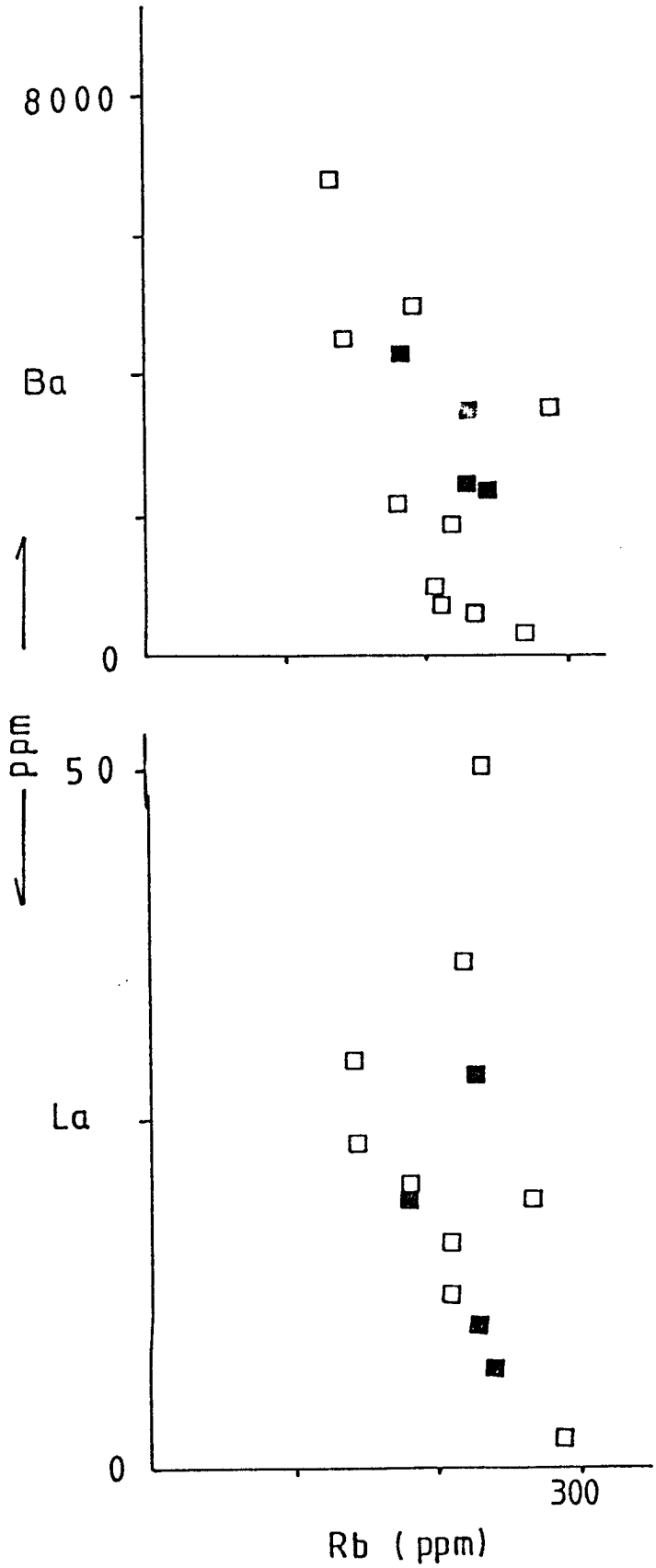

Fig. 7.7 Variation of Ba and La with Rb in the Mivula Hill syenite.

□ — *syenite* ■ — *dyke*

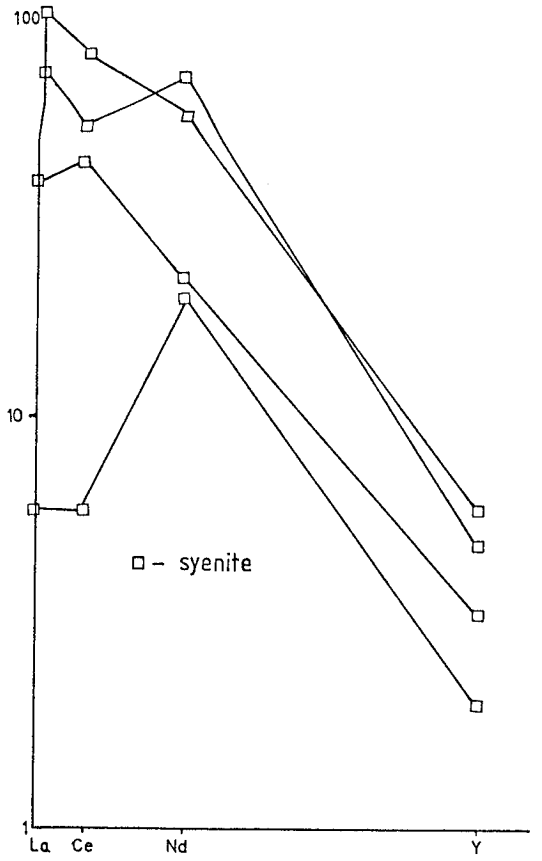

Fig. 7.8 Chondrite normalised REE diagram for the Mivula Hill syenite.

6.9 Petrogenesis.

The Mivula Hill syenite shows a smaller range in SiO_2 than the Sinda and Chipata syenites which has presumably resulted in the lack of any obvious systematic trends on the Harker diagrams (Fig. 7.4) However, disregarding samples M1, M8 and M23, it may be argued that the remaining analyses show some systematic decrease in MgO, FeO and CaO and an increase in Al_2O_3 and K_2O whilst Na_2O remains relatively constant. The variation suggests fractional crystallization of a ferromagnesian mineral such as pyroxene or amphibole, both of which are present in the rocks whilst the increase of the K_2O/Na_2O ratio may be attributed to the crystallization of nepheline. The constancy of Na_2O would require approximately 30% nepheline to be crystallizing.

The aberrant samples M1, M8 and M23 are high in Na_2O and Al_2O_3, low in the ferromagnesian elements and have average contents of K_2O. This suggests accumulation of nepheline. In accord with this, the rocks consist of euhedral nepheline and alkali feldspar with few mafics.

The variation of the FeO*/FeO*+MgO ratios (Fig. 7.5) is also in agreement with fractional crystallization involving mafic phases.

However, the large variation at constant values of FeO*/FeO*+MgO of 0.89 and 0.97 is again indicative of a crystal accumulation process.

Inspection of the FeO*/FeO*MgO diagram shows that the range in element variation at the constant values of this ratio exceeds the range of the FeO*/FeO*+MgO of

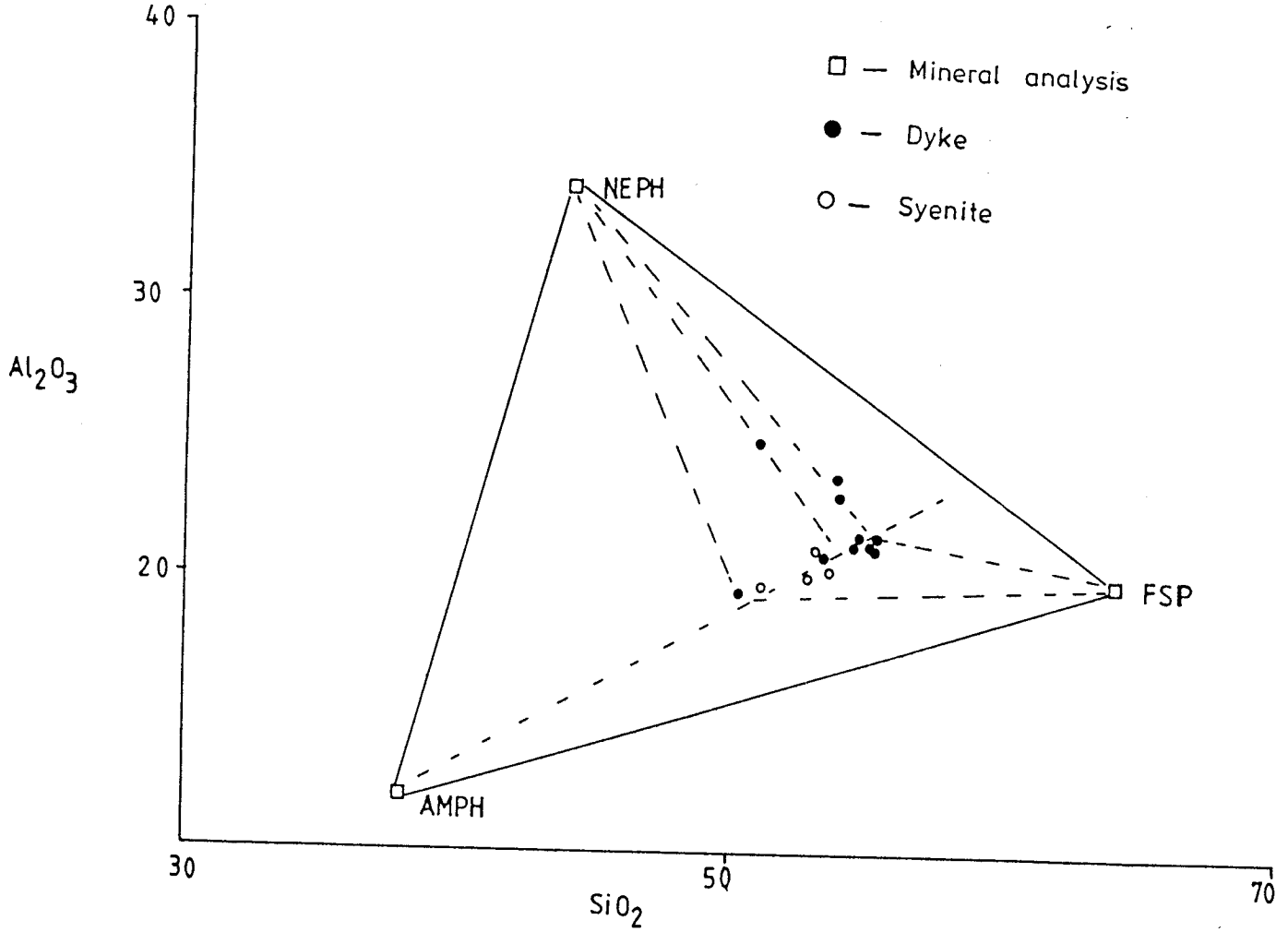

Fig. 7.9 Possible trend of fractionation of the Miyula intrusion

the analysed samples suggesting that crystal accumulation or the variation in the proportion of crystals and trapped liquid was more dominant in controlling the chemical variation than fractional crystallization.

The Harker diagram for Al_2O_3 for which mineral data have been plotted (Fig. 7.9) shows that this trend could be explicable by mixtures of alkali feldspar and nepheline in nearly constant proportions with decreasing amounts of amphibole.

Thus the major element data, in conjunction with the mafic composition of the dykes intruding the main syenite, suggest that the chemistry of the Mivula syenite reflects mixtures of floated cumulates of feldspar and nepheline with various proportions of liquid crystallizing a mafic mineral, namely amphibole.

CHAPTER SEVEN

Geochronologic study of the Mivula Hill syenite

7.1 Results.

Twelve samples from the syenite were selected for analysis. Rb/Sr ratios were determined by X-ray fluorescence spectrometry to an accuracy of about ± 1%. Standard ion exchange procedures were employed in the chemical preparation of the samples. Sr was loaded on single tantalum filaments and isotopic measurements were made on a mass spectrometer. The Rb-Sr data for the syenite are given in table 7.1. $^{87}Rb/^{86}Sr$ has been calculated according to the standard formula: $^{87}Rb/^{86}Sr = Rb/Sr\ (2.70 + 0.283\ (^{87}Sr/^{86}Sr)$ (40). Results of the twelve samples are plotted on a $^{87}Rb/^{86}Sr$ graph shown as figure 7.1. The points show a certain degree of scatter, especially those with high Rb/Sr ratios. The scatter in the points may be attributed to a considerable degree of secondary alteration seen in samples M3, M15, and M24 and to weathering in sample M18.On this basis, samples M3, M15, M18 and M24 are excluded from the regression analysis. Regression of the remaining samples gives an isochron age of 1341±16 Ma with an initial $^{87}Sr/^{86}Sr$ ratio of .7028±0.0001 (Table 7.2, Fig. 7.2). The results are reported at the one sigma level. The low initial ratio suggests an origin in the deep crust or upper mantle.

Table 7.1

Mivula Hill sodalite syenite Rb-Sr results.

Sample No.	Rb(PPM)	Sr(PPM)	$^{87}Rb/^{86}Sr$	$^{87}Sr/^{86}Sr$
M2	140	212	.16576±.0017	.70627±.002
M3	167	629	.67213±.0015	.71428±.00007
M6	240	1810	.33333±.0033	.70878±.0002
M7	237	2340	.25645±.0026	.70795±.0002
M9	220	1180	.47119±.0047	.7116399±0.0002
M11	202	1420	.35796±.0038	.70969±0.0002
M13	265	1300	.51272±.0051	.71241±0.0002
M15	503	475	2.7069±.0018	.73215±.00009
M16	285	1060	.67401±.0068	.71623±0.0002
M18	409	1220	.51299±.0063	.71795±.0002
M21	131	2170	.17486±.0017	.70612±0.0002
M24	321	609	1.3400±.0018	.72397±.00005

Table 7.2 Results used in isochron plot

Sample No.	X	STD X	Y	STD Y	VERT.DEV.
M2	0.1657600	0.0017000	0.7062700	0.0002000	0.0002823
M6	0.3333300	0.0033000	0.7087800	0.0002000	-0.0004298
M7	0.2564500	0.0026000	0.7079500	0.0002000	0.0002185
M9	0.4711900	0.0047000	0.7116399	0.0002000	-0.0002206
M11	0.3579600	0.0038000	0.7096900	0.0002000	0.0000066
M13	0.5127200	0.0051000	0.7124100	0.0002000	-0.0002491
M16	0.6740100	0.0068000	0.7162300	0.0002000	0.0004696
M21	0.1748600	0.0017000	0.7061200	0.0002000	-0.0000427

INTERCEPT = 0.702800 S.D. = 0.000112

SLOPE = 0.019228 S.D. = 0.000236

MSWD = 2.24

INITIAL RATIO = 0.7028+-0.0001

AGE 1341.07 +- 16.64M.Y. (1 SIGMA)

STUDENT T = 2.45

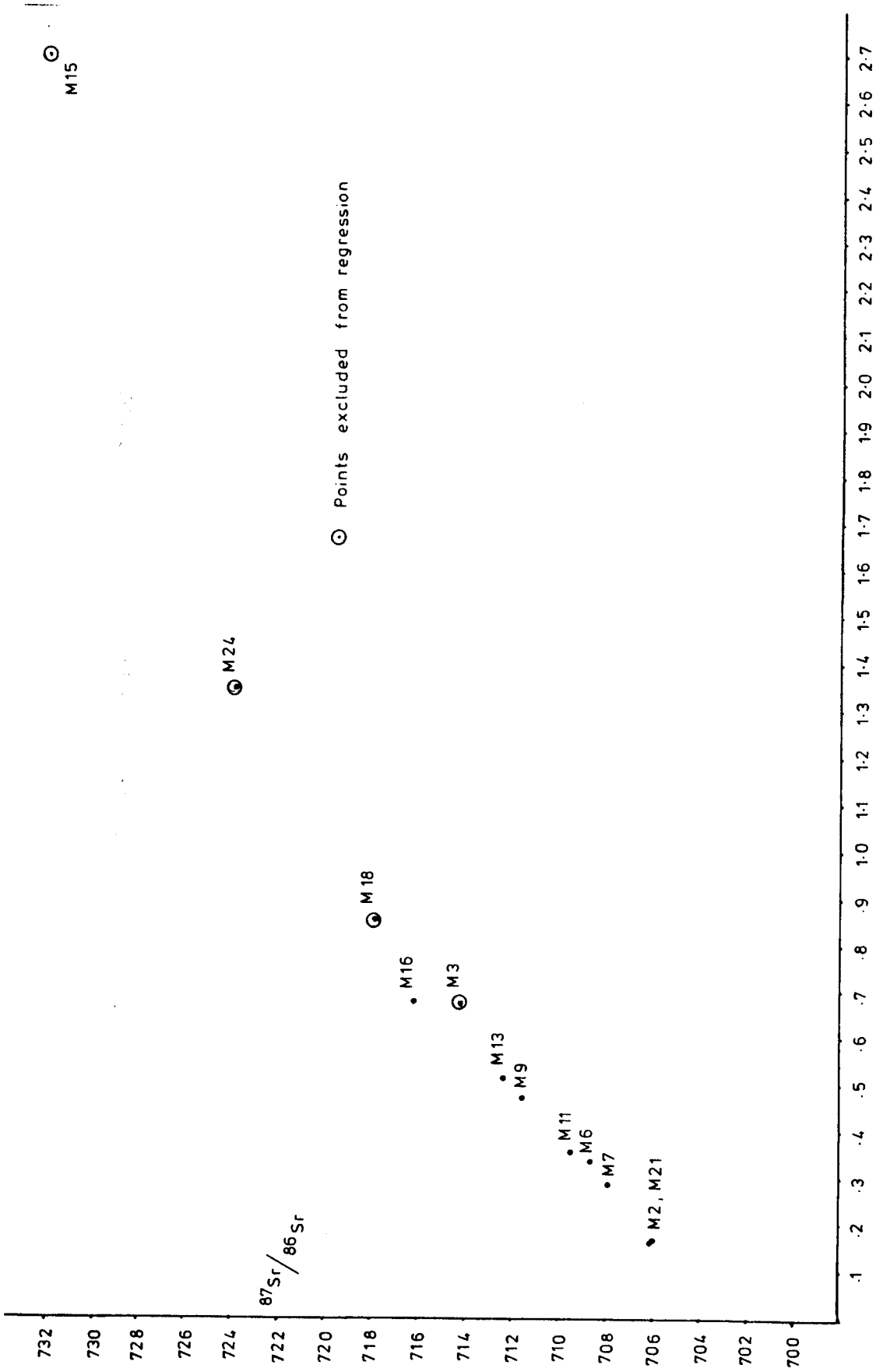

Fig. 8.0 Rb-Sr plot of samples from the Mivula Hill syenite.

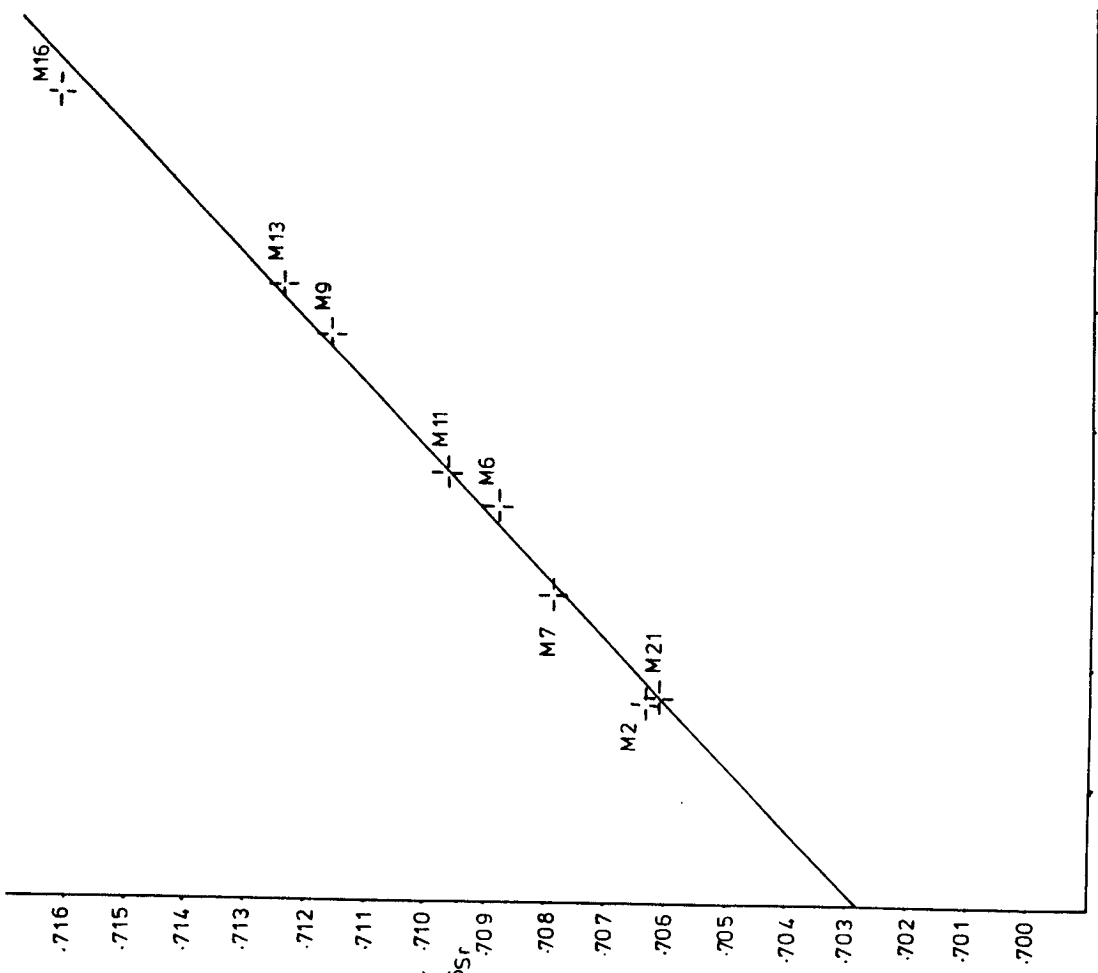

Fig. 8.1 Rb-Sr whole rock isochron of the Mivula Hill syenite.

7.21 Discussion

The age obtained for the Mivula sodalite syenite is in disagreement with previous age determinations on the intrusion and its enclosing rocks. The Mivula syenite has been previously dated at 550 Ma by a K-Ar mineral age (41). K-Ar whole rock and mineral ages from the Mafingi group rocks in which the syenite is intrusive range from 770-330 Ma. The available data also indicates that the Mafingi group was deformed for the first time during the Irumide orogeny (18).

The 550 Ma age of the Mivula syenite reported by Snelling is interpreted as a mineral re-equilibration age reflecting the Mozambiquain phase of the Pan African orogeny whose dates in Malawi range from 400 - 700 Ma(17). The mineral ages shown by the Mafingi group rocks are also a reflection of the same orogenic episode. Furthermore, the determination of whole rock ages on sedimentary and metasedimentary units is questionable (Brueckner pers. comm.).

Hence it is concluded that the Mivula Hill syenite was intruded into the Mafingi group sediments about 1341±16 Ma ago. The initial strontium ratio is suggestive of a mantle origin for the syenite. Recent Rb-Sr studies have shown that Irumide plutonism is widespread in the region. Among the Irumide plutonics are included the Dzalanyama, Mcezi, Lwakwa, Mwenga and Wililo granites from Malawi having Rb-Sr whole rock ages ranging from 1132±43 Ma to 1016±55 Ma and the Lusenga syenite in Northern Zambia which has an age of 1134±8 Ma (42, 43).

The establishment of an Irumide age for the Mivula syenite confirms the pre Irumide age for the deposition of the Mafingi group (18).

CHAPTER EIGHT

Conclusions

8.1 Sinda Syenites

The Sinda syenites are a petrogenetically related N-S trending string of intrusions which can be divided into two groups.

Petrographically the Lusandwa and Mayira intrusions comprise porphyritic and porphyroclastic rocks ranging from mafic pyroxene syenite through hornblende syenite to leucosyenite. The Pule, Seya and Tantha intrusions are in contrast wholly uniform, granular hornblende syenites.

Chemically, the Lusandwa and Mayira intrusions follow an alkaline trend, whilst the Pule, Seya and Tantha intrusions trend towards calc-alkaline compositions, (Fig. 6.2).

The chemical variation in the Lusandwa and Mayira intrusions are attributed to fractional crystallization and clearly reflect the presence of a crystalline assemblage in equilibrium with an evolving liquid. The mineral chemistry data is in agreement with fractional crystallization, showing an increase in the FeO*/FeO*+ MgO ratio of the mafic minerals from the mafic to the felsic rocks.((Fig. 5.5).

The trace element chemistry of the apatite rich rocks within the Mayira intrusion indicate that their constituent minerals crystallized in equilibrium with a chemically similar magma. The FeO*/MgO ratio of the pyroxene from the apatite rocks indicate that these crystallized from less evolved liquids than that from which the exposed pyroxene syenite crystallized. To account for the evolution of the liquid and for the crystal sorting into

apatite -pyroxene and apatite-feldspar rocks, crystal settling and gravity settling is invoked to have been active during the early stages of crystallization. This makes it possible that the concentric layering in the Lusandwa intrusion is a deformed igneous laminnation. Furthermore, the suggestion of the operation of crystal settling processes at an early stage of crystallization suggests that more of these apatite rich bodies may be present at depth in the Lusandwa intrusion.

No completely satisfactory model can be established to explain the evolution of the Pule, Seya and Tantha intrusions. The variation of the major elements and Cr is consistent with fractional crystallization whilst the variation of the incompatible elements is not obviously so although it may be explained by a change in KD values and control by minor phases.

The increase of Ba with SiO_2 (Fig. 6.5) however, strongly suggests accumulation of alkali feldspar and the decrease of Zr, Nb and Y (Fig. 6.5) consistent with dilution of magma by different amounts of crystals. Furthermore, the porphyroclastic textures which the rocks show indicate that they were emplaced as a mixture of crystals and liquid, supporting the crystal-liquid mixing model.

Whichever model is chosen for the Pule, Seya and Tantha intrusions, it is evident that they were derived from the Lusandwa and Mayira magma at some stage of its evolution but their subsequent evolution and crystallization was governed by different processes. Their sill-like structure and petrographical homogeneity suggests that they crystallized at a higher level and more rapidly. (36).

8.2 Chipata syenites

The Lunkhwakwa and Bandawe intrusions in the Chipata area are petrographically and chemically distinct from each other.

The Lunkhwakwa intrusion consists of an oversaturated pyroxene syenite whilst the Bandawe intrusion is an undersaturated nepheline syenite.

Major element variation in the Lunkhwakwa syenite is attributed to fractional crystallization of an alkaline syenite magma whilst the correspondence of high Ba and Sr and low Nb and Zr in some samples indicate that there was some accumulation of alkali feldspar by either crystal settling, flotation or in situ growth with little trapped liquid (75).

The relatively flat Rb and LREE trends in the intrusion (Fig. 7.1) suggest a relatively low crystallization temperature for the intrusion at which the Rb and LREE KD values were close to unity (76). This is in agreement with the petrography of the alkali feldspar which is completely exsolved into microcline and albite, and with the crystallization of sphene at the expense of Fe-Ti oxides.

Element variation in the Bandawe intrusion may also be explained by a combination of fractional crystallization and feldspar accumulation. The distribution of the LREE however, appears to have been controlled by amphibole crystallization.

8.3 Mivula Hill nepheline syenite.

The Mivula Hill nepheline syenite is a layered intrusion which is a product of crystal fractionation processes.

The variation of the major elements with both SiO_2 and FeO*/FeO*+MgO as fractionation indices (Figs. 7.4, 7.5) suggest that part of the element variation can be accounted for by fractional crystallization whilst the scatter in Al_2O_3 and Na_2O and the element variation at constant FeO*/FeO*+MgO values suggest that crystal accumulation involving alkali feldspar and nepheline took place. Crystal-liquid mixing involving the accumulated phases and a mafic liquid, principally crystallizing amphibole, appears to account for a large portion of the chemical variations observed in the intrusion.

Despite yielding an isochron age which places the intrusion of the Mivula magma close to the peak of the Kibaran orogenesis, there is a general lack of features characteristic of a syn-orogenic intrusion (71).

The layered nature of the intrusion suggests crystallization under relatively quiet tectonic conditions rather than in an orogenic environment. Petrographically, the syenite is homogeneous and lacks in both foliated and metamorphic textures typical of orogenic intrusions (71).

Furthermore, the petrographic features of the fenitic rocks (chapter 4) at the roof of the intrusion indicate deformation of the country rocks prior to the fenitisation process, hence prior to the emplacement of the intrusion.

The apparent contradiction between the petrographical and chemical data is at present still difficult to resolve owing to the lack of detailed field data on the relationship between the intrusion and the surrounding country rocks and points to the need for more petrological work. However, if the petrographical evidence is accepted to indicate a cratonic setting for the Mivula intrusion,

then the 1340 Ma isochron age obtained on the intrusion implies that some constraints must be placed on the upper age limit of Irumide deformation in Zambia.

8.4 Petrological implications.

The syenite intrusions of the Sinda and Chipata areas are located within the Malawi province of the Mozambique orogenic belt, a triangular region which is bounded by the Lake Malawi rift in the east, the Luangwa rift in the west and the Zambezi rift in the south.

The available geochronological data indicate that the intrusions are late-tectonic and were emplaced during the waning stages of the Pan African orogeny.

The Mivula intrusion, in contrast to the other intrusions, is located within the Irumide belt, a product of Kibaran orogenesis. The 1340±16 Ma Rb-Sr whole rock isochron age obtained on the intrusion is highly equivocal as it is close to the ages obtained for the peak of Kibaran orogenesis. The syenite intrudes thoroughly recrystallized rocks of the Mafingi Group which have been assigned to the Kibaran orogeny (18). This relationship indicates that the intrusion is post-tectonic, in which case the 1340 Ma age may indicate an early closure of Kibaran orogenesis in this part of Zambia.

Chemically, the syenite intrusions of the Sinda and Chipata areas are characterized by higher contents of K, P, Ba, Sr and REE than the average syenite whilst the Mivula syenite is chemically comparable to the average nepheline syenite except for high Ba and Sr.

On alkalinity indices vs SiO_2 variation diagrams (Fig. 6.1), the intrusions show decreasing alkalinity from the Mivula intrusion to the Sinda intrusions. Corresponding to this, the AFM diagrams (Figs. 6.4c and 7.0) show a

progressive increase of the Na_2O+K_2O:MgO ratio with a decrease in the FeO component. The chemistry of the pyroxenes from the Sinda and Chipata syenites (Fig. 5.4) also reflect the increasing degree of alkalinity of the intrusions.

The tectonic setting of the Sinda and Chipata intrusions is of particular significance both locally and regionally. Continental alkaline rocks are normally located in stable cratonic regions often associated with crustal arching and rifting (78). The close association of the alkaline rocks of eastern Zambia with orogenesis however suggests that the rift environment is a general case which applies to particular alkaline rock types-typically extremely fractionated and peralkaline (36), and that alkaline rocks may be associated with orogenesis, but have been little studied.

The unusual chemical features of the Sinda and Chipata intrusions, namely the high concentrations of the incompatible elements (K,P,Ba,Sr and REE) may be a primary feature of the magmas, introduced into them by metasomatic fluids from the mantle (98). The mobile orogenic environment perhaps represents zones of weakness in the largely cratonic environment of the African continent through which fluids from the mantle, activated by regional tectonics, were channelled. These fluids would necessarily be hot, thereby causing partial melting of the upper mantle or lower crust resulting in the generation of these magmas.

The increasing alkaline nature of the magmas, at least from the Sinda to the Chipata area, may therefore either reflect different degrees of partial melting or different depths of origin of the magmas.

REFERENCES

1. Drysdall, A.R., Thieme, J. G. and Johnson, R.L. Geological Map of the Republic of Zambia. Scale 1:1000,000 Geol. Surv. Dept. 1974-1975.

2. Phillips, K.A. The geology of the Sinda area: explanation of Degree sheet 1431, N.E. Quarter. Rep. geol Surv. N. Rhod. 9, 1960, 27pp.

3. _____ The geology of the Lusandwa River area: explanation of Degree Sheet 1331, S.E. Quarter. Rep. geol. Surv. Zambia 13, 1964, pp1-21.

4. _____ The geology of the Petauke and Mwanjawanthu area, explanation of Degree Sheet 1431, N.W. Quarter and part of S.W. Quarter Rep. geol. Surv. Zambia. 15, 1965, 28pp.

5. Mukumba, W.C,K. The Petrology and the associated sulphides mineralisation of the syenitic rocks in east Chilembwe, Petauke, Univ. Zambia spec. proj. report (unpublished) 1980 52pp.

6. Mujokotwaki, G. Phosphate (apatite)-rich bodies of Chilembwe in Sinda West PL 183. Geol. soc. Zambia newslett, 23, 1982, pp6-7

7. Felton, D.R. The geology of the Machinje Hills area: explanation of Degree Sheet 1331, N.W. Quarter Rep. geol. Surv. Zambia 35, 1973, pp1-16.

8. Newton, A.R. and Drysdall, A.R. Further data on an amphibole from Mivula Hill. Rec. geol. Surv. N. Rhod. 1960, pp26-29.

9. Adams, F.D. and Osborne, F.F. On two nepheline-sodalite syenites from new localities in N. Rhodesia. Can. Journ. Res. 6, 1932, pp571-576.

10. Newton, A.R. On the syenite of Mivula Hill, E. Province. Rec. geol. Surv. N. Rhod. 1959, pp14-17.

11. Vavrda, I. The geology of the Chipata area: explanation of Degree Sheet 1331 S.E. Quarter. geol. Surv. Zambia 41, 1974, 21pp.

12. Phillips, K.A. The plutonic histroy of the Sinda area: Sheet 1431, N.E. Quarter. Rec. geol. Surv. N. Rhodesia. 1959, pp3-5.

13. Bailey, D.K. Notes on the petrography of the Msoro Ring Complex, E. Province. Rec. geol. Surv. N. Rhod., 1956, pp18-19.

14. Brewer, M.S. Interim report of the geochronology results in the ODM/IGS age determination project, Zambia and Malawi. Geol. Soc. Zambia, Symp. on Pre-Katangan geol. of Zambia. 1978, pp5-8.

15. Barr, M.W.C. The geology of the Sasare area: explanation of Degree Sheet 1331, S.W. Quarter. Rep. geol. Surv. Zambia 30 1972, 70pp.

16. Munyanyiwa, H. The Petrological and trace element study of the Mulungushi metavolcanics. Univ. of Zambia spec. proj. report (unpublished) 1983, 50pp.

17. Carter, G.S. and Bennett, J.D. The geology and mineral resources of Malawi. Bull. geol. Surv. Malawi 6, 1973, pp8-36.

18. Fitches, W. R. Sedimentation and tectonics at the northeast end of the Irumide orogenic belt, N. Malawi and Zambia. Geol. Rundsch. 60, 1971, pp589-619.

19. Daly, M. and Unrug, R., The Muva supergroup of Northern Zambia: a craton to mobile belt sedimentary sequence Trans. geol. soc. S. Africa 85, 1983, pp155-165.

20. Ray, A.K. Lithostratigraphic succession of Zambia. Stratigraphic Committee, Geol. Surv. of Zambia,1984.

21. Dodson, M.H., Cavanagh, B.J., Thatcher, E.C. and Aftalion, M. Age limits for the Ubendian metamorphic episode in Northern Malawi. Geol. Mag., 112, 1975, pp403-410.

22. Andersen, L.S. and Unrug, R., Geodynamic evolution of the Bangweulu block, Northern Zambia. Geol. Soc. Zambia Proterozoic 83 Int. Conf. 1983, 52pp.

23. Cahen, L., Snelling, N.J., Delhal, J., Vail, J.R., Bonhomme, M. and Ledent, D. (1984). The Geochronology and Evolution of Africa. Oxford. pp95-143.

24. Floor, P., Alkaline gneisses. In Sørensen, H. (ed) (1974). The alkaline rocks John Wiley & Sons. pp124-140.

25. Turner, D.C., The alkaline rocks of Zambia. Geol. Soc. Zambia workshop. 29-30 March, 1985. Abst.

26. Czamanske, G.K. and Mihålik, P., Oxidation during magmatic differentiation, Finnmarka Complex, Oslo area, Norway: Part I, the opaque oxides. Jn Pet. 13/3, 1972, pp493-509.

27. Frasl, G., Anzeichen schumelzflussigen amd hochtemperierten Wachstums an den grossen Kalifeldspaten einiger Porphyrgranite, Porphyrgranitgneise und Augengneise Osterreichs Jb Geol. B.A., Wien, 97, 1954, pp71-134.

28. Droop, G.T.R., A clinopyroxene paragenesis of albite-epidote-amphibolite facies in meta-syenites from the Southeast Tauern Window, Austria Jn. Pet. 23/2, 1982, pp163-185.

29. Richardson, S.W., The petrology of the metamorphosed syenite in Glen Dessarry, Inverness-shire Q.Jn. geol. soc. Lond. 124, 1968 pp9-51.

30. Kempe, D.R.C., The Kilonwa syenite, Tanzania Q.Jn. geol. soc. Lond. 124, 1968 pp91-100.

31. Bonin, B. and Martin R.F., Coexisting alkali feldspars in felsic members of the Cauro-Bastelica ring complex, Corsica Lithos 7, pp23-28.

32. Martin, R.F. and Bonin, M., Water and magma genesis: the association hypersolvus granite-subsolvus granite. Can. Min. 14, 1976 pp228-237.

33. Bloomfield, K., Aegirine gneisses in Central Malawi Q.Jn. geol. soc. Lond. 123, 1967, pp93-98.

34. Coolen, J.J.M.M., Chemical petrology of the Furna granulite complex, S. Tanzania. G.V.A. paper of geology 1, 13, 1980, ppl2-18.

35. Size, W.B., Petrology of the Red Hill syenite Complex New Hampshire. Geol. Soc. Am. Bull. V83, 1972, pp3747-3760.

36. Sørensen, H., Alkali syenites, feldspathoidal syenites and related lavas. In Sørensen, H. (ed) 1974, The Alkaline rocks, John Wiley. pp22-48.

37. Wellman, T.R., The stability of sodalite in a synthetic syenite plus aqueous chloride fluid system. Jn Pet. 11 1, 1970, pp49-71.

38. Barker, D.S., Phase relations in the system $NaAlSiO_4$-SiO_2-NaCl-H_2O at 400-800^{o}C and 1 Kbar and petrologic implications Jn. Geol. 84, 1976 pp28-32.

39. Parsons, I., The Klokken gabbro - syenite complex, South Greenland: Cryptic variation and origin of inversely graded layering. Jn. Pet. 20 pt 4, 1979, pp653-694.

40. Faure, G., (1977) Principles of Isotope geology. John Wiley & Sons. 464pp.

41. Bloomfield, K., Orogenic and post-orogenic plutonism in Malawi. In Clifford, T.N. and Gass, I.G., eds. (1970) African Magmatism and Tectonics Oliver & Boyd. Edinburgh. ppll9-153.

42. Haslam, H.W., Brewer, M.S., Darbyshire, D.P.F. and Davis, A Irumide and post-Mozambiquian plutonism in Malawi. Geol. Mag. 120, 1, 1983, pp21-35.

43. Brewer, M.S., Haslam, H.W., Darbyshire, D.P.F., and Davis, A.E., Rb-Sr age determinations in the Bangweulu Block, Luapula Province, Zambia. Rep. Inst. Geol. Sci. 79/5, 1979, llpp.

44. Cawthorn, G.R. and Collerson, K.D., The recalculation of pyroxene end-member parameters and the estimation of ferrous and ferric iron content from electron microprobe analyses. Am. Min. 59, 1974, ppl203-1208.

45. Larsen, L.M., Clinopyroxenes and Co-existing mafic minerals from the alkaline Ilimaussaq intrusions, S. Greenland. Jn. Pet. 17, 2, 1976 p258-287.

46. Wilkinson, J.F.G., Clinopyroxenes from the Square Top intrusion, Nundle, New South Wales. Min. Mag. 35, 276, 1966, ppl061-1070.

47. Leake, B.E., Nomenclature of amphiboles. Min. Mag. 42, 1978 pp533-563.

48. Nash, W.P. and Wilkinson, J.F.G., Shonkin Sag Laccolith, Montana. I. Mafic minerals and estimates of temperature, pressure, oxygen fugacity and silica activity Cont. Min. Pet 25, 1970, pp241-269

49. Stephenson, N.C.N., Coexisting hornblendes and biotites from Precambrian gneisses of the south coast of Western Australia. Lithos 10, 1977, pp9-27.

50. Deer, W.A., Howie, R.A., and Zussman, J. (1966) An introduction to the rock-forming minerals. Longman. 519pp.

51. Brooks, C.K., Engell, J., Larsen, L.M. and Pedersen, A.K., Mineralogy of the Werner Bjerge alkaline complex, East Greenland. Meddr om Grønland, Geosci., 7, 1982, 35pp.

52. Norrish, K. and Chappell, B.W., X-ray fluorescence spectrometry. In Zussman, J (ed) 1977, Physical methods in determinative mineralogy, 2nd ed. Academic Press, London. pp201-272.

53. Currie, K.L. The alkaline rocks of Canada. Geol. Surv. Canada Bull 239, 1976 228pp.

54. Wright, J.B. A simple alkalinity ratio and its application to questions of non-orogenic granites. Geol. Mag. v104, 4, 1969, pp370-384.

55. Robinson, D. and Leake, B.E. Sedimentary and igneous trends on AFM diagrams. Geol. Mag. 112, 1975 pp305-307.

56. Taylor, S.R. The application of trace element data to problems in petrology. Phys. Chem. Earth 6, 1965, pp133-213.

57. Turekian, K.K. and Wedepohl, K.H. Distribution of the elements in some major units of the earth's crust. Bull geol. soc. Amer. 72, 1961 pp175-192.

58. Masuda, A., Nakamura, N. and Tanaka, T. Fine structures of mutually normalised rare-earth patterns of chondrites. Geochim. Cosmochim Acta 37, 1973, pp239-248.

59. Smith, T.E., Tetley, N. and Hudec P.P. Proterozoic mafic syenites from Baker Lake N.W.T. Canada Prec. Res. 13, 2/3, 1980 pp167-179.

60. Stephenson, D. Alkali clinopyroxenes from nepheline syenites of the south Øôroq Centre, South Greenland. Lithos 5, 1972 pp187-201.

61. Irvine, T.N. and Baragar, W.R.A. A guide to the chemical classification of the common volcanic rocks. Can. Jn. Earth Sci. 8, 1971 pp523-548.

62. McDonald, R. The petrology of alkaline dykes from the Tugtutoq area, South Greenland. Bull geol. soc. Denmark 19, 1969, pp257-282.

63. Emeleus, C.H. and Harry, W.T. The Igaliko nepheline syenite complex. General description. Bull. Grønlands geol. Unders. 85, 1970, 115pp.

64. McDonald, R. The role of fractional crystallization in the formation of the alkaline rocks. In Sørensen, H. (ed) 1974, The Alkaline rocks. John Wiley pp442-458.

65. Sørensen, H. Rythmic igneous layering in peralkaline intrusions. Lithos 2, 1968, pp261-283.

66. Coombs, D.S. and Wilkinson J.F.G. Lineages and fractionation trends in unsaturated volcanic rocks from the East Otago volcanic province (New Zealand) and related rocks. Jn. Pet. v10, 3, 1969, pp440-501.

67. Emeleus, C.H. Structural and petrographic observations on layered granites from Southern Greenland. Spec. Pap. Min. Soc. Ameri., 1, 1963, pp22-29.

68. Bateman, P.C. and Chappell, B.W. Crystallization, fractionation and solidification of the Tuolumne Intrusive Series, Yosemite National Park, California. Bull. geol. Soc. Amer. v90, 1, 1979, pp465-482.

69. Stephenson, D. The South Øoroq Centre nepheline syenites South Greenland. Grøns. geol. Unders

70. Noble, D.c., Howman, H.R., Hebert, A.J., Silberman, M.L. Hercopoulos, C.E., Fabbi, B.P. and Hedge, C.E. Chemical and isotopic constraints on the origin of low silica andesite from the Andes of Central Peru, Geology 3, 1975, pp501-504.

71. Appleyard, E.C. Syn-orogenic igneous alkaline rocks of eastern Ontario and northern Norway. Lithos 7, 1974, pp147-169.

72. Heier, K.S. Geochemistry of the nepheline syenite on Stjernøy, north Norway. Nor. geol. Tidsskr. 44, 1964, pp205-215.

73. Sturt, B.A. and Ramsay, D.M. The alkaline complex of the Breivikbotn area, sørøy, northern Norway. Norges. geol. Unders. 231, 1965, pp1-164.

74. Pitcher, W.S. The nature, ascent and emplacement of granitic magmas. Jn. Geol. Soc. London, 136, 1979, pp627-662.

75. Campbell, I.H. and Arndt, N.T. Pyroxene accumulation in spinifex-textured rocks. Geol. Mag. 119/6, 1982 pp605-610.

76. Henderson, P. (1982). Inorganic geochemistry. Pergamon press 35pp.

77. Bailey, J.C. Geochemistry of igneous rocks. Lecture notes. 1979, pp32-33.

78. Bailey, D.K. Continental rifting and alkaline magmatism. In Sørensen, H. (ed) 1974. The alkaline rocks. John Wiley and Sons. pp148-160.

79. Butakora, E.L. Regional distribution and tectonic relations of the alkaline rocks of Siberia. In Sørensen, H. (ed) 1974. The alkaline rocks. John Wiley and Sons pp172-174.

80. Barker, D.S. North American feldspathoidal rocks in space and time. Geol. Soc. Am. Bull. 80, 1969. pp2369-2372.

81. Upton, B.G.J. The alkaline province of S.W. Greenland In Sørensen, H. (ed) 1974. The alkalin rocks. John Wiley and Sons pp221-230.

82. Vlasov, K.A., Kuzmenko, M.V. and Eskova E.M. (1966). The Lovozero alkaline massif. Oliver and Boyd. 624pp.

83. Streicksen, A and Hunzicker, J.C. On the origin and age of the nepheline syenite massif. of Ditro (Rumania). Rep. Schweiz. Min. Petr. Mitt., 54/1, 1974, pp60-76.

84. Hassib, A. and Annersten, H. Blue sodalite. Can. Min. 17/1, 1979 pp39.

85. Bloomfield, K., Deans, T. and Wells, M.K. The Ilomba alkaline complex, northern Malawi and associated uranium-niobium mineralisatio Inst. Geol. Sci 57, 1981, pp1-21.

86. Taylor, D. The sodalite group of minerals. Cont. Min. Petr. 16, 1967, pp172-174.

87. Edgar, A.D. Experimental studies. In Sørensen, H. (ed) 1974. The alkaline rocks. John Wiley and Sons pp380-389.

88. Currie, K.L., Curtis, L.W. and Gittins, J. Petrology of the Red Wine alkaline complex, Central Labrador and a comparison with the Ilimaussaq complex, S.W. Greenland. Geol. Surv. Can. Paper 75-1A, 1974 20pp.

89. Payne, J.G. Geology and geochemistry of the Blue Mountain nepheline syenite, Can. Jn. E. Sci. 4/2, 1968, pp259-273.

90. Duke, N.A. and Edgar, A.D. Petrology of the Blue Mountain and Bigwood felsic alkaline complexes of the Grenville province of Ontario. Can. Jn. E. Sci. 14/4, 1977, pp280-300.

91. Brock, P.W.G. Metasomatic and intrusive nepheline bearing rocks from Mbozi syenite-gabbro complex SW. Tanzania. Can. Jn. E. Sci. 5/3 1968, pp387-419.

92. Oyawoye, M.O. The petrology of a potassic syenite and its associated biotite pyroxenite at Shaki, W. Nigeria. Cont. Min. Pet. 16, 1967, pp115-138.

93. Appleyard. E.C. Nepheline gneisses of the Wolfe Belt, Lyndock Township, Ontario. Can. Jn. E. Sci. 4/3, 1967, pp371-395.

94. Gellatly, D.C. and Hornung, G. Metasomatic nepheline bearing gneisses from Darkainle, Somali Republic. Jn. Geol. 76/6, 1968, pp678-691.

95. Curtis, L.W. and Gittins, J. Aluminous and titaniferous clinopyroxenes from regionally metamorphosed agpaitic rocks in Central Labrador. HJn. Pet. 20/1; 1979, pp165-186.

96. Cox, K.G., Bell, J.D. and Pankhurst, R.J. (1979). The interpretation of igneous rocks. Allen and Unwin, London 450pp.

97. Jensen, B.B. Patterns of trace element partitionin Geochim. Cosmochim. Acta 37 1973. pp2227-2242.

98. Andreoli, M. and Hart, R. Evidence for a mid-late Proterozoic metallogenic event in southern Africa - inferences for the coeval evolution of Zambia. Geol Soc. Zambia Workshop. 29-30th March 1985. Abst.

99. Newton, A.R. and Drysdall, A.R. Further data on an amphibole from Mivula Hill. Rec. Geol. Surv. N. Rhodesia. 1959, p. 26-29